Swansea University
Prifysgol Abertawe

Novel Nanostructured Anodes for Green Energy Battery Storage

Master of Science by Research

Authored By:
Kayla McGoon-James

Supervisor: Prof. Richard E. Palmer
Co-Supervisor: Dr. Chris Phillips
Sponsored by: Johnson Matthey

M2A COATED

UKRI Engineering and Physical Sciences Research Council

UNDEB EWROPEAIDD EUROPEAN UNION
Llywodraeth Cymru Welsh Government
Cronfa Gymdeithasol Ewrop European Social Fund

Abstract

The quest to increase the lithium storage capacity of anodes in lithium-ion batteries is a prominent goal in battery research. The conventional graphitic Carbon-based anode material achieves a maximum capacity of 372 mAh g^{-1}, limited by the stoichiometry of the lithiated state Lithium Carbide (LiC_6). To overcome this limitation, Silicon anodes offer a theoretical storage capacity approximately ten times higher, albeit accompanied by a significant volume expansion issue. This study firstly explores various methods of fabricating composite materials as anodes, when combining Graphite and Silicon. The studies include the use of nano particle graphite as well as a physical method of nanoparticles deposition with a Matrix Assembly Clusters Source (MACS). The project was inspired by the ultimate prospect of employing cluster (nanoparticle) beam implantation techniques to embed small Silicon Nanoclusters, sized between 1-3 nm, into a porous carbon host. The utilization of such small Silicon particle sizes, embedded between Graphite particles, might possibly solve the volume expansion problem while retaining the benefit of additional storage density.

Anodes were made using various graphites as reference active materials, both conventionally sized (D50 8.4 µm) and Graphite nano powder to aid homogenous dispersion, and with the addition of Silicon Nanoparticles. These were made into slurries with Carbon Black and binder and cast on to foil prior to assembly into half-cells with lithium metal. The reference anodes made using conventional graphite performed as expected, with specific capacities close to expected values. However, when using Nano Graphite, the morphology of the powder caused significant drying and processing issues, that made it difficult to reliably cast the anode, causing delamination and ultimately higher instances of cell failure and lower specific capacity. Integration of the Silicon nano powder gave some evidence of improved results, but data were inconsistent and hindered by processing issues and high instances cell failure.

First demonstrative experiments utilising the MACS approach, which offers the advantage of integrating Silicon with larger Graphite particles, gave composite anodes that were able to be readily processed into an anode in the same way as conventional Graphite, without delamination or excessive cell failure. The resultant half-cells gave slightly higher capacity than reference Graphite cells, but more work is needed to develop and verify the processing to validate the extent of the Silicon coating on the Graphite and confirm its effect on capacity.

Acknowledgements

Firstly, I would like to extend my gratitude to the team at M2A Coated, the European Social Fund, and UKRI for granting me this incredible opportunity. I am immensely grateful to my sponsor Johnson Matthey, my industrial supervisors Dr. Enrico Petrucco and Dr. James Cookson and a special thank you to Thomas Samuels, for his invaluable help in battery testing and fabrication. I would like to acknowledge and thank all the talented individuals at the Energy Safety Research Institute Battery Research Lab and WCPC, for welcoming me with open arms. Your extensive knowledge and expertise in the battery sector serve as a constant source of inspiration. I express my gratitude to the Swansea University Nanomaterials Lab for the enlightening monthly discussions, shared knowledge, and pub quizzes. Without your support, this year would have been significantly less gratifying. I greatly admire your work ethic, patience, and talent. Thank you, Morris Matthews, Sarah Stock, Filip Krzymieniecki, Pavan Kumar, Henry Hoddinott, Sean Lethbridge, James McCormack, and Milos Baljozovic, Anton Marunsenko, Dr. Ashely Willow, Dr. Haytham Hussain, Nathan Reynolds, Dan Gillard, and Dr. Dan Jones. A very special acknowledgment goes to my supervisor, Prof. Richard Palmer, for believing in me even when I doubted myself, and for his unwavering support and encouragement throughout this challenging journey. I would also like to thank my co- supervisor, Dr. Yubiao Niu, for his calm demeaner and insightful expertise in TEM characterization and James Mcgettrick for his contribution to XPS analysis. I am especially grateful to Dr. Chris Phillips for his immense support, admirable patience, extensive knowledge, and constant guidance. The advice and meetings with Dr. Phillips have made a significant contribution to the success of this project. Finally, I want to express my gratitude to my friends and family for their words of encouragement and to Liam for his ever-present support.

Authors Contribution

The work presented in this thesis was conducted by the author under guidance of my supervisor Prof. R. E Palmer and my co-supervisors Dr. Chris Phillips and Dr. Yubiao Nui. This documenthas been proofread by Dr. Chris Phillips and Prof. R. E Palmer.

Declarations

This work has not previously been accepted in substance for any degree and is not being concurrently submitted in candidature for any degree.

Signed…*KaylaMJ*.....

Date.....31/05/2023….....

This thesis is the result of my own investigations, except where otherwise stated. Other sources are acknowledged by footnotes giving explicit references. A bibliography is appended.

Signed…*KaylaMJ*.....

Date.....31/05/2023….....

I hereby give consent for my thesis, if accepted, to be available for electronic sharing

Signed…*KaylaMJ*.....

Date. 31/05/2023.....

The University's ethical procedures have been followed and, where appropriate, that ethical approval has been granted.

Signed... *KaylaMJ*.....

Date..... 31/05/2023.....

Table of Contents

1 Chapter 1 – Introduction and Background 16

1.1 Introduction and Thesis Overview 16

1.2 The basics of battery chemistry 17

1.3 A brief history of battery evolution 20

1.3.1 A brief history of Lithium-ion batteries 21

1.4 Basic Electrochemistry of Lithium-ion Batteries 22

1.5 Anode Materials 25

1.5.1 Lithium 25

1.5.2 Graphite 26

1.6 Silicon and Silicon Carbon Nanocomposites 28

1.7 Conclusion 29

2 Chapter 2 Experimental Techniques 31

2.1 Introduction to Experimental Techniques 31

2.2 Materials 31

2.3 Material Characterization 34

2.3.1 Scanning Electron Microscopy (SEM) 34

2.3.2 Transmission electron microscopy (TEM) 34

2.3.3 Energy Dispersive X-ray Spectroscopy 35

2.3.4 X-ray photoelectron spectroscopy 35

2.4 Battery fabrication 36

2.4.1 Slurry Preparation 37

2.4.2 Electrode Preparation 37

2.5 Coin cell fabrication 41

2.6 Electrochemical testing 42

2.6.1 Galvanostatic Cycling – Cycle Test 42

2.6.2 Rate Test (Waterfall test) 44

2.7 Conclusion – Experimental Techniques 45

3 Chapter 3- Results and Discussion 47

3.1 Introduction 47

3.2 Material Characterization and Electrode Fabrication 48

3.3 Graphite Powder Characterization 48

3.4 Nano Graphite Powder Characterization 49

3.5 Silicon Nanoparticles Powder Characterization 50

3.6 Anode Powder Characterization Closure 51

3.7 Slurry and Electrode Fabrication 52

3.8 Graphite Slurry and Electrode Preparation 52

3.9 Nano Graphite Slurry and Electrode Preparation 53

3.10 Graphite + Silicon Nanoparticles and Nano graphite + Silicon Nanoparticles Slurry and Electrode Preparation 54

3.10.1 Method 1 55

3.10.2 Method 2 55

3.11 Slurry Preparation Closure 56

3.12 Electrode Characterization 57

3.13 Graphite + Silicon Nanoparticles Electrode SEM image Comparison 58

3.14 Nano Graphite + Silicon Nanoparticles Electrode SEM image comparison..... 59

3.15 X-ray Photoelectron Spectroscopy (XPS)..... 60

3.16 Characterization Closure 64

3.17 Electrochemical Testing Results and Discussion..... 65

3.18 Graphite (Reference Cell) Electrochemical Results..... 66

3.19 Nano Graphite Electrochemical Results 69

3.20 Graphite + Silicon nanoparticles Cell Electrochemical Results 72

3.21 Nano Graphite + Silicon Nanoparticles Rate Test Results 74

3.22 Anode Type Electrochemical Results Comparison 79

3.23 Electrochemical Testing Results Closure 80

4 Chapter 4.0 Feasibility Study: Matrix Assembly Cluster Source 82

4.1 Introduction..... 82

4.1 Background 82

4.1 Fabricate Graphite + Silicon nanocomposites using the Matrix Assembly Cluster Source 83

4.1.1 Experimental techniques..... 84

4.2 Results and Discussion (Preliminary) 90

4.2.1 Powder and Electrode Characterization..... 90

4.2.2 Electrochemical Results (Preliminary) 92

4.2 Overall Project Closure, Discussion and Future Works....96

5 Bibliography 98

Appendix 110

A1. Coin Cell Table 110

A2. Graphite Electrochemical Results 112

A3. Nano Graphite Electrochemical Tests....113

A4. Full XPS Results 114

A5. Silicon loading theory. 115

List of Tables

Table 2-1 – List of Anode Materials *32*

Table 2-2 – List of Anodes and Nanocomposites fabricated in the Project and intended ratio of silicon nanoparticles. *33*

Table 2-3 – Coin cell Parts List *33*

Table 3-1 - XPS Stoichiometry table for Electrodes *64*

Table 4-1 - XPS stoichiometric results for MACS Powder (Graphite + Silicon Clusters) and Electrode of MACS Graphite + Silicon Clusters Nanocomposite *90*

Table A 0-1 - Cell Type Table *110*

Table A 0-2 Full stoichiometric XPS Results *114*

List of Figures

Figure 1-1- Diagram comparing the volumetric and gravimetric energy densities of most common secondary battery systems (5) 18

Figure 1-2 - Landmarks in the history of Battery Technology (12) 21

Figure 1-3 - Schematic of a cylindrical lithium-ion battery (19) 24

Figure 1-4 - Schematic of Lithium-ion battery working principle (99). 24

Figure 1-5 - Three generations of Lithium-ion batteries (28) 25

Figure 1-6 - Graphite Structure of two staking sequences ABAB (2H), (B) Schematic diagram of Graphite Coordination structure in electrolyte (34) 27

Figure 2-2 - a) Fritsch Pulverisette 23 mini ball miller (52) b) Lab Automatic bar coater XB-300 c) MSK-AFA-II Automatic Thick Film Coater d) MSK-HRP-01 Hot Rolling Cylinder Press (53) e) Precision Disc Cutter from Cambridge Energy (54). 40

Figure 2-3 - a) Coin cell stack disassembled and arranged in a Glove Box and b) a schematic of coin cell stack arrangement. 41

Figure 2-4 - Galvanostatic Plots examples (61) 44

Figure 3-1 - 78000 x STEM HAADF image of thin film of Graphite SFG15; b) 310 kx STEM HAADF c) STEM HAADF of Graphite. Images captured by Dr. Yubiao Nui and Doctoral Student Sean Lethbridge 48

Figure 3 2 - a) STEM HAADF TEM micrograph of powder form PiKem Nano Graphite >30 nanometres, showing the microstructure of the Nano Graphite nanoflakes b) higher magnification c) higher magnification. Images captured by Dr. Yubiao Nui and Doctoral Student Sean Lethbridge 49

Figure 3-3 - a) of Silicon Nanoparticles (20 nm scale bar) b) Silicon Nanoparticles EDX image (20 nm scale bar) (Image captured by Dr. Yubiao Nui). 51

Figure 3-4 - Casting Method Testing a) Bar Coating, b) Thick Film Casting, c) Tape Casting 52

Figure 3-5 – Nano Graphite dried @ 45°C for 24 hours and b) dried at 35°C for 48 hours……54

Figure 3-6 - Step by Step Process of the Graphite + Silicon and Nano Graphite + Silicon slurry preparation - Method 2 56

Figure 3-7 - SEM micrograph of Graphite anode showing 5-15 nm particle sizing (a) and b) Graphite electrode at higher magnification showing the laminar structure of the Graphite electrodes. Images Captured by Doctoral student Dan Gillard at Swansea University. 58

Figure 3-8 - a) Graphite SEM Micrographs and b) Graphite + Silicon Nanoparticles SEM image at an increased magnification. Images Captured by Doctoral student Dan Gillard at Swansea University.....59

Figure 3-9 - a) Nano Graphite electrode micrograph exhibiting thermal cracking after drying at 45°C b) higher maginification and c) micrograph of Nano Graphite +Silicon nanoparticles eletcrode for comparison to show pre and post silicon nanoparticle addtion. Images capturedby Doctoral Student Dan Gillard at Swansea Universtiy. 60

Figure 3-10 - XPS Graph of Electrodes: Graphite (G) (red), Nano Graphite (NG) (blue) Graphite + Silicon Nanoparticles (G + SiNP)(black) Nano Graphite + Silicon Nanoparticles (NG + SiNP) (green and gold). Discussed in Chapter 4: MACS Graphite + Silicon (grey) and MACS Graphite + Silicon clusters (pink) – Graph and XPS analysis prepared by Dr. James Mcgettrick at Swansea University.....62

Figure 3-11 - Graphite Rate Test Capacity vs Cycle Number (C represents C-rate). The cell is tested at different charge rates to test cell retention and degradation under varying charge and discharge conditions. 66

Figure 3-12 - Graphite Rate Test Voltage Vs Capacity.....67

Figure 3-13 - Graphite Cycle Life Test (C/10) – Capacity Vs Cycle Number at constant C-rate of C/10. ..... *67*

Figure 3-14 - Graphite Cycle Life Test – Voltage Vs Capacity *68*

Figure 3-15 Nano Graphite Rate Test – Capacity Vs Cycle Number (C represents C-rate). The cell is tested at different charge rates to test cell retention and degradation under varying charge and discharge conditions. *69*

Figure 3-16 – Nano Graphite Rate Test Results Voltage Vs Capacity at a constant C-rate of C/10. ..... *70*

Figure 3-17 – Nano Graphite Cycle Life Test – Capacity Vs Cycle Number at a constant C-rate of C/10. ..... *70*

Figure 3-18 – Nano Graphite Cycle Life Test – Voltage Vs Capacity at a constant C-rate of C/10, ... *71*

Figure 3-19 - Graphite + Silicon Cycle Life Test, Capacity Vs Cycle Number at a constant C-rate of C/10. ..... *73*

Figure 3-20 - Graphite Cycle Life Test (2) – Capacity Vs Cycle Number Constant C-rate of C/10. ..... *73*

Figure 3-21 – Nano Graphite + Silicon Nanoparticles Rate Test – Capacity Vs Cycle Number (C stands for C-rate). The cell is tested at different charge rates to test cell retention and degradation under varying charge and discharge conditions. *75*

Figure 3-22 – Nano Graphite + Silicon Nanoparticles Rate Test Voltage Vs Capacity at constant C-rate of C/10. ..... *75*

Figure 3-23 -Nano Graphite + Silicon Cycle Life Test Capacity Vs Cycle Number at constant C-rate of C/10. ..... *76*

Figure 3-24 – Nano Graphite + Silicon Cycle Life Test Capacity Vs Voltage at constant C-rate of C/10. ..... *76*

Figure 3-25- SEM images of a) Nano Graphite + Silicon electrodes before 60 cycles b) after 60 cycles and c) after 60 cycles showing porous and degraded surface. Images captured by Doctoral student Dan Gillard at Swansea University.

.....76

Figure 3-26 –Anode Comparison Graph (Best Performing Cells).....76

Figure 4-1 - MACS Schematic of inside the vacuum chamber showing the cold head and matrix assembly working principle.....85

Figure 4-2 - MACS at WCPC - Swansea University April 2022 86

Figure 4-3- Engineering Rendering of the MACS created by doctoral student Morris Matthews. 86

Figure 4-5 - MACS Graphite + Silicon Electrodes 88

Figure 4-6 – a) SEM image of Graphite electrode b) SEM image of MACS Graphite + Silicon Electrode. Images captured and prepared by Doctoral student Dan Gillard. 91

Figure 4-7 - Rate Test, MACS Cells 1. 92

Figure A0-1 - Graphite Rate Test Result Cell 2.....112

Figure A0-2 - Graphite Cycle Life Test Result Cell 3 (C/10) 113

Figure A0-3 – Nano Graphite Rate Test Cell 2 113

Figure A0-4 – Nano Graphite Cycle Life Test Cell 3 114

Chapter 1 – Introduction and Background

1.1 Introduction and Thesis Overview

The world is currently facing a climate crisis, necessitating urgent efforts to transition towards sustainable energy sources and mitigate the detrimental effects of fossil fuel consumption. As part of this global endeavour, the development of electrical energy storage devices (EES) has gained significant attention, aiming to support the integration of renewable energy and ensure a reliable power supply. Among various EES technologies, batteries have emerged as a key solution due to their portability, scalability, and high energy density (1).

Lithium-ion batteries have revolutionized portable electronics and electric vehicle markets due to their excellent performance characteristics. However, the current graphitic carbon-based anode material, with a maximum capacity of $372mAhg^{-1}$. To overcome this limitation, silicon (Si) anodes have attracted significant interest owing to their high theoretical storage capacity, which is an order of magnitude greater than that of graphitic carbon-based anodes. Nevertheless, there are major challenge associated with Silicon anodes, due to intermetallic alloying upon Silicon's reaction to Lithium causing significant volume expansion during cycling, leading to electrode degradation and reduced battery lifespan (2).

To address the volumetric expansion issue and exploit the high-capacity potential of Si anodes, the concept of incorporating Si nanoparticles into a carbon host has gained prominence. The synergy between Si and carbon materials offers enhanced capacity, increased electrical conductivity, and improved tolerance to volume changes during cycling (2). One promising approach is the use of nanocomposite anodes consisting of Si nanoparticles embedded within a porous carbon matrix.

This thesis aims to investigate the effectiveness of nanocomposite anodes for enhancing the lithium storage capacity in lithium-ion batteries. Furthermore, it explores the novel Matrix Assembly Cluster Source (MACS) method as a means of embedding Si nanoclusters, ranging in size from 1-3nm, into the porous carbon host. The MACS technique, a cluster beam implantation method, enables precise control over cluster size and offers opportunities for optimizing battery performance (2). The targeted objective is to achieve a Si loading of 6% in the carbon host material.

Prior to focusing on the MACS method, various methods of fabricating nanocomposite anodes, including graphite and Silicon nanoparticles and nano graphite and silicon nanoparticles, were explored to compare their performance and feasibility. Additionally, the installation of a dedicated electron beam evaporator is currently underway to load Si atoms into the MACS matrix, thereby enabling the production of well-defined Si nanocluster beams. Battery testing will be performed using lab-scale coin cells, with reference materials comprising 15nm commercial Si powder particles.

By investigating the utilization of nanocomposite anodes and the innovative MACS method, this research aims to overcome the limitations of current lithium-ion battery anode materials and enhance their lithium storage capacity. The findings of this study have the potential to revolutionize battery technology, paving the way for the development of high-performance batteries capable of meeting the increasing demands of the sustainable energy landscape.

1.2 The basics of battery chemistry

A battery is an electrochemical cell that converts the chemical energy from a reaction directly into electrical energy. There are two main types of batteries: primary and secondary. Primary batteries, such as alkaline batteries, zinc-carbon batteries, and lithium metal batteries, cannot be recharged and are discarded after use (3; 1). In contrast, secondary batteries can be recharged due to the reversibility of the redox reactions that occur in the electrochemical cell. Examples

of secondary battery systems include lithium-ion batteries, nickel-cadmium (NiCd) batteries, nickel-metal hydride (Ni-MH) batteries, and lead-acid batteries (4).

Among secondary battery systems are lithium-ion batteries. These are an already ubiquitous energy storage technology due to their high energy density, long cycle life, and clean energy potential. In comparison to other battery chemistries, such as Ni-MH and lead-acid batteries, lithium-ion batteries offer a higher specific energy density and volumetric energy density, as shown in *Figure 1-1*- Diagram comparing the volumetric and gravimetric energy densities of most common secondary battery systems .

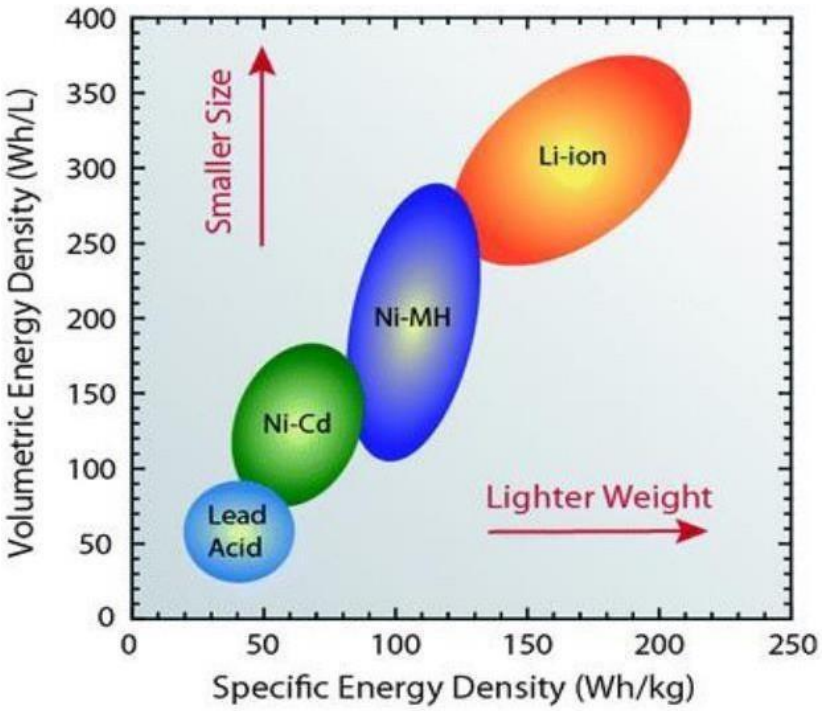

Figure 1-1- Diagram comparing the volumetric and gravimetric energy densities of most common secondary battery systems (5).

A battery is made up of a connection of multiple electrochemical cells, however, may also refer to a single cell (5). The components contained within an electrochemical cell have specific material characteristics that produce a free flow of electrons. A cell most importantly contains two electrodes with an electrochemical potential difference separated by a porous polymer

separator and a liquid or gel electrolyte. The potential difference between the anode and cathode induces an electromotive force (V) which drives a redox reaction at each electrode (5). This reaction can be split into an oxidation reaction at the anode (Eq 1) and a reduction reaction at the cathode (Eq 2). When a fully charged battery cell begins discharge, an oxidation half-reaction occurs at the anode, illustrated in *Equation (1):*

$$A \rightarrow A+ + e- \quad (1)$$

Equation 1 – Oxidation Half Reaction

The generation of positively charged ions and negatively charged electrons take place. The electrolyte solution between the two anodes is a medium that is electrically conducting through the movement of ions but insulating of electrons. These properties of the electrolyte allow for the free flow of ions to the positive electrode. An ion conducting and electron insulating porous polymer separator lies between the two electrodes to prevent short circuit of the cell. Due to the electron insulating properties of the electrolyte, negatively charged electrons are forced to travel to the anode via an external circuit and the electrical energy from this reaction is harnessed. Upon charging, a reduction reaction (2) occurs at the cathode. This continues upon charge and discharge.

$$B \rightarrow B+ + e-1 \quad (2)$$

Equation 2 - Reduction Half Reaction

The standard potential between the electrodes directly determines the cells overall electrochemical potential. A greater difference in electrochemical potential of electrodes materials equates to an increased battery voltage. Furthermore, electrode material characteristics, such as conductivity, particle size, porosity, surface area and chemical stability have a direct effect on cell electrochemical performance (6).

1.3 A brief history of battery evolution

In 1800, Italian physicist Alessandro Volta (7) invented the first electrochemical battery, the voltaic pile, using stacked copper and zinc plates separated by brin-soaked paper disks, as shown in the timeline schematic in Figure 1-2. Michael Faraday (8) later demonstrated that the voltage was a result of chemical reactions. In 1834, French scientist Gaston Planté (9) developed the lead-acid battery, a key step in battery evolution and the first rechargeable battery. It had low cost and high stability but was hindered by its carcinogenic nature and low energy density. The Ni-Cd battery followed in 1901, exhibiting excellent performance at low temperatures, but the requirement of precious metals limited its usage.

In the 1970s, lithium-based batteries (7) were developed due to the increasing demand for high-energy-density and lightweight power sources. These batteries revolutionized portable electronics and continue to be widely used today. Furthermore, the development of lithium-ion batteries in the 1980s (10) (11) marked a significant milestone in energy storage technology, offering improved safety, higher energy density, and longer cycle life. These advancements laid the foundation for the widespread adoption of lithium-ion batteries in various applications, including portable electronics, electric vehicles, and renewable energy systems. *Figure 1-2* presents the key landmarks in battery history and development.

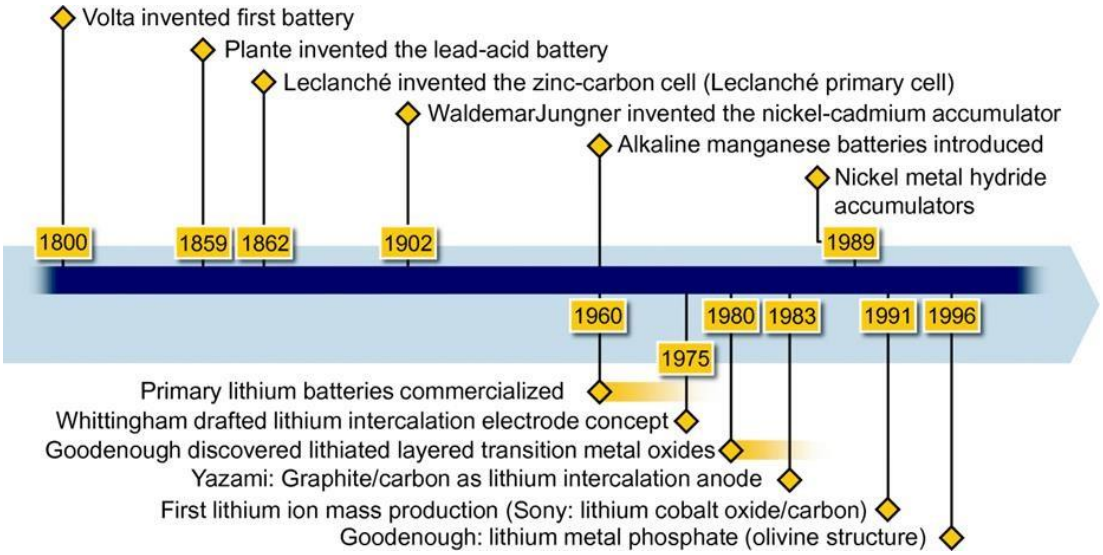

Figure 1-2 - Landmarks in the history of Battery Technology (12)

1.3.1 A brief history of Lithium-ion batteries

Since their market introduction in 1991, lithium-ion batteries (LIB's) have demonstrated an evolutionary potential for a variety of applications, not only dominating the small-scale battery market for their use in consumer electrics but have now been implemented as the battery of choice for electric vehicles such as hybrid (HEV), plug-in (PHEV) and fully electric vehicles (13). Finally, they have shown significant value for their use in stationary energy storage for intermittent energy sources like wind and solar (14) (15). The success of lithium-ion batteries is due to their high specific energy (100-265 Wh/kg) energy density (250-693 W.h/L), high reliability and ever reducing cost when compared to other battery technologies in the market (16). The use of transition metal compounds as a cathode material allows for a reversible evolution of both electronic structure and crystal structure to ensure balance during lithiation and prevention of the lattice structure collapse (17).

Lithium metal was discovered in 1817 by Arfwedson and Berzelius (16) but experimentation of the electrochemical use of lithium metal came almost a century later in 1912 under G.N Lewis (8). Lithium metal holds excellent physical properties, including low density (0.534g

cm^{-3}), high specific capacity (3860 $mAhg^{-1}$) and a low redox potential (-304V vs SHE) (17). Despite its promise, the high reactivity of lithium metal creates a technological challenge in the safety of lithium-based battery engineering. This led to the need for replacement of an unreactive metal anode material for commercialization. Thus, compounds capable of donating lithium ions (Li+) are used alternatively (18).

In the 1970s, Michael Stanley Whittingham drafted the concept of lithium intercalation using lithium metal and titanium sulphide as the electrode materials, laying the groundwork for further development (19). In the same period, Jurgen Otto Besenhard demonstrated the concept of intercalation chemistry using graphite and cathodic metal oxides as the anode and cathodes respectively (20). Samar Basu demonstrated the intercalation of lithium in graphite, an important concept in battery chemistry. However, batteries built in this time rapidly deteriorated after recharge, resulting in a poor cycle life (21). In the 1980s, research on the reversible electrochemical intercalation of positively charged lithium ions in graphitic carbon, by Rachid Yazami, allowed for great improvements in cycle life (22). Around the 1980s, much attention was concentrated toward the development of materials for the positive electrode, the cathode. In 1986, Akira Yoshino's 'soft carbon anode' along with Goodenough's LCO cathode and carbon ester-based electrolyte patented the world's first commercial lithium-ion battery, which was produced and sold by Sony and Asahi Kasei in 1991. Since then, much investment has been put into developing these technologies (23).

1.4 Basic Electrochemistry of Lithium-ion Batteries

Lithium-ion batteries (LIBs) are widely used due to their high energy density, low self-discharge rate, and long cycle life. The performance of LIBs is measured by various parameters including specific capacity, rate capacity, coulombic efficiency, and cycle life. Specific capacity refers to the amount of energy released per unit volume or mass, and it is determined by the number of positive lithium ions that travel between the positive and negative electrodes

during battery cycling. Coulombic efficiency, on the other hand, is the ratio of discharge capacity after a full charge and charging capacity of the same cycle (24). Rate capacity relates to the size of the current in a battery, and cycle life refers to the number of times a battery can be charged and discharged before 80% capacity deterioration (19).

The basic components of LIBs include anode, cathode, electrolyte, separator, and current collector, which can be seen in the schematic *Figure 1-3* annotating the design within a cylindrical lithium-ion battery. The primary electrochemical reactions take place at the anode and cathode, with typical materials being Lithium Cobalt Oxide ($LiCoO_2$), Lithium Manganese Oxide ($LiMn2O_4$), Lithium Iron Phosphate ($LiFePO_4$ or LFP) and Lithium Manganese Cobalt oxide ($LiNiMnCoO_2$ or NMC) for cathode and typically Graphite for the anode (19). Upon charging, lithium ions are extracted from the cathode material and embedded in the anode material through a reversible intercalation reaction (25). When the battery discharges, the flow of ions and electrons takes place in the opposite direction, converting chemical to electrical energy (19), with the chemical reactions that take place outlined in *Equations (3,4,5):*

$$Cathode: LiCoCO_2 \leftrightarrow Li1-xCoCO_2 + xLix + xe- \text{ (3)}$$

Equation 3

$$Anode: 6C + xLi+ + xe- \leftrightarrow LixC_6 \text{ (4)}$$

Equation 4

$$Total\ LiCoO_2 + 6C \leftrightarrow LixC_6 + Li1-xCoO_2 \text{ (5)}$$

Equation 5

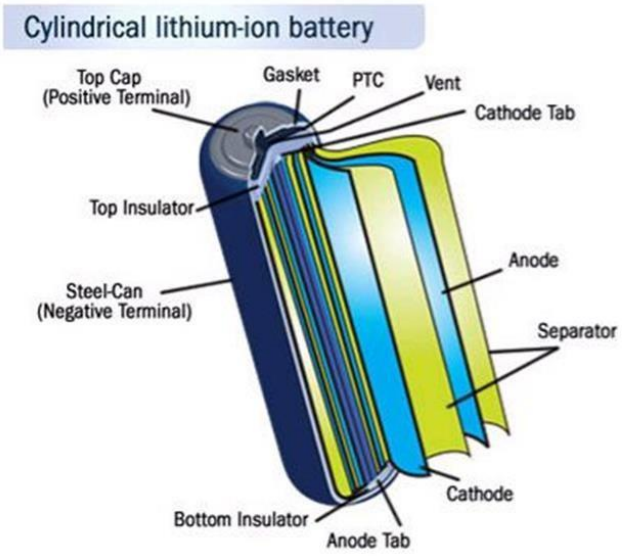

Figure 1-3 - Schematic of a cylindrical lithium-ion battery (19)

The electrolyte, usually lithium hexafluorophosphate ($LiPF_6$), facilitates the flow of electrical charge between the electrodes by maintaining a free ion exchange. *Figure 1-4* illustrates the working principles of a lithium-ion battery, with graphite as the anode and $LiCoCO_2$ as the cathode. Lithium-ion batteries with graphite anodes and LiCoO2 cathodes operate based on the movement of lithium ions between the anode and cathode during charge and discharge cycles, facilitated by a liquid electrolyte. During discharge, lithium ions move from the anode (graphite) to the cathode (LiCoO2), releasing energy; during charge, ions move back, storing energy (26).

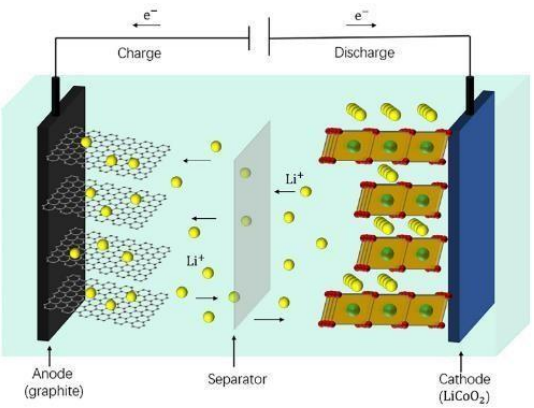

Figure 1-4 - Schematic of Lithium-ion battery working principle (99).

1.5 Anode Materials

The operational dynamics of a lithium-ion battery underscore the pivotal role of the anode material in shaping overall battery performance. Consequently, the pursuit of advanced anode materials is paramount, driven not only by performance optimization but also by considerations of cost-effectiveness and material availability. Although Graphite Significant investments are being channelled into research and development to discover anode materials that align with the demands of high-performance, market-ready lithium-ion batteries (26) (14). This collective endeavour to identify novel anode materials and enhance fabrication techniques is a focal point in the landscape of battery technology advancement (1). Particularly within the realm of hybrid and electric vehicles, the need for high-performance anode materials is pressing (27).

1.5.1 Lithium

According to theoretical energy density calculations and thermodynamic data (25), secondary system batteries using metallic lithium as an anode material have the potential for the highest energy density of any electrochemical energy storage device. This is depicted in *Figure 1-5* (26).

Gene.	Cathode	Anode	Electrolyte	Time	Market
1st	4.2V $LiCoO_2$	Coke	PC/DMC $LiPF_6$	1991-	CE
2nd	4.3 V $LiCoO_2$	NG AG $Li_4Ti_5O_{12}$	EC-DMC, $LiPF_6$	1994-	CE
	$LiMn_2O_4$,				EV
	$LiNi_{1/3}Co_{1/3}Mn_{1/3}O_2$				grid
	$LiFePO_4$				power tool
3rd	4.4-4.6 V $LiCoO_2$	Soft carbon Hard carbon SnCoC SiO_x Nano-Si/C	**EC-DMC,** **$LiPF_6$** + VC, FEC, BP, ES, PS, LiBOB, LiTFSI, Silane, LiFSI, Ionic liquid…	2005-	CE EV HEV Grid Others
	$LiNi_{x<0.5}Co_yMn_2O_2$				
	$LiNi_{0.8}Co_{0.15}Al_{0.05}O_2$				
	$LiFe_{1-x}Mn_xPO_4$				
	xLi_2MnO_3-$Li(NiCoMn)O_2$				
	$LiNi_{0.5}Mn_{1.5}O_4$				

Figure 1-5 - Three generations of Lithium-ion batteries (28)

Initially, early battery designs employed lithium metal electrodes paired with polar aprotic electrolyte solvents, which do not have a hydrogen atom bonded to an oxygen or nitrogen atom. However, this approach led to the formation of a dense surface film within the cell, impeding effective passivation (27). Over repeated charge-discharge cycles, the excessive build-up of metallic lithium deposition and lithium dendrites became problematic, with the potential to breach the separator and trigger battery short circuits. Beyond the safety concerns associated with pure lithium metal anodes, these batteries exhibited significant lithium consumption as a finite resource and experienced rapid deterioration in cycle life. Complicating matters were issues like the instability of the solid electrolyte interphase (SEI) layer growth and the progressive degradation of electrolytes, both further challenging the viability of lithium metal anodes. It's evident that substantial endeavours are required to address these challenges, with a near-term goal of developing third-generation lithium-ion batteries incorporating alternative anode materials (28). Among these, silicon-based anode materials stand out as a promising area of focus for future advancements, shaping the path toward fourth-generation LIBs.

1.5.2 Graphite

Graphite has been the standard anode material for LIBs since the 1990's. Graphite is the preferred anode material due to its safety, non-toxicity, abundance and low-cost (29).

Additionally, graphite offers a satisfactory capacity, energy density and cycle life. The preference of graphite electrode material is with virtue to the characteristics of graphite itself including low cost and chemical/electrochemical stability (30). Graphite is made up of honeycomb carbon layers which are weakly bound by van der Waals interaction illustrated in *Figure 1-6*, with a two-stacking sequence of hexagonal ABA or rhombohedral ABC stacking with an interlayer distance of 0.335 nm (31). The intercalation of guest ions in the graphite galleries is achieved through the formation of graphite intercalation compounds. As early as

1840, the attempted intercalation of H_2SO_4 into graphite was researched by Schafhaeutl et al (32). In the 1990s, a significant breakthrough was achieved in the realm of non-aqueous electrochemical cells: the successful intercalation of lithium ions into graphite (32). Illustrated in Figure 16, this process depicts how solvated ions from the electrolyte undergo a de-solvation step, facilitating the insertion of free lithium ions. This mechanism results in a high lithium-ion storage capacity of around 300 to 372 mAg-1 (26), coupled with an impressive retention rate of 90% or more even after undergoing numerous cycles at a 1C rate (33). It's worth noting that these outcomes can be subject to various influencing factors such as electrode formulation and cycling conditions. While graphite has been a key anode material in lithium-ion batteries, its ability to meet escalating market demands is being questioned due to certain limitations. Graphite's theoretical capacity for lithium-ion storage is relatively modest, around 372 mAh/g. As energy storage requirements increase in applications like electric vehicles and renewable energy storage, higher energy densities are essential (33).

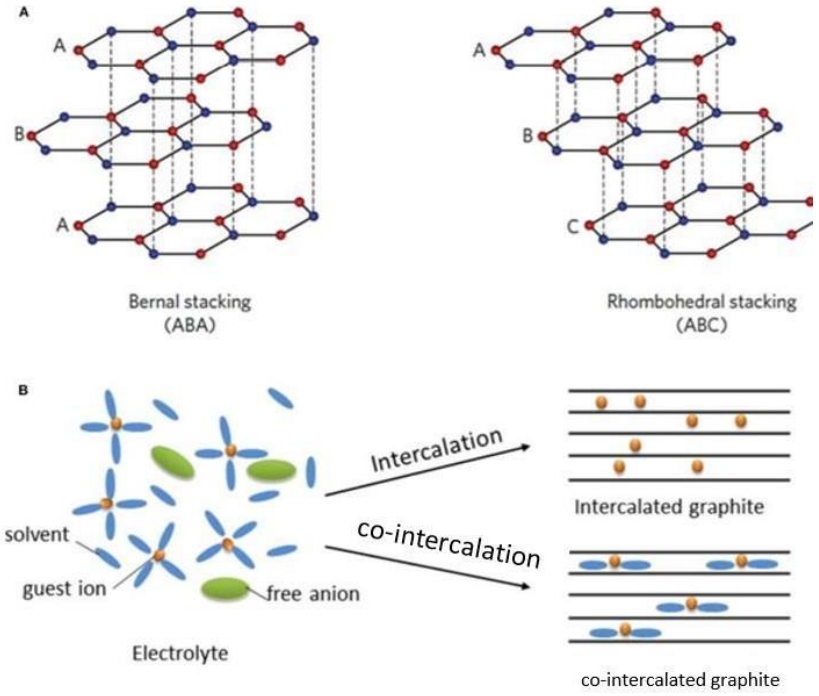

Figure 1-6 - Graphite Structure of two staking sequences ABAB (2H), (B) Schematic diagram of Graphite Coordination structure in electrolyte (34).

1.6 Silicon and Silicon Carbon Nanocomposites

To overcome the limitation of Graphite, various alternative anode materials have been explored, among which silicon has gained significant attention due to its high theoretical capacity and low discharge voltage (35).

Silicon (Si) has a theoretical capacity of 4200 mAh/g, which is about an order of magnitude higher than that of graphite (372 mAh/g) used in conventional LIBs. The high capacity of Si can significantly increase the energy density of the battery, leading to longer battery life and improved performance, (36). However, Si experiences significant volume expansion during lithiation and delithiation, leading to mechanical degradation and loss of electrical contact, which ultimately leads to poor cycling performance.

To address these issues, various strategies have been explored, including the use of nanostructured silicon, silicon-based composites, and surface modifications. Nanostructured silicon, such as silicon nanowires, nanotubes, and nano porous silicon, can mitigate the mechanical stress caused by volume expansion, resulting in improved cycling stability. For example, it has been demonstrated that using silicon nanowire battery electrodes, the issue of silicon volume change during lithium can be alleviated and maintain a discharge capacity of close to 75% maximum, with little fading during cycling (33). Silicon-based composites, such as silicon/carbon and silicon/tin/carbon, have been developed to improve the conductivity and stability of the silicon anode. Surface modifications, such as coating silicon with carbon, metal oxides, or polymers, can improve the stability of the SEI layer, reduce the electrolyte decomposition, and mitigate the volume expansion, resulting in improved cycling performance (37) (36) (38).

Recent studies have demonstrated the potential of Si-based anodes for LIBs. For instance, Li et al. reported a Si-based anode composed of Si/C nanospheres that exhibited a high reversible capacity of 2300 mAh/g after 100 cycles with a capacity retention of 78.7% at 1C rate (39).

Zhang et al. developed a Si/CNT composite anode that showed a reversible capacity of 1200 mAh/g after 100 cycles with a capacity retention of 77.8% at 1C rate (40). Xu et al. prepared a SiOx@C@Cu3Si composite anode that exhibited a high reversible capacity of 1000 mAh/g after 500 cycles with a capacity retention of 87% at 1C rate (41).

1.7 Conclusion

In conclusion, this background review has explored the progress made in the field of silicon nanoparticle-based anodes for lithium-ion batteries. The use of silicon nanoparticle-carbon composite materials has emerged as a promising alternative to traditional graphite-based anodes due to their high capacity, low operating potential, and excellent cycling stability. This is supported by studies conducted by Liu et al. (41), who reported a high specific capacity of 1575 mAh g^{-1} and good cycling stability of a silicon/carbon composite anode. Similarly, Guo et al. showed that a silicon/carbon nanofiber composite anode had a high capacity of 1068 mAh g^{-1} and excellent cycling stability up to 1000 cycles.

Studying silicon nanoparticle-based anodes is an important area of research, as the development of high-performance lithium-ion batteries is critical for the advancement of various technologies, including electric vehicles, portable electronics, and renewable energy systems. Silicon-based anodes offer the potential for significantly higher energy densities than current graphite-based anodes, which could lead to longer battery life and increased energy storage capacity. Additionally, silicon is abundant and widely available, making it an attractive and sustainable material for battery applications.

However, several challenges must be addressed to optimize the performance of silicon nanoparticle-carbon composite anodes. These challenges include issues related to synthesis methods, electrode architecture, and the structural stability of the anode material during cycling. For example, Choi et al (42). highlighted the importance of a rational electrode architecture design to mitigate volume expansion during cycling, which is a major challenge

for high theoretical capacity materials, as volume changes are due to intercalation of lithium and are inherent to high-capacity anodes (43) . Furthermore, utilizing nanostructured silicon in battery anodes mitigates volume expansion by allowing for better accommodation of the mechanical strain arising from lithiation. The increased surface area and reduced diffusion distance in nanostructured silicon enhance lithiation kinetics, minimizing stress-induced cracking (44).

Through the exploration of different methods of fabricating nanocomposite anodes and the installation of a specialized electron beam evaporator for loading Si atoms into the MACS matrix, this research aims to explore a possible advancement in silicon-based lithium-ion battery technology. The utilization of reference materials for battery testing in lab-scale coin cells using commercial Silicon nanoparticle (15 nm) powder will provide valuable insights into the performance and feasibility of the nanocomposite anodes.

The MACS technology, with its precise control over cluster size and intense beam of well-defined clusters, holds promise for optimizing battery performance. By achieving a Si loading of 6% in the carbon host material, the MACS method may provide a new method for embedding silicon clusters onto a carbon material for use in high performance lithium-ion batteries.

Chapter 2 Experimental Techniques

2.1 Introduction to Experimental Techniques

The experimental program involved the production of Graphite and Graphite plus Silicon anodes used in a half cell configuration with lithium metal as the counter electrode, to evaluate the effect of the incorporating silicon, in various forms, in with Graphite. Further to this, both regularly sized and nano sized graphite were used. This chapter details the materials used, methods to manufacture anode slurries, their deposition and subsequent use in coin cells for electrochemical testing as well as electrochemical testing methods. Further to this the materials were subjected to characterisation using Transmission Electron Microscopy, Scanning Electron Microscopy and X-ray photoelectron spectroscopy, to explore the surface morphologies and chemical compositions of the powders and electrodes used within this project, as mentioned in Chapter 1, these material properties have effects on the anode performance.

2.2 Materials

This project fabricated and tested five anode types, each with a different active material. The combinations composed of mixtures of conventionally sized Graphite (SFG15), Nano graphite, silicon nanoparticles, and carbon-silicon macro and nanocomposites, with the materials used in the electrode fabrication listed in *Table 2-1*, and the Anode names and compositions listed in *Table 2-2*.

Graphite (Timrex® SFG15 typically D90 17.9 µm) was obtained from IMERYS. Nano graphite (30nm nanospheres) was purchased from PiKem and provided by Johnson Matthey Technology Centre. Silicon nanoparticles (15nm) were purchased from ACS Material. The electrolyte used in each battery assembly is 1M $LiPF_6$ in ethylene carbonate/diethyl carbonate (EC/DEC, volume ratio 1:1) (Sigma Aldrich) which is a standard electrolyte shown to be compatible for use in both carbon and silicon-based anodes, based on previous literature (45).

2032-type coin cell, 316 Stainless Steel, and a full set including 0.5mm spacers and springs were purchased from Cambridge Solutions. Binder-free glass microfibre separators were purchased from Whatman. Lithium metal was used as the counter electrode (Sigma Aldrich). All materials for Coin cell parts and their respective sources used within this project, are listed in *Table 2-3.*

Table 2-1 – List of Anode Materials

Material	Vendor/Source	Material Property
SFG15 Graphite	**Timrex® SFG15 Graphite – IMERYS**	**Active material**
Nanographite 30nm nanospheres	**PiKem (provided by Johnson Matthey)**	**Active material**
Silicon Nanoparticles	**ACS Material**	**Active material**
TIMCAL SUPER P C45	**Sigma Aldrich**	**Conductive additive**
Carboxymethyl Cellulose (Sodium salt. Mw 250000 D. S.090)	**Sigma Aldrich**	**Binder**
Deionized Water	**N/A**	**Solvent for binder**
Lithium hexafluorophosphate (1.0M $LiPF_6$ in EC/DMC = (50/50) (v,v) battery grade)	**Sigma Aldrich**	**Electrolyte**
Lithium Metal	**Sigma Aldrich**	**Counter Electrode**

Table 2-2 – List of Anodes and Nanocomposites fabricated in the Project and intended ratio of silicon nanoparticles.

Anode Type	Carbon Silicon Ratio (Active)	Active (%)	Binder (%)	Carbon Black (%)
1. Graphite	100:0	80	10	10
2. Nano graphite	100:0	80	10	10
3. Graphite + Silicon Nanoparticles	94:6	80	10	10
4. Nano graphite + Silicon Nanoparticles	94:6	80	10	10
5. Graphite + Silicon Nanoclusters (MACS)	94:6	80	10	10

Table 2-3 – Coin cell Parts List

Part	Vendor
316 Stainless Steel Casing with seal	Cambridge Solutions
0.5mm Spacers	Cambridge Solutions
Glass Fibre Separator	Whatman

2.3 Material Characterization

Both ‘as supplied’ battery materials (active powders), casted and dried electrodes (anodes) were characterized using a range of characterization techniques, to characterize the commercially purchased powders to confirm the particle size, chemical composition and consequently the suitability for use in this project. Additionally, characterization for each anode type was essential to determine the chemical composition of each anode, in particular the silicon content of the nanocomposites, surface chemistry and particle size.

2.3.1 Scanning Electron Microscopy (SEM)

Scanning electron microscopy (SEM) and field emission gun scanning electron microscope (FEG-SEM) are effective characterization techniques to investigate the morphology of casted electrodes before cycling and after cycling. SEM works by generating a focused beam of high-energy electrons that scans across the surface of a sample, interacting with the atoms to produce signals such as backscattered electrons, secondary electrons, and characteristic X-rays. These signals are collected and processed to generate high-resolution images that reveal the surface morphology and composition of the sample (46). The ZEISS EVO LS25 SEM was used to observe surface morphology and give an idea of the overall material structure and morphology. This characterization technique was also used for imaging surface fractures, flaws, and corrosion of each electrode which is especially interesting after cycling. The scanning electron microscope relies on the detection of high-energy electrons emitted from the surface of a sample after exposure to a highly focused beam of electrons from an electron gun (47).

2.3.2 Transmission electron microscopy (TEM)

A Thermo Scientific Talos F200X scanning/transmission electron microscope (S/TEM) was used to obtain high-resolution STEM and TEM images of raw powders (Graphite, Nano graphite, Silicon nanoparticles and silicon nanocarbon nanocomposite). Transmission Electron Microscopy (TEM) works by passing a beam of electrons through an ultra-thin specimen, and the resulting interactions

and scattering of electrons provide detailed information about the sample's internal structure and composition at atomic resolution (48). The TEM was used to observe and confirm the particle size of commercially purchased powders and to study the microstructure of each raw powder material. The vacuum dried prepared through dispersing raw powders onto a 3mm diameter TEM gride (carbon coated Cu grid) by drop-casting with suitable solvents and air/vacuum-dried. The TEM images were captured by Dr Yubiao Nui and doctoral student Sean Lethbridge and contributed to the analysis of the images in this thesis.

2.3.3 Energy Dispersive X-ray Spectroscopy

Energy-Dispersive X-ray Spectroscopy (EDS) works by detecting characteristic X-rays emitted from a sample when it is bombarded with electrons in an electron microscopy setup, allowing for elemental analysis of the sample's composition (46). Energy dispersive x-ray spectroscopy (EDS) signal detection was used for 3D elemental characterization of raw powders with compositional mapping using four silicon drift detectors (SDDs) for superior sensitivity and mapping capabilities of up to 10^5 spectra/sec. This technique is essential for evaluating the true elemental composition of each powder. The energy dispersive x-ray spectroscopy detector is a feature installed as an available feature of the transmission electron microscope (TEM).

2.3.4 X-ray photoelectron spectroscopy

XPS is a characterization method that determines the elemental composition as well as the elemental state of each sample. X-ray Photoelectron Spectroscopy (XPS) works by measuring the kinetic energy of photoelectrons emitted from a sample's surface upon exposure to X-ray radiation, providing information about the elemental composition and chemical state of the surface (49). It should be noted that XPS is a surface-sensitive technique with an analysis depth of 8-10 nm. X-ray photoelectron spectroscopy (XPS) is an effective method to build an idea of the chemical composition and chemical bonds at the surface of the electrode and raw material samples and furthermore to quantify and confirm the chemical composition of components in

each electrode. The XPS data was collected using the Kratos Axis Supra, based in the Advanced Imagining of Materials at Swansea University. Surface stoichiometry was calculated using CasaXPS Version 2.3.22PR1.0. Peak areas were calculated from raw spectra using Tougaard baselines & the area adjusted using the Kratos sensitivity factor library. XPS measurements and analysis was conducted by Dr. James Mcgettrick.

2.4 Battery fabrication

The first step to battery fabrication is, to begin with, raw powder as the active and conductive component and combine this with a binding component to give a slurry. Binder acts as a binder material that holds the active materials and other components together, providing structural integrity and stability to the electrode as well as good adhesions and ensuring efficient electron and ion transport during battery operation (50). This slurry is then cast onto copper foil which acts as the current collector and dried. The dried electrode sheet is then punched, and these electrode discs are assembled into coin cells. *Figure 2.1* shows images of the slurry to electrode process. Left shows the slurry in the mixing device described in the following sections, middle displays the dried electrode after casting and right displays a punched electrode ready for coin cell fabrication and testing. The remainder of this section describes the methodology and equipment used in the battery fabrication process.

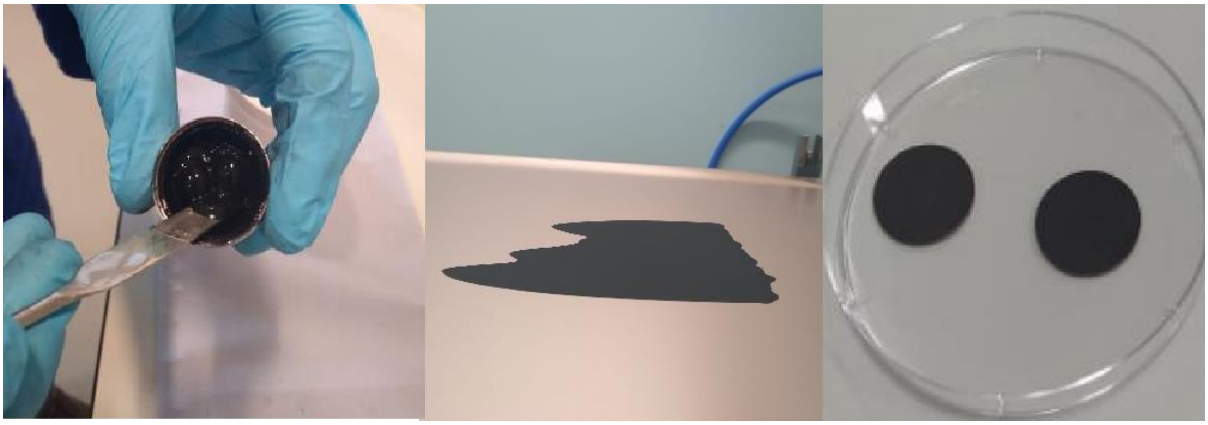

Figure 2.1 – a) Wet slurry in egg (ball mill) March 2022 b) Casted slurry on copper foil April 2022 c) Punched electrode April 2022

2.4.1 Slurry Preparation

The slurry preparation routes are similar for different materials however vary when the active material differs in particle size and elementally. The slurry mixture consists of an active material (graphite, nano graphite, graphite + silicon, nano graphite + silicon), a conductive carbon material (carbon black), a binder to adhere the materials together, and lastly a suitable solvent. Slurries tested in this project were composed of two main ratios of active material, carbon black, and binder in the ratios 70:20:10 and 80:10:10 respectively on a dry mass basis. These ratios are typical intended to optimize electrochemical performance of the battery electrodes as demonstrated in prior research *(51)*. Furthermore 70:20:10 was used initially as a basis formulation recipe. As the active material combinations behaved differently in terms of physical binding of materials, for example, nanoparticles require more binder as there is a smaller surface area to make contact in comparison to the macro-Graphite material used, which required less binder to achieve a homogeneous slurry mixture. For this reason, two different ratios were experimented with, and the results reported in Chapter 4. The binder used was carboxymethyl cellulose (CMC) (Sigma Aldrich) with deionized water as the solvent in a 4wt% CMC in water. The components of the slurry mixture were high-energy mixed using a Fritsch Pulverisette 23 mini ball miller, illustrated in *Figure 2.2.* This equipment consists of a grinding bowl *(Figure 2.1a)* that holds the slurry materials. Two grinding balls are then put into the grinding bowl and the bowl is then sealed using a rubber o-ring and pulverized at a set time and frequency (Hz) at 45 hertz/s with an additional 5µl of dilution needed.

2.4.2 Electrode Preparation

The electrodes were fabricated by coating the slurries on Cu foil. The coating process was carried out firstly by testing three varying methods, to explore which achieved the most consistent and high-quality casting. The first method tested was bar coating.

Figure 2-1*(b)* shows a diagram of the Lab Automatic Bar coater. This method consists of using the RK Control Coater, which uses the surface of a bar with wire windings of a given diameter to meter the ink evenly across the substrate at the desired speed which can be set automatically. Once the electrode was cast, it was then dried in an MTI vacuum oven at 60°C.

The second method was the hand casting method which consisted of using an electrical tape to tape down the substrate (Cu foil) and create a gap between the substrate and tape, depositing the slurry in between the tape channel. By hand, a glass rod was used to evenly spread the deposited slurry into a uniform electrode sheet.

The final casting technique used was an MSK-AFA-II Automatic Thick Film Coater, with a diagram displayed in *Figure 2.1 (c)* and the specified equipment is part of the Energy Safety Research Institute (ESRI Lab 003). The MSK-AFA-II is a mini tape casting coater consisting of a film applicator and a bottom heated vacuum platform which allows for a consistently smooth substrate (Cu foil) and the drying of electrodes after coating. To achieve an even coating, Cu foil is set on the vacuum platform and the vacuum pump is then engaged. Following this, a doctor blade calibrated to the selected thickness and is set at the film applicator and the slurry is deposited at the blade of the doctor blade and onto the Cu foil. The application speed is then set to 15 mm/s and the film coater is set to run. Once the doctor blade evenly distributes the slurry, the temperature of the heated vacuum platform is set to 45°C, stated as the appropriate drying temperature for Li-ion electrodes in the Standard Operating Procedure (SOP) recommended by the manufacturer for carbon-based slurries for li-ion batteries and the electrode is dried overnight. The thick film coater was able to achieve high uniformity in both thicknesses and surface structure of the electrode when compared with other methods and for this reason, the thick film coater was selected.

3.1.1.1 Electrode Calendaring and Drying

The casted electrode was then calendared using an MSK-HRP-01 Hot Rolling Cylinder Press. Presented in *Figure 2.1 (d)* The MSK-HRP-01 is a compact Hot Rolling Cylinder Press with a max working temperature of 100°C. This device is of use in battery design for preparing Li-ion battery electrodes after coating, to increase the active material density of the electrode and adhesion to the current collector using a pair of steel rollers (96 mm in width) with a maximum roller temperature of 100°C. The calendaring temperature was set to 50°C. The calendared electrode was then punched using a Precision Disc Cutter from Cambridge Energy Solutions, shown in *Figure 2-1 (e)* into 14 mm discs. The electrode discs were then annealed under a vacuum at 45°C, for 24 hours.

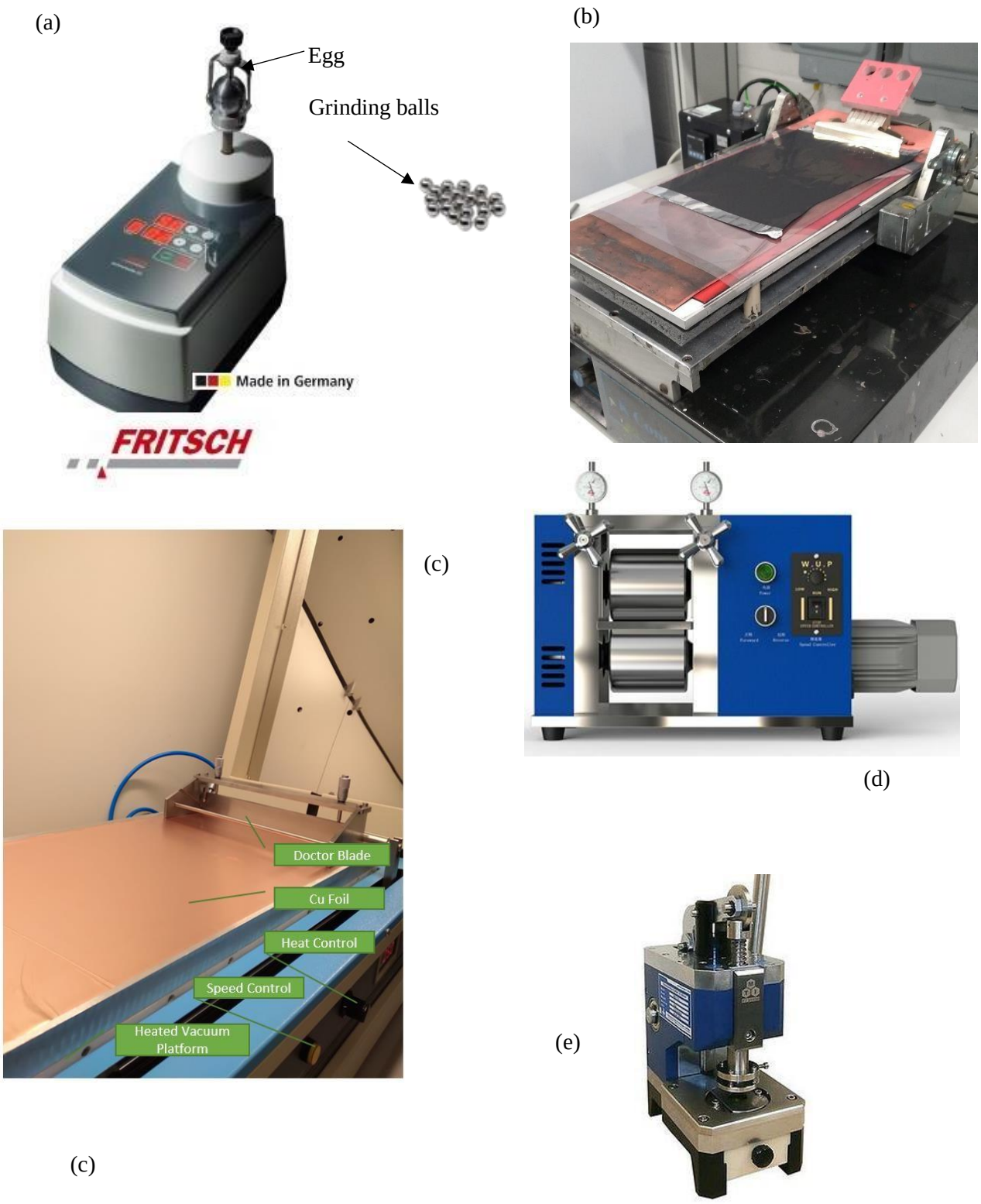

Figure 2-1 - a) Fritsch Pulverisette 23 mini ball miller (52) b) Lab Automatic bar coater XB-300 c) MSK-AFA-II Automatic Thick Film Coater d) MSK-HRP-01 Hot Rolling Cylinder Press (53) e) Precision Disc Cutter from Cambridge Energy (54).

2.5 Coin cell fabrication

Each coin cell was put together as half cells. Coin cells are widely used in the battery research sector as a suitable way to test the potential of new battery materials, even as a means of testing for large-scale applications such as grid storage, small coin cells, and half coin cells are generally suitable to test the rate and capacity capabilities of a novel battery electrode materials (55). Coin cells 2032-type (20 mm diameter and 3.2 mm thickness) were used for electrochemical testing. Each coin cell consisted of two circular metal casings, encapsulating a cell stack that is comprised of two electrodes (cathode and anode) separated by an ionically conducting and electrically insulating Whatman® glass fiber separator (GF/D, thickness 0.67 mm), wet with 1M $LiPF_6$ EC/DEC 50/50 (w/w) electrolyte to allow the passing of lithium ions from one electrode to the other. Three 0.5 mm spacers (316SS) and a spring are stacked on top (of the two electrodes and the separator) and the stack is then crimped to ensure a good electrical contact, with the arrangement illustrated in *Figure 2-2*, in the lab glovebox (left) and a schematic (right).

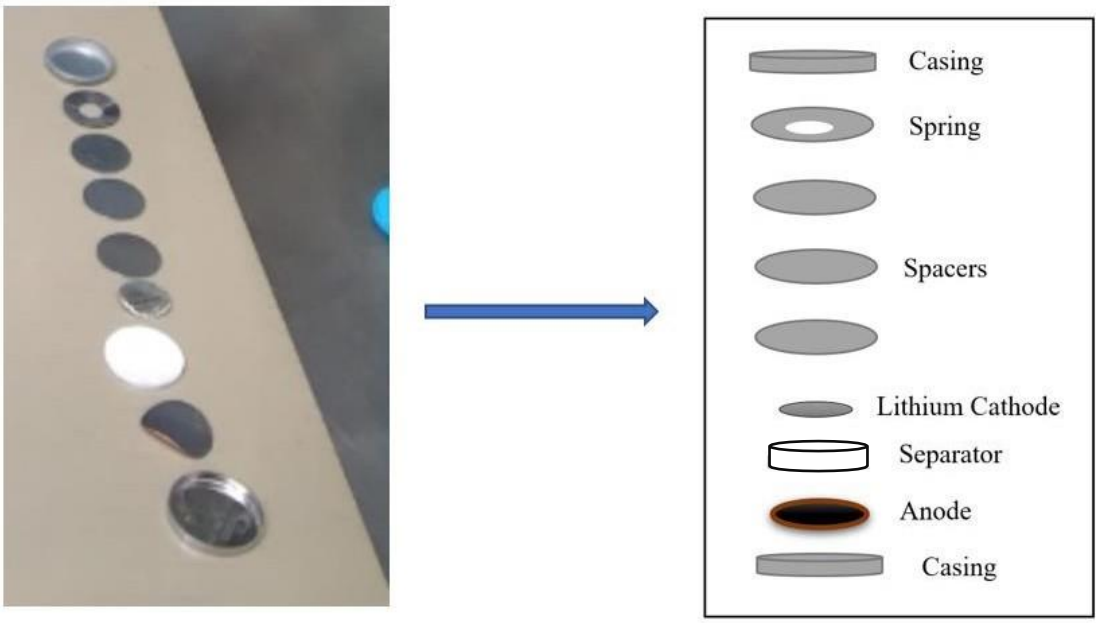

Figure 2-2 - a) Coin cell stack disassembled and arranged in a Glove Box and b) a schematic of coin cell stack arrangement.

2.6 Electrochemical testing

The fundamental electrochemical testing parameters of a coin cell are charge/discharge specific capacities (mAh/g) cycle life, rate performance and voltage profiles.

The specific charge/discharge capacities define the amount of electrical charge the material can deliver per gram of material. Furthermore, the higher the specific capacity of the electrode material, the more lithium ions can bind to the electrode, resulting in a larger storage capacity in the lithium-ion battery (56). Cycle life is defined as the number of cycles (full charge and discharge) a cell can perform before its capacity drops and visibly reduces performance (57). Rate tests provide a quantitative measure of the corrosion rate of a battery material by alternating the applied current over time and this test allows the characterization of the SEI layer (58). While all slurries were prepared at Swansea University, testing was conducted at both Swansea University and Johnson Matthey Technology Centre, Sonning Common.

2.6.1 Galvanostatic Cycling – Cycle Test

Galvanostatic cycling (GC) testing refers to an electrochemical testing technique by which an electrode is cycled against a constant current while immersed in an electrolyte. A current is applied to drive an electrochemical reaction, followed by a reverse current to drive the reverse reaction. This method calculates the total input/output capacities with a specified voltage window over repeated cycle. This is achieved through controlling the current between the working electrode and the counter electrode, measuring linear polarization resistance. Charge and discharge currents are conducted with respect to the mass of the individual anodes and is expressed in mA/g. By also knowing the theoretical capacity of a material, the C-rate can be calculated using *Equation 6.*

$$Active\ mass\ of\ electrode\ (g) \times theoretical\ capacity\ (\frac{mAh}{g}) = 1C(C\ Rate\ )(mAh)$$

Equation 6 – C-rate Equation

For example, 1C is a full discharge in 1 hour and C/10 is a discharge over 10 hours. Several important metrics can be retrieved from this type of testing. Important metrics and diagrams measured by this type of electrochemical testing and are outlined as follows; specific capacity given by mAh/g, which represents the electrode materials electrical storage capacity per gram of material. Coulombic efficiency describes the ratio of discharge capacity after a full charge and the charging capacity of the same cycle (59). Voltage profile curves given by U/I vs, time curve, which represent the Gibbs free energy reaction (60), and clearly represents the upper and lower voltage limits as well as the cycle time. On this time curve, all cycles are easily identifiable and symmetrical charge and discharge stages represent good coulombic efficiency. Cycle life graph is given by Cycle number vs time where 1 cycle represents a full charge and discharge, based on the applied C rate. Long galvanostatic cycling (cycle test) were conducted using BioLogic battery tester, BasyTech battery testing and MACCOR battery tester (MACCOR USA). Although Biologic, BasyTech, and MACCOR battery testing systems are all used for evaluating the performance of batteries, they differ in the way they display results and the features they offer. These systems utilize similar testing principles, including measuring voltage, current, and capacity, but each system has its own preferred methods for displaying and analysing data. MACCOR was the testing equipment available in Johnson Matthey, while BasyTech, Biologic and Astrol were available to test at the laboratory. All tests were carried out at room temperature.

A galvanostatic charge plot, as shown in *Figure 2-3*, is a graphical representation of the capacity of a battery or electrochemical cell as a function of the number of charge-discharge cycles it has undergone. The capacity of a battery or cell refers to the amount of energy it can store or deliver at a given time. The x-axis of a galvanostatic charge plot typically represents the number of charge-discharge cycles, while the y-axis represents the specific capacity of the battery or cell, which is the capacity per unit mass or volume. *Figure 2.3* shows an example of

the types of galvanostatic charge plots that represent the electrochemical performance of a li-ion battery. In this plot, the specific capacity of the battery decreases slightly with increasing number of charge-discharge cycles. This is a common trend in batteries and is due to a variety of factors, including the formation of a solid electrolyte interface (SEI) on the electrodes and the gradual deterioration of the electrodes themselves over time. It is important to note that the specific capacity of a battery or cell can also be affected by other factors, such as the charging and discharging rate, the temperature and humidity of the environment, and the quality of the materials used in the cell.

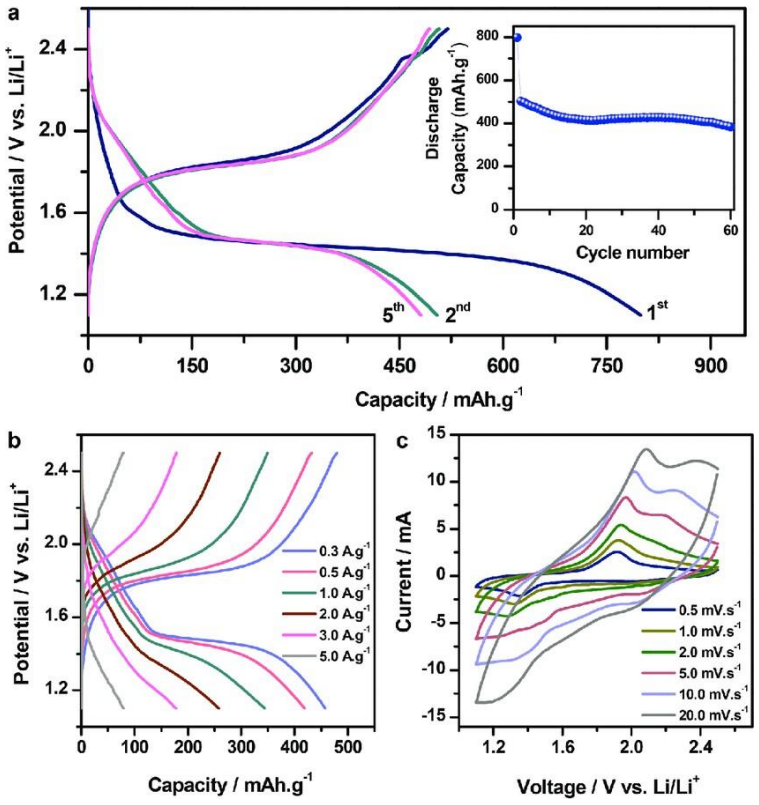

Figure 2-3 - Galvanostatic Plots examples (61)

2.6.2 Rate Test (Waterfall test)

Rate performance testing, also known as waterfall testing, is a type of galvanostatic testing performance and is determined by observing a cell's performance over different current

densities, the battery charging and discharging performance is determined by applying constant charge-discharge ratios, in this case, by applying sequences with a range of different C rates - C/10, C/5, C/2, C, 0.5C, C, for 10 cycles each. By observing the capacity fade every 10 cycles, when applying each C rate, gives an insight of the corrosion rate, long-term stability, and performance degradation of the working electrode, under varying charging and discharging conditions (62).

The cycle life test or battery cycling test is a typical experiment for testing a battery's long-term stability through observing capacity fade (mAh/g) vs cycle number and voltage vs cycle number (63). The cycle number is the time that a battery takes to complete a full charge and discharge cycle. During this test, the battery is charged and discharged at the desired C rate (C/10) and specified voltage window (-0.05 V to 1.0 V) over 100 cycles or until cell failure. This test typically shows a drop in capacity as C rate is increased, as demonstrated in *Figure 2-5.*

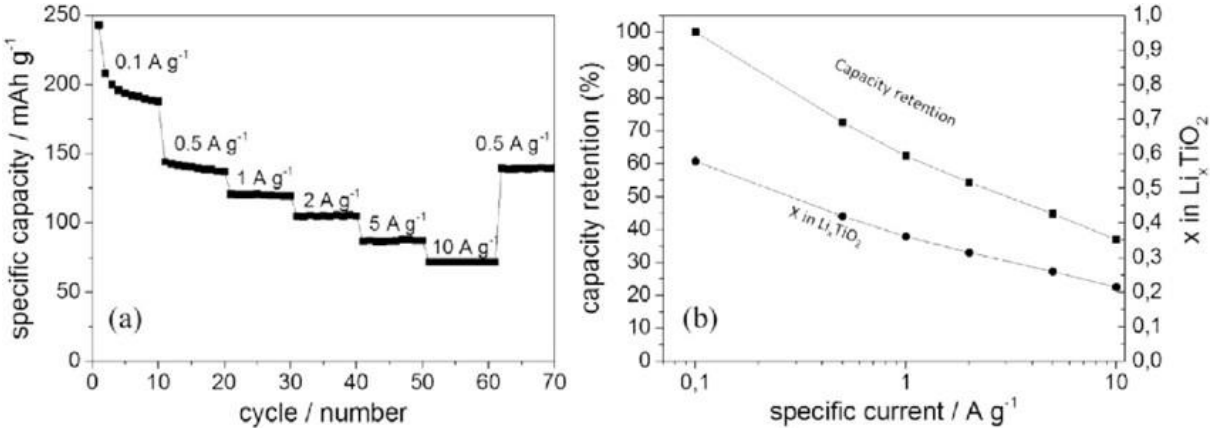

Figure 2-5 - Example of a Lithium-ion battery rate test retrieved from (64).

2.7 Conclusion – Experimental Techniques

In conclusion, this study emphasized the importance of gaining a comprehensive understanding of the experimental techniques and processes involved in battery testing, particularly when formulating with diverse active materials. The extensive learning experience and utilization of

various experimental techniques have provided a solid foundation for obtaining reliable and meaningful results. By mastering these techniques, the necessary tools facilitated the ability to navigate the complexities of battery research and ensure the accuracy and reproducibility of findings.

Chapter 3- Results and Discussion

3.1 Introduction

In this chapter, the design of silicon-carbon composite anodes for lithium-ion batteries is presented, along with an analysis of the electrochemical results obtained from the experimental methods adopted throughout the project. The methodology used in this study included the use of two different silicon-carbon composite materials: Graphite + Silicon Nanoparticles and Nano graphite + Silicon Nanoparticles, which were evaluated and compared in terms of their electrochemical performance against a reference cell composed of Graphite and compared in terms of their fabrication process and overall electrochemical performance. Given the range of powder morphologies, separate studies are required to evaluate the best methods to disperse and deposit materials used within this project. (See *Table 2-2).*

The experimental methods employed in this study include, galvanostatic charge-discharge testing, which were used to evaluate the electrochemical performance of the nanocomposite materials. The data obtained from these tests were then used to compare the performance of the different materials as a potential novel anode material and to identify the factors that contribute to their varying levels of performance.

3.2 Material Characterization and Electrode Fabrication

This section describes the characteristics of the supplied powders in terms of their morphology, crystal structure and particle size using methods described in Chapter 2.2, to ensure that the above characteristics align with the commercial descriptions and in parallel identify discrepancies that may occur.

3.3 Graphite Powder Characterization

Figure 3.1 illustrates STEM-HAADF images of Graphite SFG15 at different scale bars; 200 nm, 50 nm and 2 µm to allow a more detailed picture of the true crystal structure of the graphite form at an atomic level. *Figure (3.1a)* shows a close-up STEM-HAADF image (scale bar 2µm) of bulk graphite (SFG15) in which the graphite flake structure can be observed. It can be observed that the particle is roughly 8 µm, when comparing with the scale bar. The TIMREX-SFG15 data sheet specifies the material has a particle size (D50 of 8.4 micron) meaning that half the particles are under this size, and furthermore smaller particle sizes can be seen in *Figure 3-1 b) and Figure 3-1 c).* In terms of microanalysis, most importantly, the images satisfy the investigation of Graphite particle size that the commercial powder is as expected and can therefore be used with confidence as a reference cell.

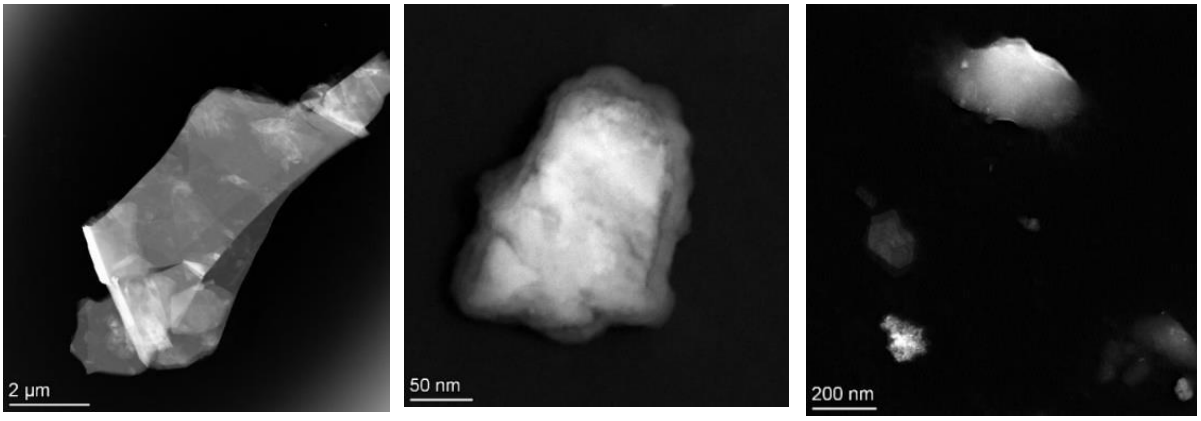

a *b* *c*

Figure 3-1 - 78000 x STEM HAADF image of thin film of Graphite SFG15; b) 310 kx STEM HAADF c) STEM HAADF of Graphite. Images captured by Dr. Yubiao Nui and Doctoral Student Sean Lethbridge.

3.4 Nano Graphite Powder Characterization

The crystal structure and particle size distribution of the untreated Nano graphite powder (30 nm Nano graphite Spheres PiKem) was characterized using transmission electron microscopy (TEM). Figure *3-2* presents three STEM HAADF images of the Nano graphite powder with particle sizes less than 30 nm. *Figure 3-2a)* shows a high-angle annular dark-field (HAADF) STEM image of the untreated Nano graphite powder at 500 nm scale bars, where the crystalline structure of the carbon grains can be observed, which look comparatively smaller to the SFG15 and approximately 30 nm when compared with the 500 nm scale bar. *Figure 3-2 b)* shows an image with a 50 nm scale bar, which again reveals the average particle size distribution of the Nano graphite to be around 15-30 nm, consistent with the description of the particles as being >30 nm in size. *Figure 3-2 c)* shows a magnified micrograph taken at a phase-contrast setting, providing a clearer image of the Nano graphite particle size. The STEM HAADF images reveal consistency within particle size of >30 nm, of the particles in study.

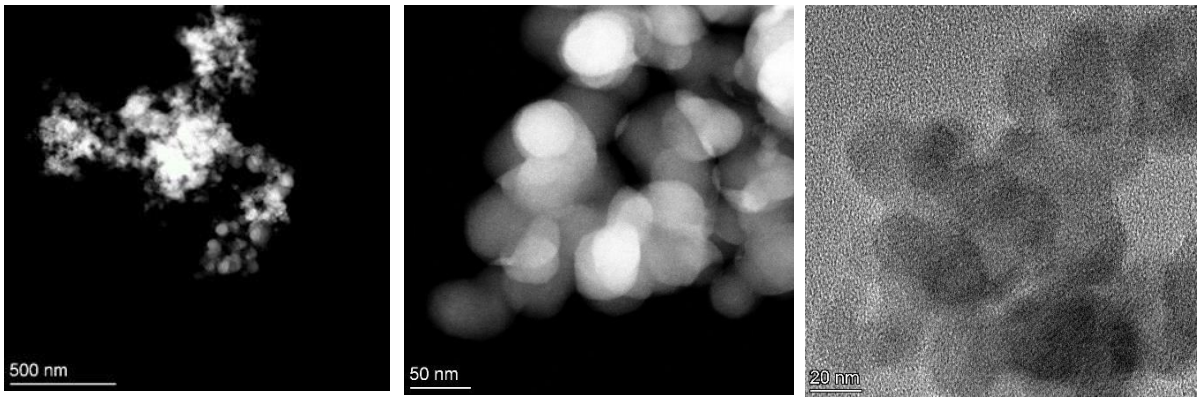

a) b) c)

Figure 3-2 - a) STEM HAADF TEM micrograph of powder form PiKem Nano graphite >30 nanometres, showing the microstructure of the nano graphite nanoflakes b) higher magnification c) higher magnification. Images captured by Dr Yubiao Nui and Doctoral Student Sean Lethbridge.

3.5 Silicon Nanoparticles Powder Characterization

The transmission electron microscope micrographs in *Figure 3-3* provide a detailed examination of the Silicon Nanoparticles (15nm) powder (ACS materials). The image in a) exhibits is compared to a 50nm scale bar, while the image in b) reveals a TEM image of the Silicon Nanoparticles after mixing with Nano graphite. Both images confirm the presence of a clear and even distribution of spherical particles with 15nm diameter.

The EDS image, *Figure 3-3 b)* indicates that the predominant chemical composition of the particles is silicon, with some signs of oxidation present on the outer edges of the particles. However, this oxidation possibly could be attributed to the process of transferring the powder to TEM grids for observation. The EDS images at a magnification, with a scale bar of 20nm reveal the presence of 15 nm spheres of nano-graphite, and furthermore images utilize colour mapping to highlight the presence of carbon (red), silicon (blue), and signs of oxidation (green spots) within the powder (65). While TEM and EDS provide valuable insight into the microstructure and composition of the silicon nanoparticles powder, it is important to note that these techniques do not quantitatively determine the chemical composition. This information is obtained using X-ray Photoelectron Spectroscopy (XPS).

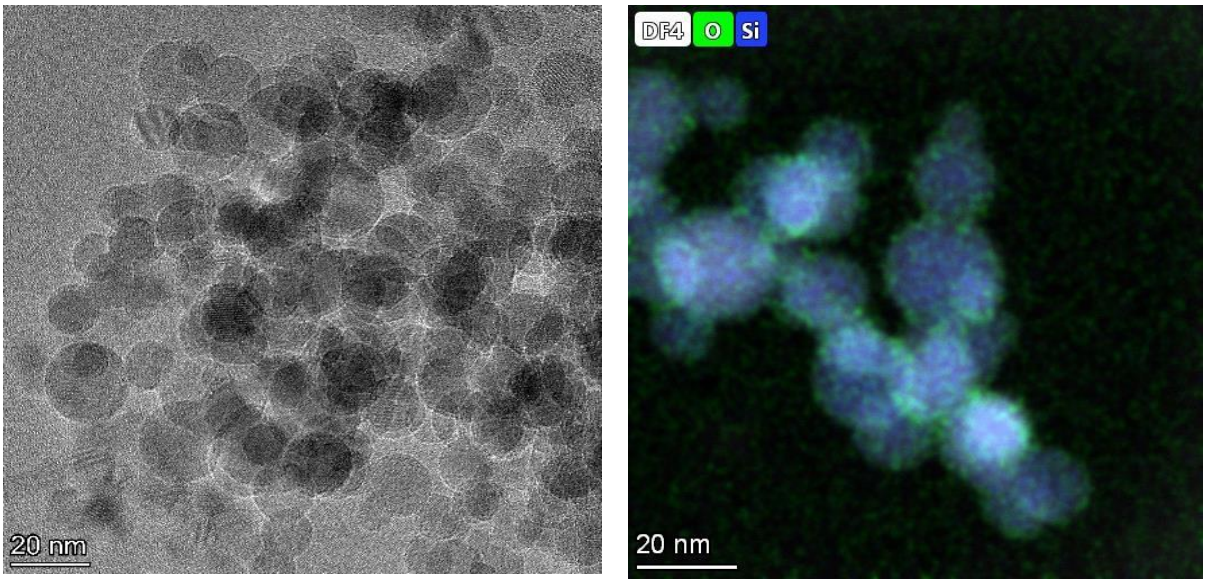

a) b)

Figure 3-3 - a) of Si nanoparticles (20 nm scale bar) b) Si nanoparticles EDX image (20 nm scale bar) (Image captured by Dr. Yubiao Nui).

3.6 Anode Powder Characterization Closure

The STEM HAADF and TEM analyses reveal distinct differences in crystal structure and particle size distribution between graphite, nano graphite, and silicon nanoparticles. Graphite exhibits a expected morphology and particle size, nano graphite has a polycrystalline arrangement of atoms with a flake-like morphology, and silicon nanoparticles display a nano flake structure with a clear and even 15 nm size distribution of particles. Furthermore, each material has an expected chemical composition, particle size and structure. The insights gained from these analyses provide essential information such as the chemical composition and particle size of each material and into the differences in structure and composition of each material, providing confidence in the materials suitability for the project.

3.7 Slurry and Electrode Fabrication

All anodes were prepared by mixing active powders (Graphite, Nano graphite, Graphite + Silicon Nanoparticles, Nano graphite + Silicon Nanoparticles) described in Section 2.3 with carbon black Super-P (conductive material) and Carboxymethyl cellulose (CMC binder). A few coating methods (Section 2.3.2) were trialled for the Graphite reference anode to select the optimum method for ongoing testing. As mentioned in Section 2.3.2, various methods for casting are required due to the varying material characteristics of the materials being compared in this study.

3.8 Graphite Slurry and Electrode Preparation

The Graphite slurry was prepared using the methodology outlined in Section 2.3.

Figure 3.4 illustrates the results of each casting method described in Section 2.3.2 showing the consistent homogenous casting that the Thick Film Coater (b) was able to achieve when compared with the XB-300 Laboratory Bar Coater (a) and Tape Casting (c).

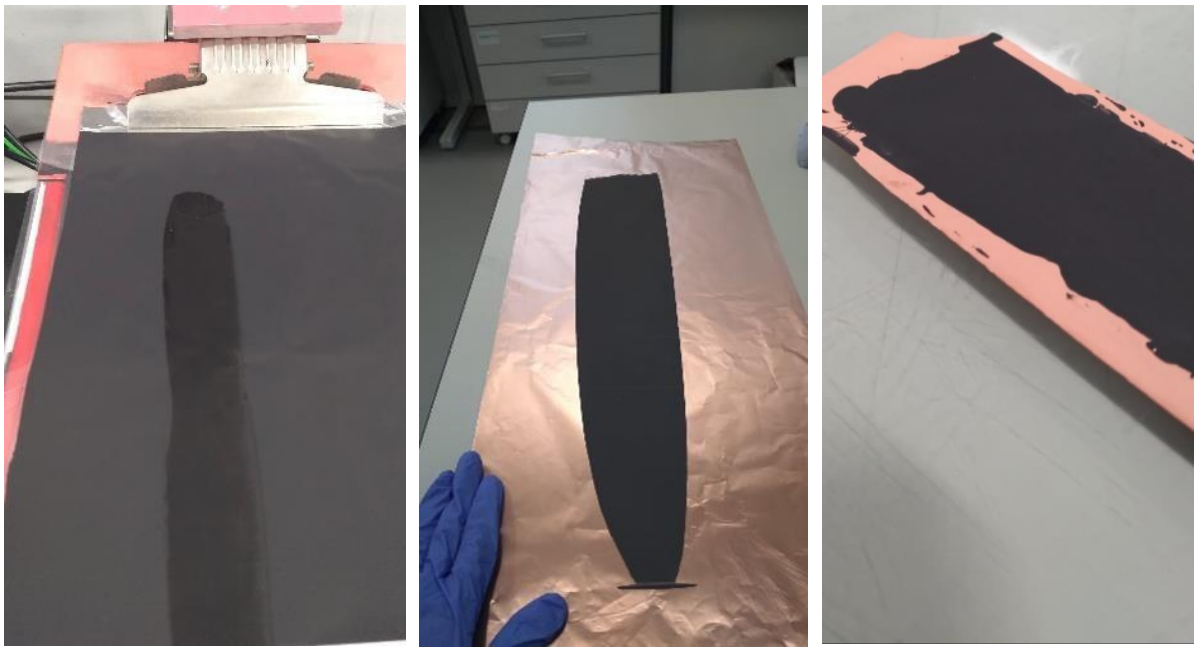

a) b) c)

Figure 3-4 - Casting Method Testing a) Bar Coating, b) Thick Film Casting, c) Tape Casting

After evaluating different methods for preparing the materials, it was found that the film coater method provided the best results in terms of consistency of the slurry casting and reproducibility for each anode type. This is due to the automation features and vacuum platform to hold the substrate taught, as opposed to a manual approach for methods a and c. Therefore, the film coater method was selected as the preferred method and used for the remaining preparation of the materials.

3.9 Nano graphite Slurry and Electrode Preparation

The slurry preparation and casting technique for the Nano graphite electrode followed the procedures described in section 2 but with the incorporation of 15 µl of deionized water added in increments of 5 µl. To achieve a uniform mixture, 10 minutes of mixing was performed after each addition, owing to the challenging nature of working with nanoparticles. The Nano graphite mixture was initially dried at 45°C for 24 hours, but this resulted in cracking of the electrode slurry (as shown in *Figure 3-5a).* The high temperature caused rapid expansion of the electrode, leading to tensile stresses and cracking. By using a lower drying temperature of 35ºC for 48 hours, the likelihood of cracking was reduced because the Nano graphite electrode was able to heat up gradually. This is shown in *Figure 3-5*, which shows an uncracked nano graphite electrode casting after drying. The lower temperature also reduced the overall amount of expansion, which helped to further reduce the risk of thermal cracking. It is important to note that the optimal drying temperature will depend on the specific materials and formulations used in the electrode slurry, as well as the desired properties of the final product. Therefore, it may be necessary to experiment with different temperatures and heating rates to find the optimal conditions for electrode drying, especially when working with novel materials.

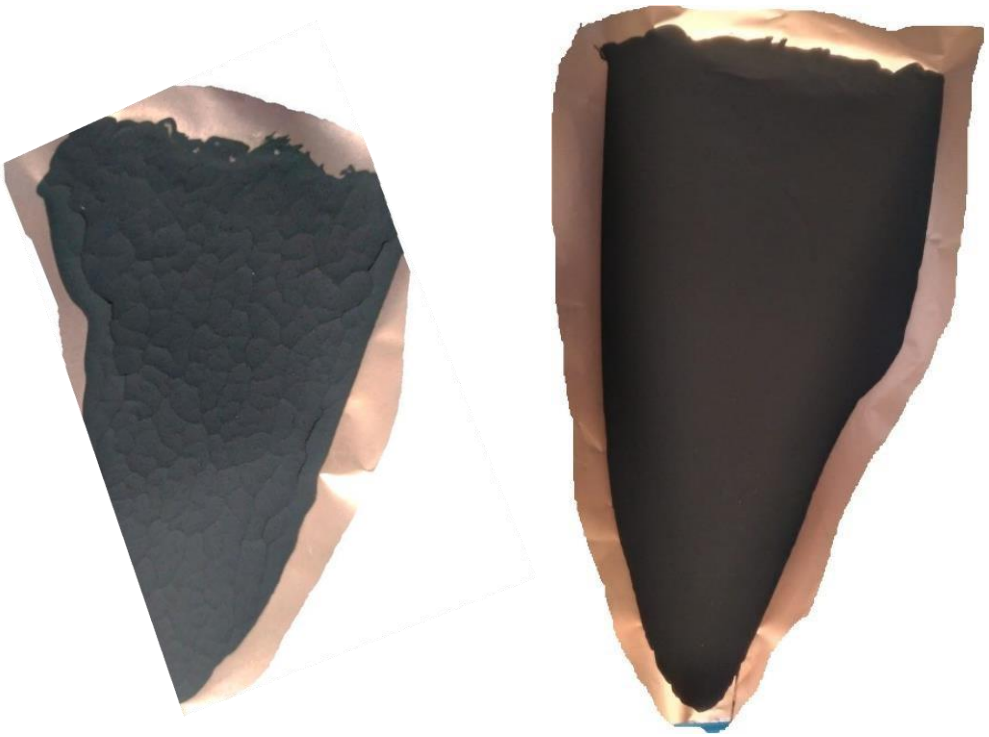

a) b)

Figure 3-5 – Nano graphite dried @ 45°C for 24 hours and b) dried at 35°C for 48 hours.

3.10 Graphite + Silicon Nanoparticles and Nano Graphite + Silicon Nanoparticles Slurry and Electrode Preparation

The slurry preparation, casting, and electrode fabrication of the Graphite + Silicon Nanoparticles was explored using two methods. Firstly, where the graphite and silicon powders were first milled together, and second where the silicon was added to the pre-milled slurry. The challenges of working with novel nano composites proved challenging to smoothly incorporate Silicon nanoparticles within the carbon electrode slurry, in particular slurry mixing and drying. Furthermore, various methods were explored to improve mixing times and homogenous electrode casting. After the method provided a slurry that was challenging to cast, the second

method was then explored. The second method was inspired by a study from *Patil et al.* (66), that explores the fabrication of highly silicon-nano graphite aerogel-based anodes for lithium-ion batteries, where the methodology describes the addition of silicon to a pre milled slurry.

3.10.1 Method 1

Graphite SFG15 + Silicon Nanoparticles electrode was composed of 94 wt% Graphite SFG15 and 6 wt% Silicon nanoparticles as active material. To prepare, 94 mg of carbon and 6 mg of Si nanoparticles were milled in a Fritsch Pulverisette 23 Mini Mill Grinder at 45Hz for 10 mins until adequate mixing was achieved between the powders. The mixture was combined for 10 mins as this was the tested time it took to achieve a homogenous mixture to the eye. A study by Zhou et al. (67) investigated the effects of mixing time on the performance of lithium-ion battery electrodes. They found that the mixing time had a significant impact on the morphology, porosity, and electrochemical properties of the electrode. They also found that the optimal mixing time varied depending on the specific electrode material and slurry formulation. Since this study focused on the comparison of anode materials and not optimal mixing time to improve performance, the key factor when looking at mixing times and frequency was to keep consistency throughout the slurries where possible and furthermore 10 minutes of mixing was sufficient with the reference cell and so this is assumed to be the case with the remaining cells. 10 wt% CMC (carboxymethylcellulose) binder was then added to the mixture along with 10% Super P (TIMCAL) Carbon Black. The mixing process and addition of deionized water was identical to that of the Nano graphite.

3.10.2 Method 2

Method 2 differed from Method 1 in that firstly Graphite (IMERYS), CMC and Carbon Black were combined in the Fritsch Pulverisette 23 Mini Mill Grinder at 45 hertz for 10 minutes until well combined into a wet slurry mixture and the Silicon Nanoparticles (ACS materials) were added to the wet slurry mixture which was then milled using the same method as Nano graphite.

Figure 3-6 illustrates the step-by-step process conducted in Method 2. The electrode preparation and coin cell fabrication followed the identical methodology used for the reference Graphite cell (Section 3.1.2.2) and Nano graphite (Section 3.1.2.3) and both methods were used and electrochemically tested in coin cells.

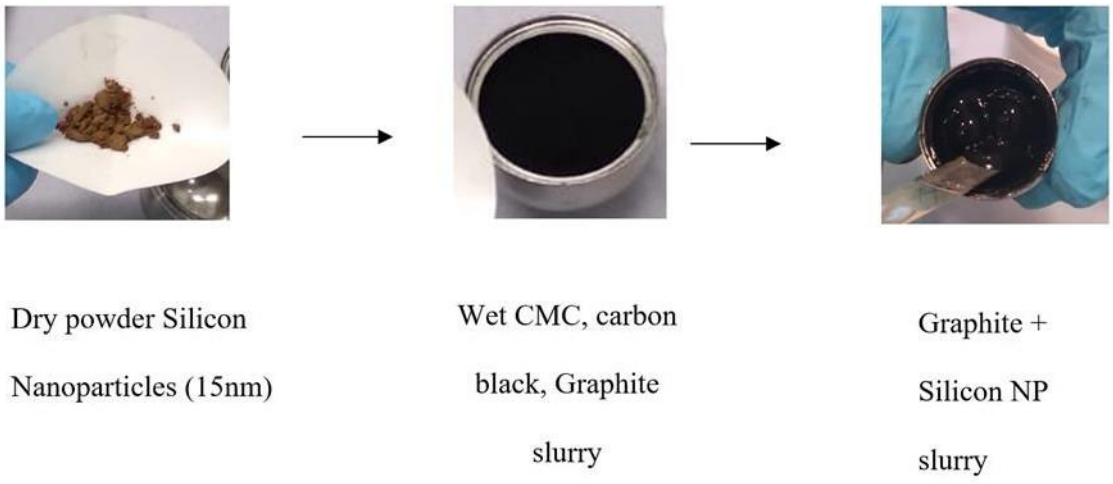

Figure 3-6 - Step by Step Process of the Graphite + Silicon and Nano graphite + Silicon slurry preparation - Method 2

3.11 Slurry Preparation Closure

In conclusion, the preparation and fabrication of various electrode materials, (Graphite, Nano graphite, Graphite + Silicon Nanoparticles and Nano graphite + Silicon Nanoparticles), require different methods due to their particle size, surface area, and nature of nanomaterials. While the Thick Film Coater was found to be the best method for Graphite slurry, the Nano graphite electrode still experienced stability issues such as cracking during drying. To mitigate these issues, a lower drying temperature of 35°C for 48 hours was found to be effective. However, it is important to note that the optimal drying temperature will depend on the specific materials and formulations used in the electrode slurry, as well as the desired properties of the final product.

In conclusion, the preparation of electrode slurries is a critical step in the fabrication of lithium-ion batteries. It is important to recognize that different carbon morphologies require different preparation methods due to differences in particle size, surface area, and nature of nanomaterials. As highlighted in this study, the drying process can lead to issues such as cracking and delamination, especially for nanomaterials. The challenges of slurry preparation are compounded by the fact that different anode materials require different preparation methods, making it difficult to develop a one-size-fits-all approach. The results of this study demonstrate some difficulties with methodology of fabricating a silicon carbon nanocomposite. Furthermore, the importance of investigating the characteristics of electrode slurries, including layer stability and the identification of materials within the electrodes, to provide insight into the dispersion of the slurry. To improve the electrode slurry preparation step in the future, it is recommended to thoroughly characterize materials prior to the slurry preparation step, to optimize the drying and mixing process to avoid cracking and delamination, material investigation and iterative testing.

3.12 Electrode Characterization

The parameters analysed included the surface morphology, pore size, and the presence of cracks and scratches, which can impact the electrode's performance. The stability of the electrode layer was also evaluated, as well as the dispersion of the slurry, to ensure consistent electrode quality. Additionally, the presence of silicon within the Graphite + Silicon Nanoparticles and Nano graphite + Silicon Nanoparticles electrodes was investigated.

Scanning electron microscopy (SEM) was used to analyse the surface morphology, composition, and microstructure of the graphite electrode material as deposited onto Cu foil after formation of the electrode with the methodology of this described in Chapter 2. XPS was used to characterize the chemical composition of the electrodes.

3.13 Graphite + Silicon Nanoparticles Electrode SEM image Comparison

Figure 3-7 [redacted] presents an SEM image of the Graphite electrode compared with the Graphite + Silicon Nanoparticles electrode (fabrication method described in *3.10*) before cycling, both showing high surface area of Graphite flakes bonded with CMC in a stacked arrangement. The electrode SEM microphase of both images look similar with the presence after the addition of silicon nanoparticles unable to be identified on the surface morphology of the electrode, which could be concluded to the small particle size and significant size difference of the graphite flakes and silicon nanoparticles. As this is a surface morphology analysis, this type of characterization may not have picked up the presence of the small silicon nanoparticles.

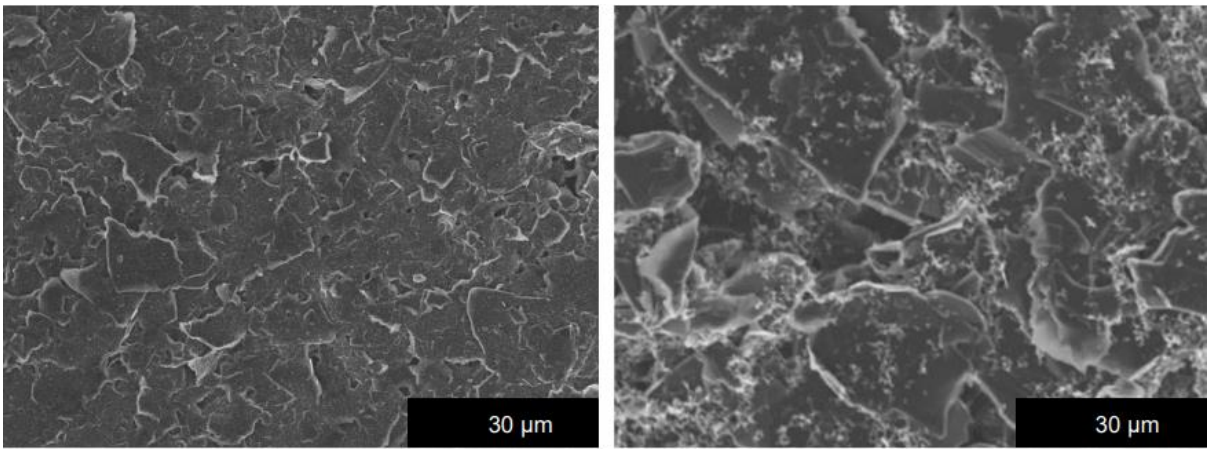

(a) (b)

Figure 3-7 - SEM micrograph of graphite anode showing 5-15 nm particle sizing (a) and b) Graphite electrode at higher magnification showing the laminar structure of the graphite electrodes. Images Captured by Doctoral student Dan Gillard at Swansea University.

3.14 Nano Graphite + Silicon Nanoparticles Electrode SEMimage comparison

Figure 3-9 show a micrograph of the Nano graphite electrode. The image clearly shows the presence of thermal cracking, which is further highlighted in *Figure 3.9b,* where an enlarged micrograph is presented with thermal cracking after drying the electrode at 45ºC, prominently displayed in the top left corner, as indicated by the red line. The SEM analysis provides valuable insights into the structural properties of the Nano graphite electrode and the effects of thermal treatment on its integrity. This highlights small scale discrete mechanism of electrode cracking as opposed to microcracks, giving an insight into the nano graphite electrode layer and its stability. *Figure 3.9b* (Nano graphite electrode) and *Figure 3.9c* present a comparison of the nano graphite micrograph before and after the addition of silicon respectively. Much like *Figure 3.8,* the presence of silicon within the Nano graphite + Silicon Nanoparticles electrode cannot be visually identified from the images. Both micrographs reveal a microstructure that is less porous in comparison to Graphite + Silicon Nanoparticles micrographs. Additionally, the presence of small <30 nm carbon "flakes" can also be observed. The absence of large graphitic flakes and well-bonded microstructure seen in the SEM images can be considered as positive indicators of a good electrode performance, which was found in a study by Li et al. (68), where it was found that well-bonded graphene coatings with small flakes and few defects resulted in improved electrochemical performance compared to coatings with larger flakes and more defects. They attributed this to the increased surface area and improved electronic conductivity of the well-bonded coatings (69).

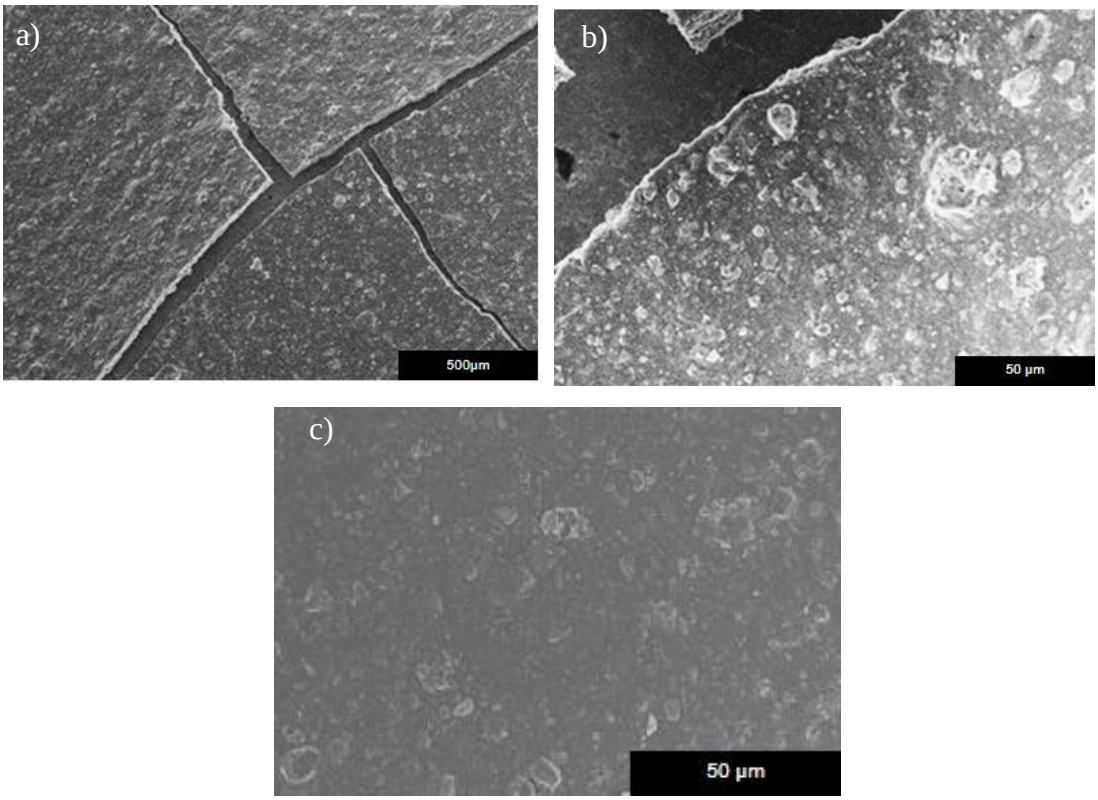

Figure 3-9 - a) Nano Graphite electrode micrograph exhibiting thermal cracking after drying at 45°C b) higher maginification and c) micrograph of Nano Graphite + Silicon Nanoparticles eletcrode for comparison to show pre and post silicon nanoparticle addtion. Images captured by Doctoral Student Dan Gillard at Swansea Universtiy.

3.15 X-ray Photoelectron Spectroscopy (XPS)

X-ray photoelectron spectroscopy (XPS) was employed to conduct a surface analysis of the chemical composition of the interphase on the electrodes. Furthermore, XPS is used in this study to determine the chemical composition of the electrode surfaces studying the elemental composition of the Graphite and Nano graphite electrodes after the addition of 6% silicon nanoparticles and understanding weather the expected chemical composition is what is present in the electrodes. The XPS is also used in this study as a tool to identify information on surface reactions and identify any impurities that may be present and consequently affecting the electrode performance and stability (70).

For graphite, the XPS spectrum typically shows a characteristic peak at around 284 eV corresponding to the C 1s energy level. This peak can be deconvoluted into different components corresponding to different chemical environments of carbon atoms in graphite, such as sp2-hybridized carbon atoms in graphene layers, sp3-hybridized carbon atoms in amorphous carbon, or carbon atoms bonded to other elements such as oxygen or nitrogen (71). The XPS chart is presented in *Figure 3-10*, with the XPS results from the MACS described in Chapter4

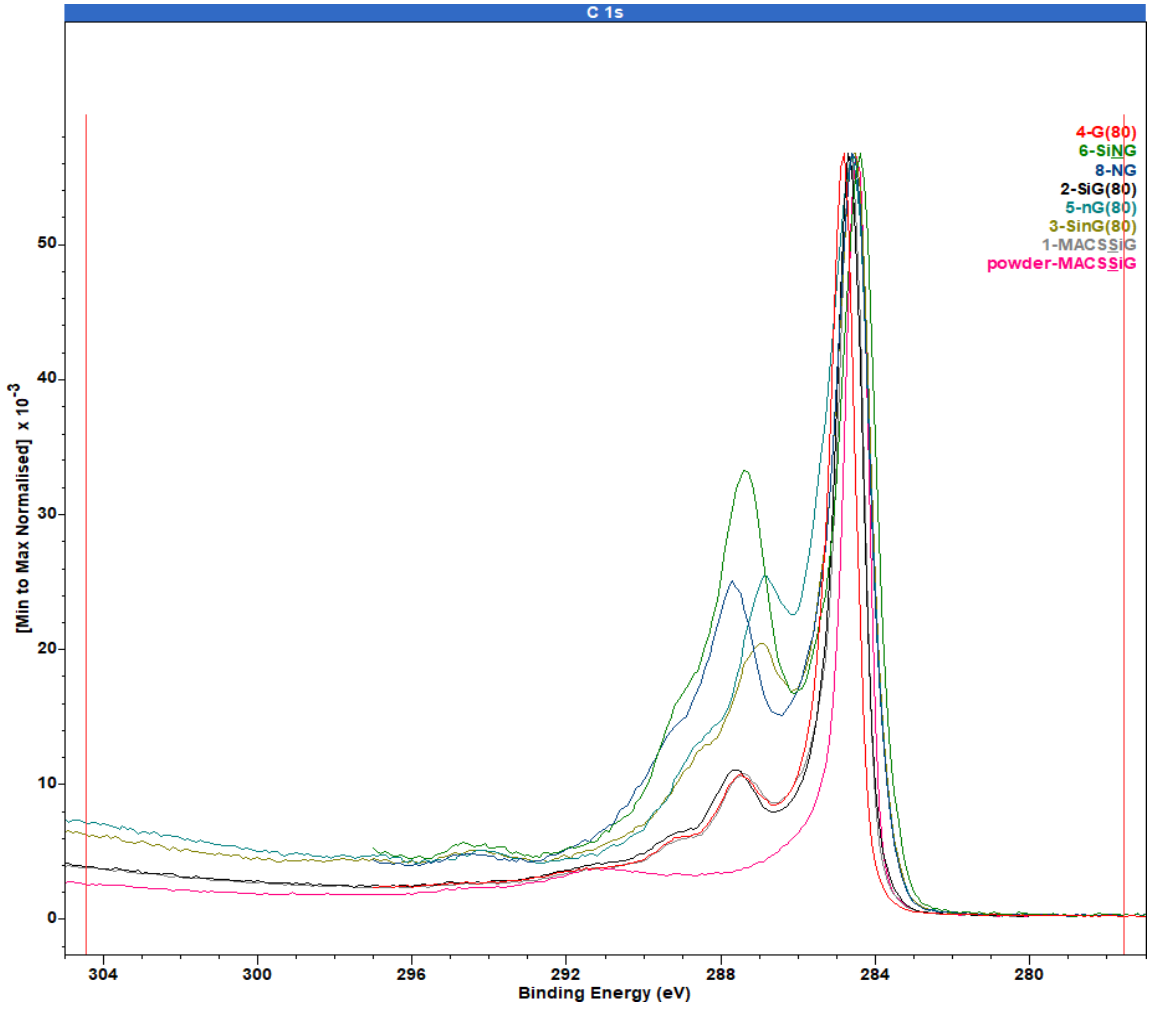

Figure 3-10 - XPS Graph of Electrodes: Graphite (G) (red), Nano graphite (NG) (blue) Graphite + silicon nanoparticles (G + SiNP)(black) nano graphite + silicon nanoparticles (NG + SiNP) (green and gold). Discussed in Chapter 4: MACS Graphite + silicon (grey) and MACS Graphite + Silicon clusters (pink) – Graph and XPS analysis prepared by Dr James Mcgettrick at Swansea University.

Table 3-1 presents the average XPS stoichiometric results of the four anode types that are being compared within this study (see Table 0-2, Appendix for full results). The XPS interaction volume is approximately 10nm limited by the inelastic mean free path (IMFP) of the electrons. Graphite (G) is highlighted in pink, Nano graphite (NG) is highlighted in yellow. Graphite + Silicon Nanoparticles is highlighted in green and Nano graphite + Silicon Nanoparticles is highlighted in blue. The electrodes were fabricated with 80 wt.% active material, 10 wt.% CMC binder, and 10 wt.% Timrex® SuperP 45.

These results indicate that the pre-cycling graphite electrode exhibits an average of 83% carbon, with 0.16% silicon, which is assumed to be an impurity. XPS analysis of graphite typically shows only carbon signals, as graphite is composed of carbon atoms arranged in a hexagonal lattice. Silicon, on the other hand, is a distinct element and would not be naturally present in graphite in XPS analysis unless intentionally added or deposited (72) (73) (74).

The interaction volume is approximately 10nm. Both Graphite and Graphite + Silicon Nanoparticles electrodes demonstrate an expected 80% carbon composition, which forms the bulk of the active material. The elemental composition of these active materials does not reveal any unexpected impurities. However, the anticipated 6% composition of Silicon Nanoparticles in the Nano graphite electrode averages at 2.1%. This discrepancy could be attributed to several factors. Firstly, the size difference between graphite and silicon nanoparticles could lead to under-detection of the smaller silicon particles by the XPS technique, resulting in an underestimation of the actual silicon content (71). Secondly, the assumption that carbon is graphitized, as this material is labelled as nano-graphite, may not always be accurate, leading to potential inaccuracies in the silicon content estimation (72; 64). Thirdly, if the silicon nanoparticles are not uniformly distributed on the surface of the graphite particles, XPS may not detect all the silicon atoms present, leading to an underestimation of the silicon content (73). Lastly, surface contamination with other elements or compounds could interfere with the XPS analysis and lead to an incorrect measurement of the silicon content. The XPS penetrates to approximately 10 nm, so it may be passing through the thin layers of silicon. However, it is also possible that silicon may not be present in the material and further investigation is needed to confirm its presence or absence. The chemical composition of the Nano graphite electrode shows a lower-than-expected ratio of 80% active material, confirms the negligible presence of impurities on the surface of the Nano graphite electrode. The chemical composition of the Nano graphite + Silicon nanoparticles electrode indicate an average carbon composition of 63.3%,

silicon composition of 3.3%, with a maximum of 5.3% and a minimum of 2.4%. This suggests an uneven distribution of Silicon within each electrode. The Carbon composition, at an average of 62.7%, is consistent, however the similarity between a lower Carbon content than expected in both XPS analysis involving Nano graphite, suggests that the small 30 nm carbon particles may not be accurately detected by the XPS.

Table 3-1 - XPS Stoichiometry table for Electrodes.

Sample Identifier	Al 2p component %	C 1s %	Cl 2p %	Cu 2p1/2 %	Cu 2p3/2 %	Fe 2p %	Na 1s %	O 1s %	Si 2p %
G	0	83.7	0	0	0	0.5	1.8	13.2	0.2
NG	1.3	69.3	0	0.01	0.02	0.2	1.7	25.4	2
Gr+NSi	0	81.25	0	0	0	0	1.7	14.9	2.1
NGr +NSi	0.7	63.3	0.4	0.04	0.07	1.3	0.2	30.3	5.3

3.16 Characterization Closure

The electrode characterization and comparison of Graphite and Nano Graphite electrodes before and after the addition of silicon do not show any obvious changes or presence of Silicon nanoparticles.

The XPS analysis highlights, with the range of chemical compositions, with the remaining cell compositions found in the Appendix, the challenges in ensuring consistency across coin cell samples due to various manual mechanical tasks and the potential for human error and inconsistencies across these tasks. Therefore, it may be difficult to accurately compare active materials as other uncontrollable factors may also be present. Moreover, it is important to carefully consider the experimental conditions and data analysis methods when performing XPS analysis to accurately determine the elemental composition of the electrodes, confirming why this technique alone is not adequate and is therefore done in parallel with SEM and TEM

to verify the particle size and distribution in the sample, which may help explain any discrepancies observed in the XPS analysis.

3.17 Electrochemical Testing Results and Discussion

The electrochemical performance of the electrodes was evaluated in a half coin cell configuration, using lithium metal as the counter electrode and graphite or graphite/silicon nano/composites as the working electrode. This section will discuss the results and comparison of the electrochemical performance of the Graphite, Nano graphite, Graphite + Silicon and Nano graphite + Silicon Nanoparticles, with the main goal of identifying the effects of silicon addition to both Graphite and Nano graphite and if it solves issues such as silicon's concomitant volume expansion and subsequent rapid capacity loss seen in many studies outlined in Chapter 1.

The results presented below represent the best outcomes achieved for each cell type. However, it is important to note that the results were quite diverse, and a significant number of cells failed during testing. In such cases, additional information, and data pertaining to remaining cells are included in the appendix for reference. To provide further context, *Table A.1* in the appendix lists all coin cells manufactured for testing, including details of the testing location and whether they passed or failed. The decision to conduct tests at both sites was based on experience and to utilize the MACCOR electrochemical testing software. Cell electrochemical performance was evaluated through galvanostatic charge/discharge cycling at a fixed voltage window of -0.05 V to 1.00 V versus lithium and altering current rates every 10 cycles starting at C/20, C/10, C/5, C/2, C, 2C, C (see Chapter 2). The cycle life test results for each anode are presented in this section using the cycle life testing methodology as described in Chapter 2. All cells were cycled at a constant current of C/10.

3.18 Graphite (Reference Cell) Electrochemical Results

The following section presents the electrochemical results for the graphite datum cell and was tested in a half coin cell formation, using both rate testing and cycle life testing.

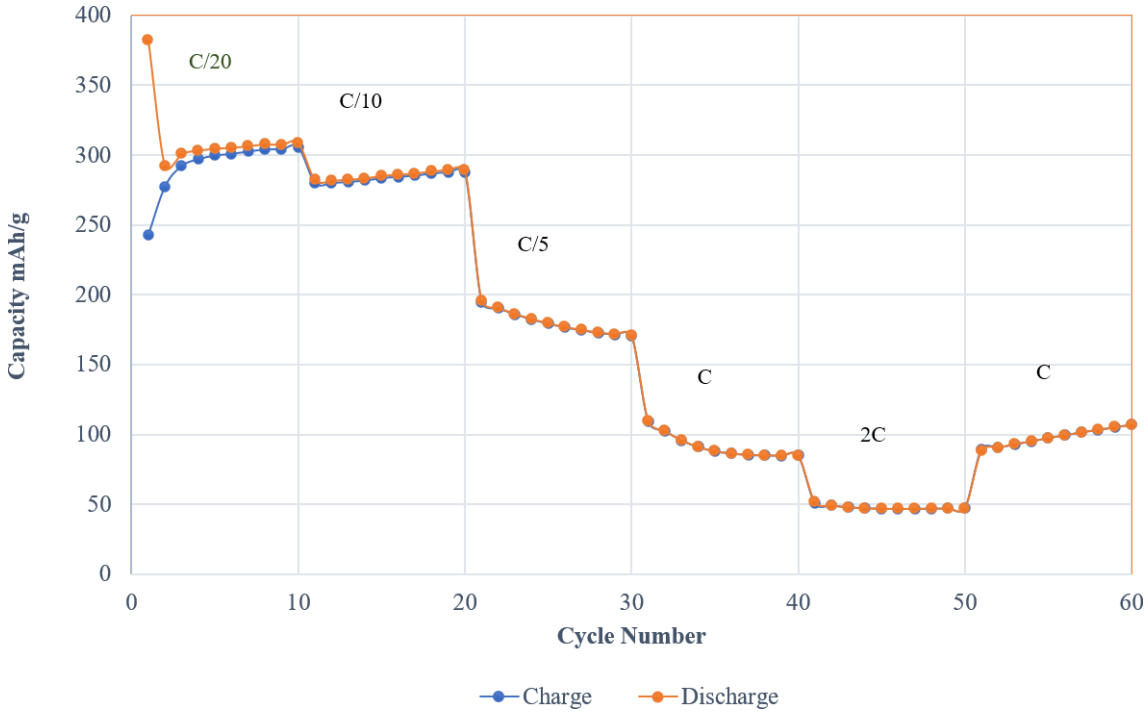

Figure 3-11 - Graphite Rate Test Capacity vs Cycle Number (C represents C-rate). The cell is tested at different charge rates to test cell retention and degradation under varying charge and discharge conditions.

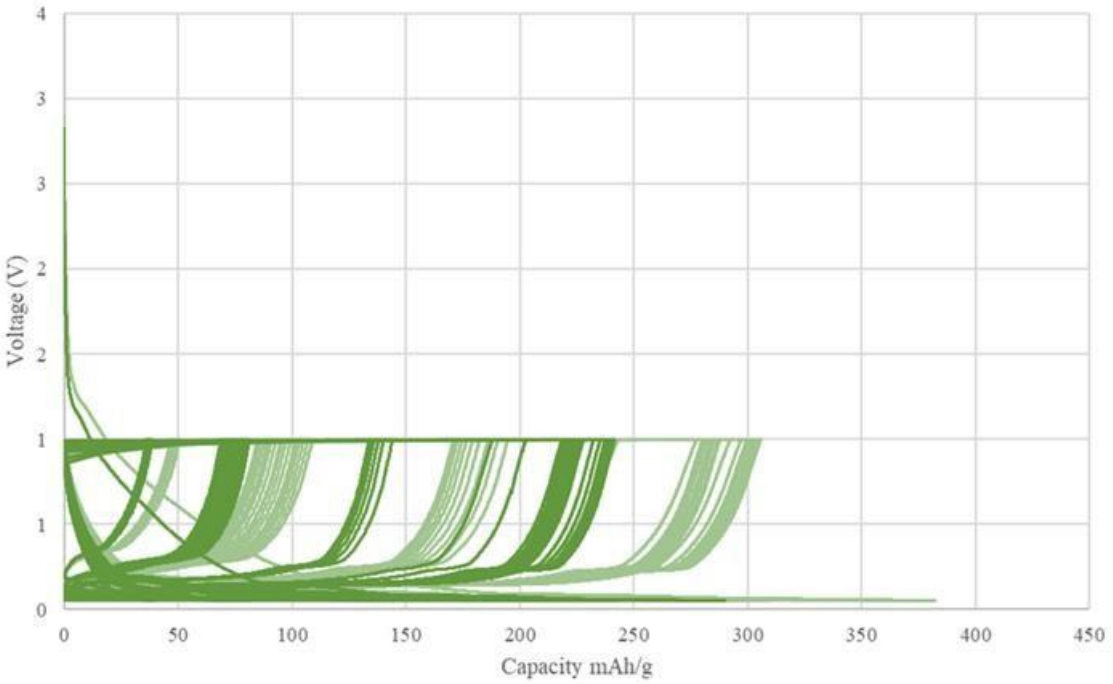

Figure 3-12 - Graphite Rate Test Voltage Vs Capacity

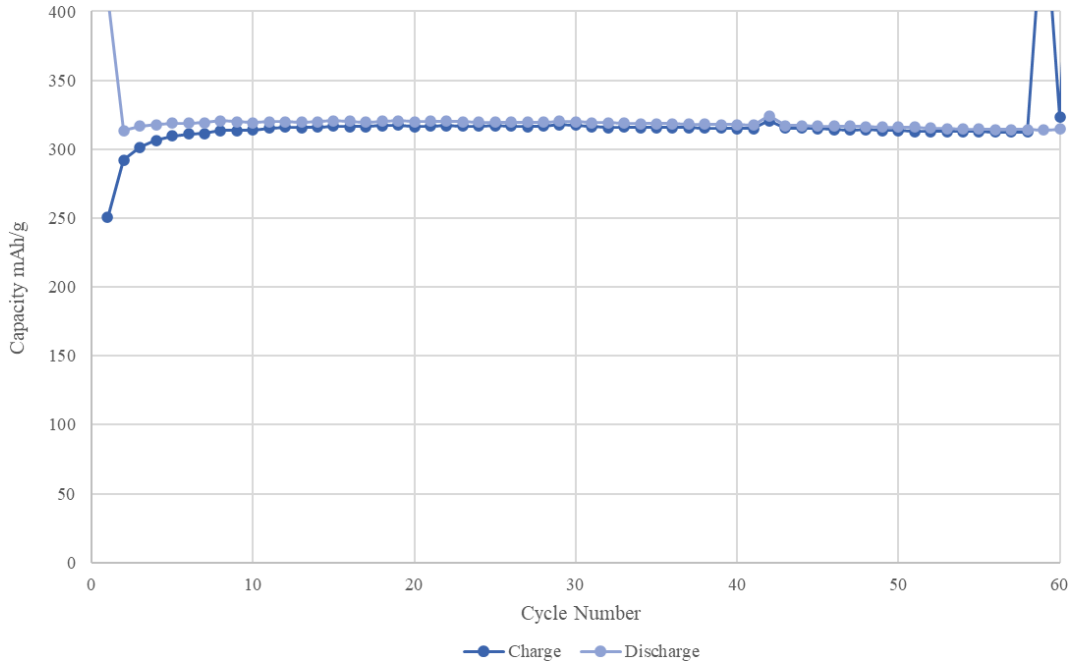

Figure 3-13 - Graphite Cycle Life Test (C/10) – Capacity Vs Cycle Number at constant C-rate of C/10.

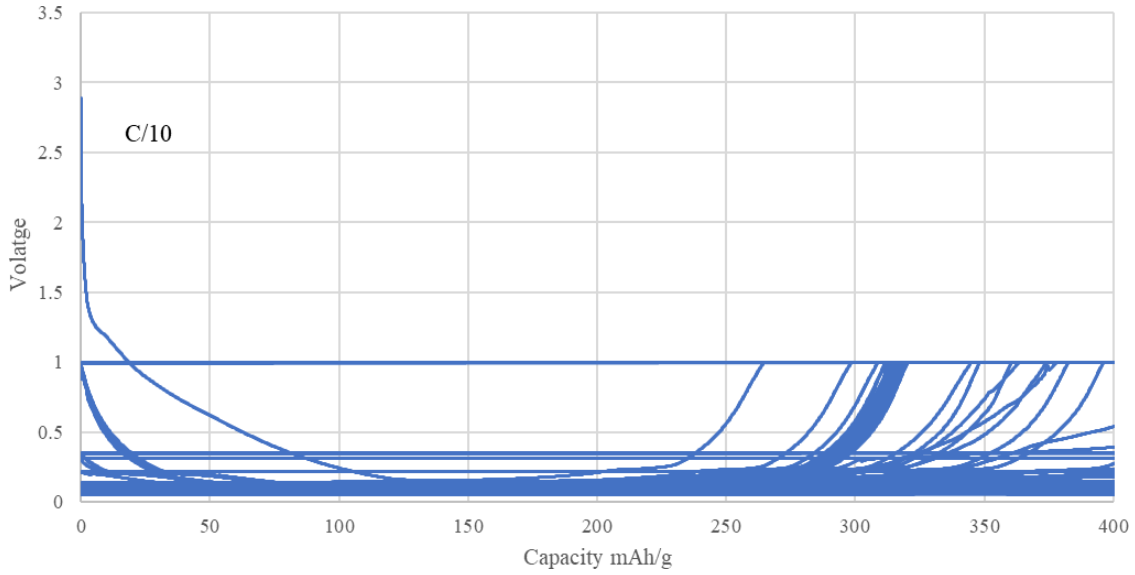

Figure 3-14 - Graphite Cycle Life Test – Voltage Vs Capacity

The performance of the Graphite Cell used as a datum cell demonstrated consistent and reproducible results. A total of 12 datum cells were made and tested however only 4 cells produced usable results. Ideally, a set of 5 consistent results would be preferred. In the rate test shown in *Figure 3-11* at C/20, an initial capacity of 387 mAh/g was observed, which decreased to 300 mAh/g after the first cycle. As known the capacity loss in the first cycle is attributed to the formation of the solid-electrolyte interphase layer (41). The capacity retention at 2C discharge/charge rate, after 30 cycles, was found to be 91%. The overall retention rate from C/20 to 1C, after 60 cycles, was approximately 30%. The voltage profile of the Graphite electrode was investigated in the voltage window of 0.05-1.00V, and the results shown in *Figure 3-12. and Figure 3-14. Figure 3-13* presents a cycle life test and the voltage profile from this data, showing a consistent discharge capacity of >300 mAh/g and capacity retention rate of 100% after 60 cycles. The voltage profile exhibits a stable cycling cell. These results align well with existing literature (75) (76) notably study by Fu et al., (77) where a comparable initial reversible capacity of 350 mAh/g and 86% retention after 500 cycles was reported. The graphite cell demonstrated the best performance among the tested cells, while the appendix

provides additional insights, including some variations due to methodology experimentation. These findings instil confidence in the coin cell fabrication methodology and establish the graphite cell as a reliable reference for future studies in this field. Overall, this section successfully achieved its objective of establishing a robust datum cell and methodology for slurry and coin cell fabrication, providing a satisfactory comparison for the varying anode types for electrochemical testing.

3.19 Nano Graphite Electrochemical Results

The following section presents the electrochemical results and discussion of the Nano graphite anode cells to see the effects on electrochemical performance when using Nano graphite as opposed to graphite, which were tested in a half coin cell formation, using both rate testing and cycle life testing.

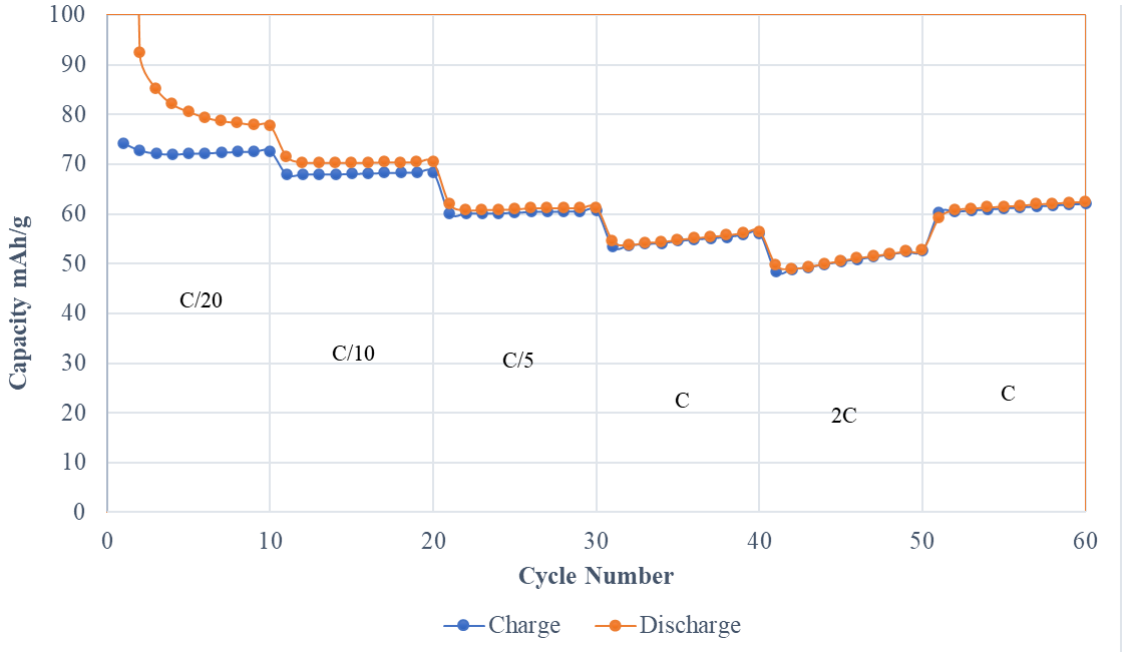

Figure 3-15 Nano graphite Rate Test – Capacity Vs Cycle Number (C represents C-rate). The cell is tested at different charge rates to test cell retention and degradation under varying charge and discharge conditions.

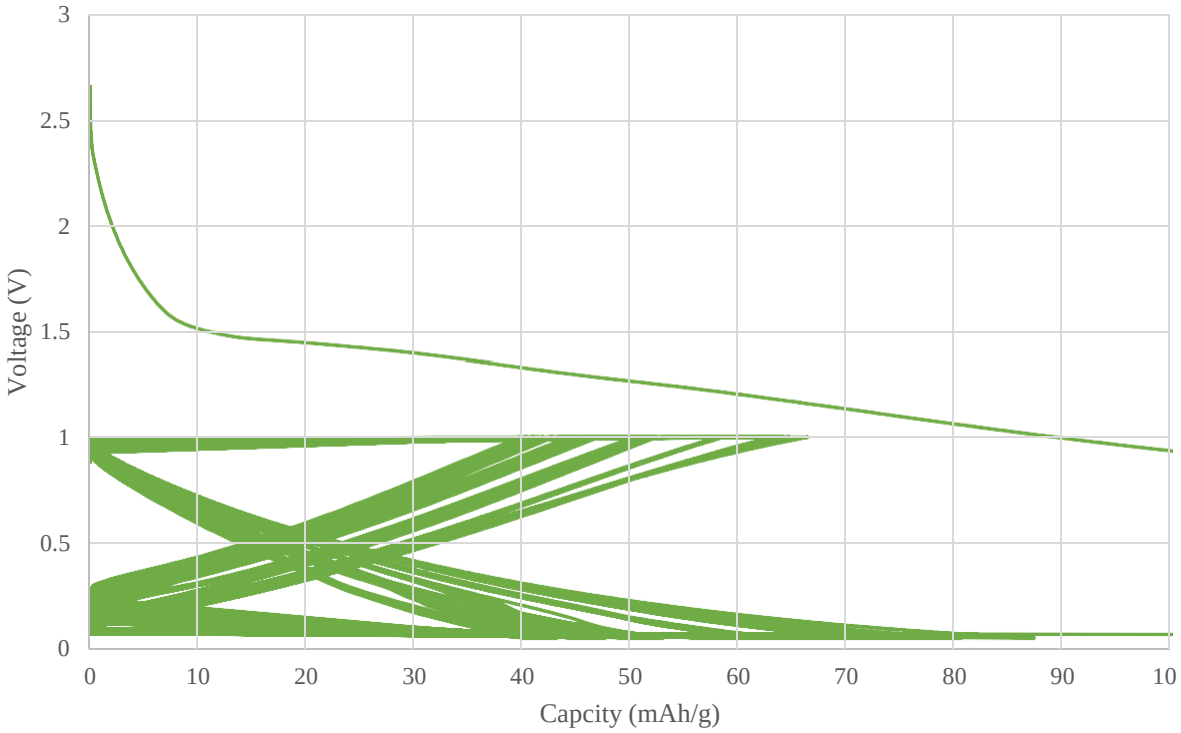

Figure 3-16 – Nano graphite Rate Test Results Voltage Vs Capacity at a constant C-rate of C/10.

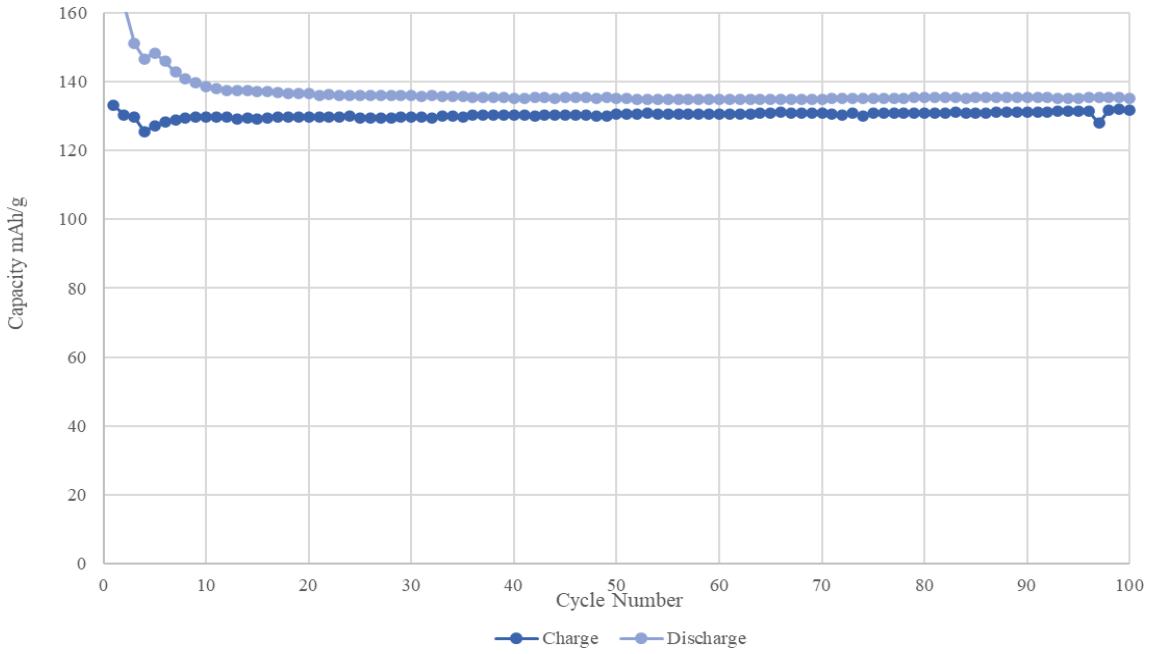

Figure 3-17 – Nano graphite Cycle Life Test – Capacity Vs Cycle Number at a constant C-rate of C/10.

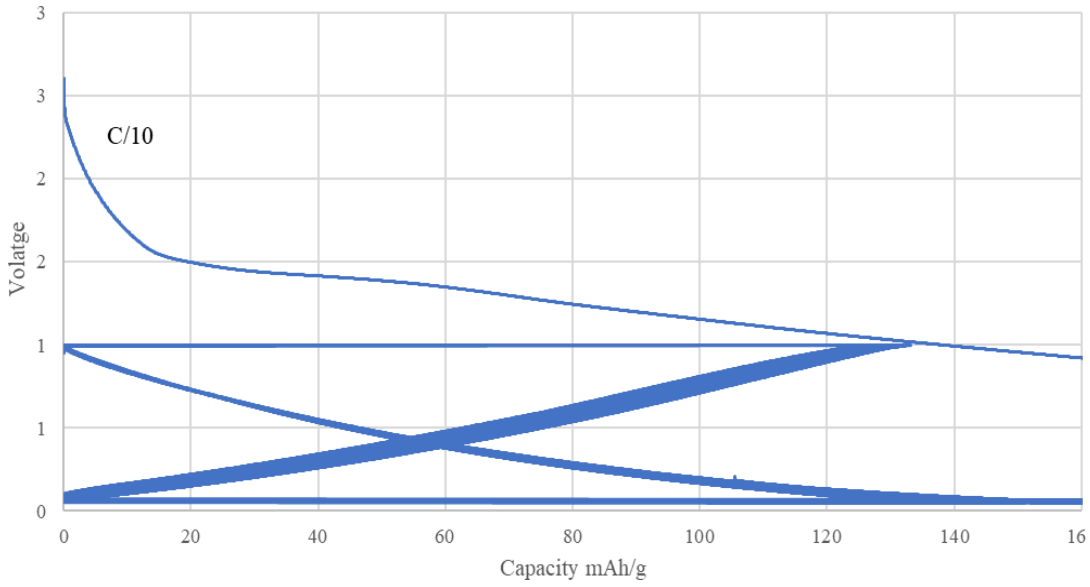

Figure 3-18 – Nano graphite Cycle Life Test – Voltage Vs Capacity at a constant C-rate of C/10,

The results obtained from the nano graphite cell testing were varied, with some anomalous results and consistently low capacities across most cells. The discharge capacity over the first cycle of the rate test is 91 mAh/g, with a capacity retention rate from cell 30 to 60 of 109% and an overall retention rate of 66%. The specific capacity is four times lower capacity than the datum cell. In the cycle life test, an initial discharge capacity of 150 mAh/g and a final discharge capacity of 135 $mAhg^{-1}$ giving a retention rate of 90% after 100 cycles. There could be several reasons for a higher retention rate and lower capacity than particle size and morphology of the nano graphite cell, due to its smaller particle size can offer a unique morphology as shown in the SEM micrograph of the nano graphite powder (*Figure 3-2)* and nano graphite electrode *(Figure 3-3),* with a hierarchical architecture which can offer improved electrochemical kinetics, and furthermore higher capacity retention but a lower specific capacity (78). The observed low specific capacity rate can be attributed to inherent properties of the material rather than significant process issues, as the only variable under consideration is the active material itself. It has also been found that poor performance is at times observed with nano graphite anodes and can suffer significant capacity fade and limited cycling stability

due to formation of an unstable solid-electrolyte interphase (SEI) layer (79) . Furthermore, the nano graphite material proved to be challenging to work with, with issues arising in the casting and slurry stage of the manufacturing process, such as thermal cracking, as shown in *Figure 3-5* with the anode layer delaminating from the copper foil, and the SEM image *(Figure 3-9).* Overall, our results suggest that nano graphite may not perform as well as other materials in battery applications and further research is necessary to better understand its limitations and overcome the challenges associated with working with this material.

3.20 Graphite + Silicon Nanoparticles Cell ElectrochemicalResults

The following section presents the Graphite + Silicon nanoparticles anode electrochemical results to see the effects on electrochemical performance of a graphite anode after the addition of silicon nanoparticles which were tested in a half coin cell formation, using both rate testing and cycle life testing.

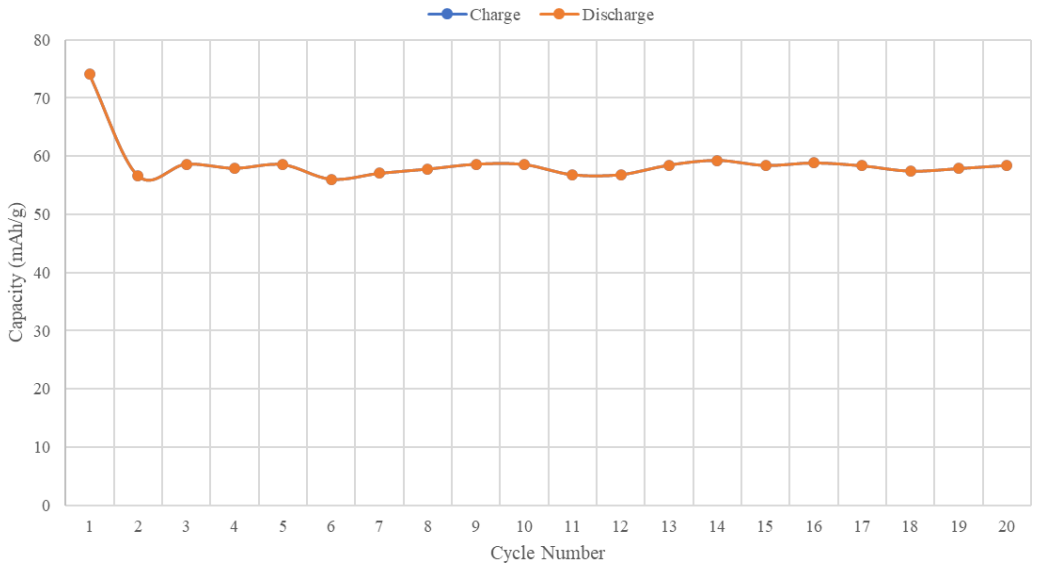

Figure 3-19 - Graphite + Silicon Cycle Life Test, Capacity Vs Cycle Number at a constant C-rate of C/10.

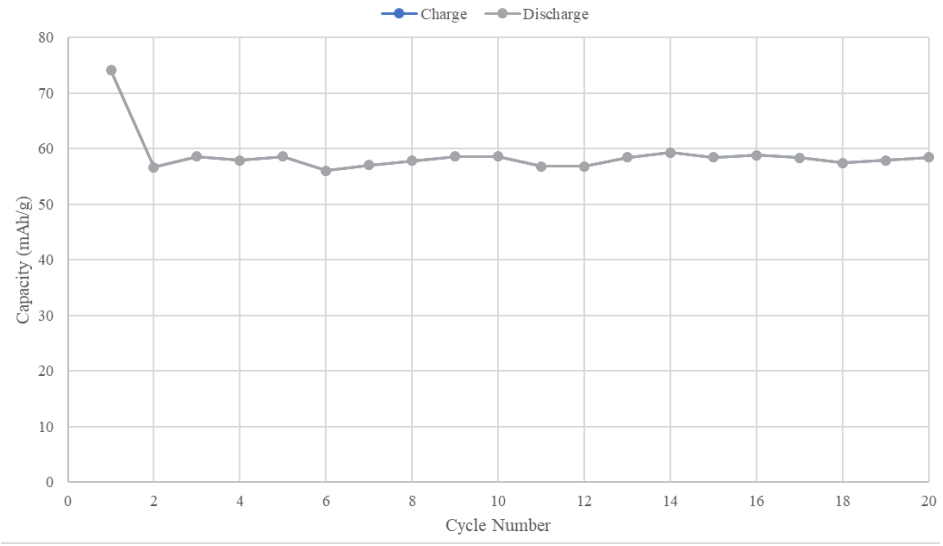

Figure 3-20 - Graphite Cycle Life Test (2) – Capacity Vs Cycle Number Constant C-rate of C/10.

The three Graphite + Silicon Nanoparticles cells that were tested using a rate test setting all experience cell failure after cycle one. The Graphite + Silicon Nanoparticles cycle life tests 1 and 2 exhibited an initial discharge capacity of 75mAh/g, approximately four times lower than the datum cell as presented in *Figure 3-19 and Figure 3-20*. After cycle one and formation of the SEI layer, capacity dropped to 57 mAh/g with a final capacity at cycle 20 and a capacity

retention rate of 100%. Both cells failed after cycle 20, which is significantly premature when compared to the graphite datum cell and nano graphite cells, which failed at cell 60 and 100 respectively. There was no gradual capacity loss but a catastrophic failure. Graphite can be a tough framework for loading (80), and often undergoes a complex process when building graphite silicon composites and the electrochemical results may reflect that the simplistic mixing approach when fabricating the Graphite + silicon nanocomposite may not suffice. Based on the results, the addition of Silicon nanoparticles has extremely hindered the cell performance. Previous studies have encountered challenges associated with addition of silicon to graphite anodes due to the volume expansion of silicon which can cause cycling stability and poor electrical conductivity of silicon which can reduce the overall electrical conductivity of the electrode and result in higher resistance to electron transfer (81) (82). However, it is worth acknowledging the limitations of an electrochemical study, limited comparison literature and the complexity of the parameters that could have played a role in the end results. The SEM images in *Figure 3-9a* and *Figure 3-9b* do not show any significant difference in the morphology of the electrode before and after the addition of the silicon nanoparticles.

Furthermore, the observed results emphasize the importance of carefully considering the impact of active material additions on cell performance and highlight the need for further optimization to achieve desirable outcomes.

3.21 Nano Graphite + Silicon Nanoparticles Rate TestResults

The following graphs, *Figure 3-21, and Figure 3-22*, show the rate test and voltage profile results of the nano graphite + silicon nanoparticles to examine the effects of the addition of silicon nanoparticles on the electrochemical performance of the anodes which were tested in a half coin cell formation, using both rate testing and cycle life testing.

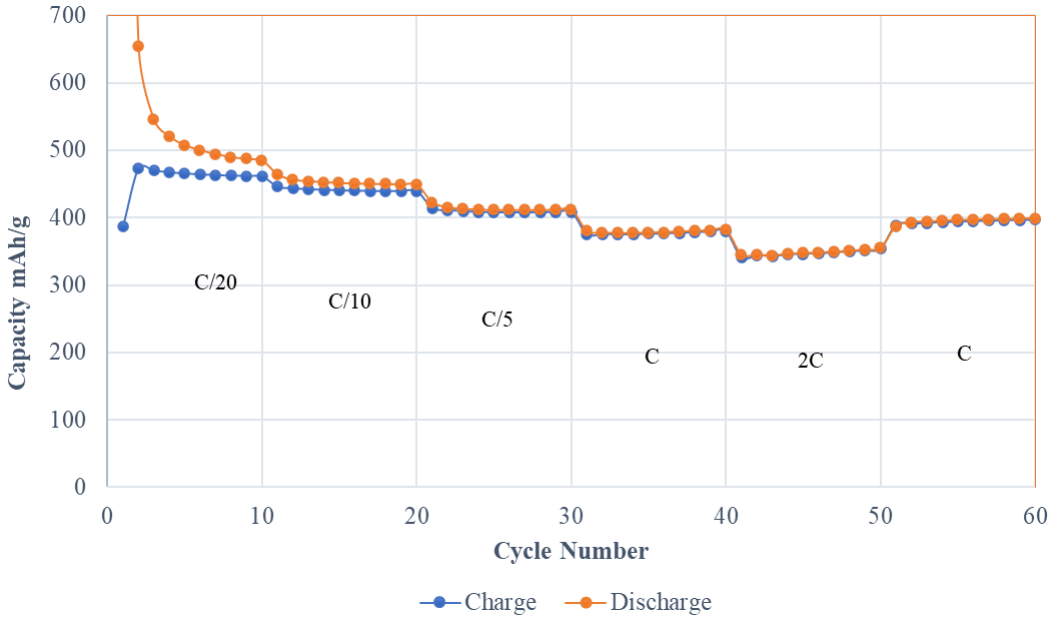

Figure 3-21 – Nano graphite + Silicon Nanoparticles Rate Test – Capacity Vs Cycle Number (C standsfor C-rate). The cell is tested at different charge rates to test cell retention and degradation under varying charge and discharge conditions.

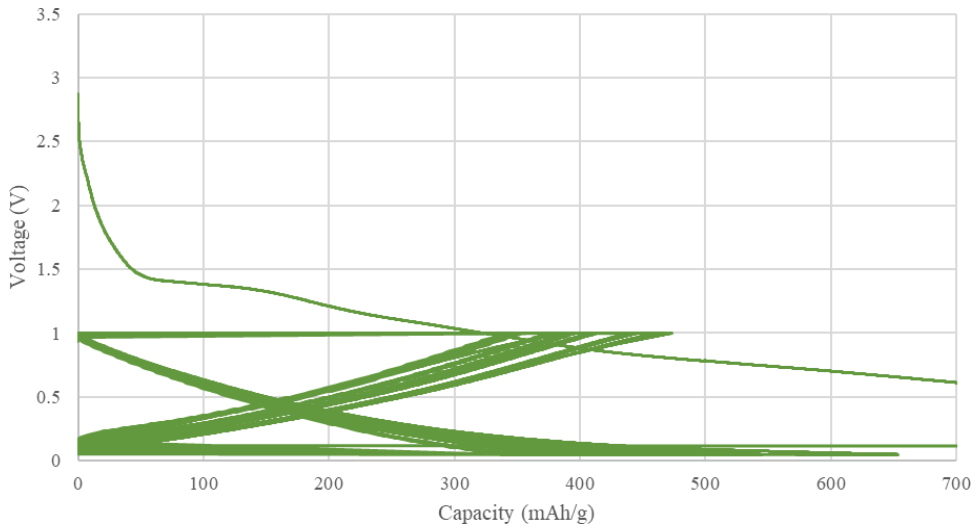

Figure 3-22 – Nano graphite + Silicon Nanoparticles Rate Test Voltage Vs Capacity at constantC-rate of C/10.

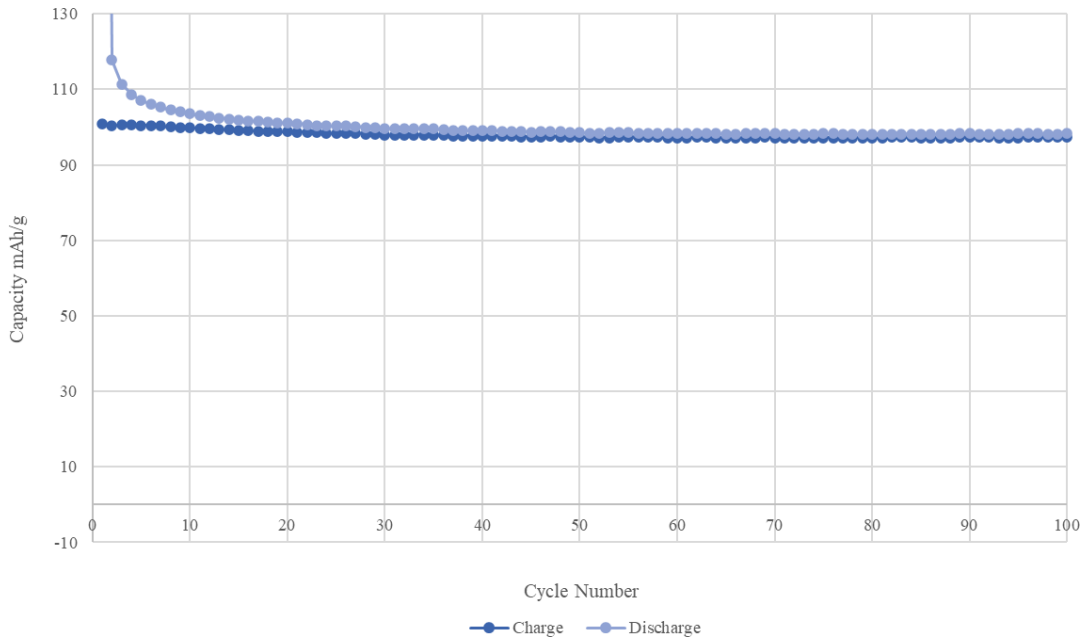

Figure 3-23 -Nano Graphite + Silicon Nanoparticles Cycle Life Test Capacity Vs Cycle Number at constant C-rate of C/10.

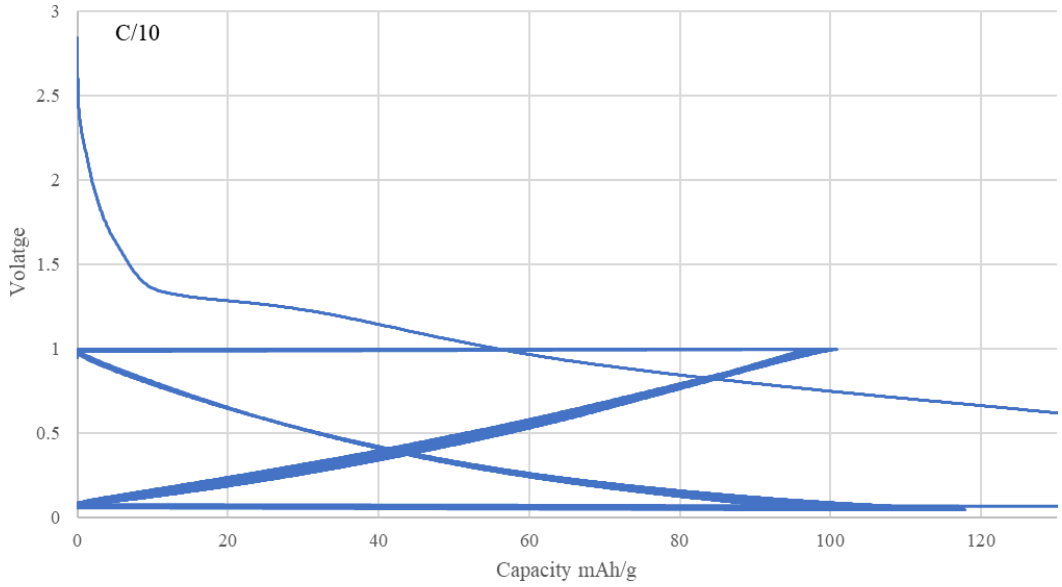

Figure 3.24 – Nano Graphite + Silicon Nanoparticles Cycle Life Test Capacity Vs Voltage at constant C-rate ofC/10.

The electrochemical rate testing of Nano Graphite + Silicon composite cell, shown in *Figure 3-21* exhibits an initial discharge capacity of 680 mAh/g dropping to 550 mAh/g at cycle 2 at C/20. Cycling from 1C for 10, 2C for 10 and 1C for 10, the cell experienced a good capacity retention of 102% and an overall capacity retention of 60%, for 60 cycles.

The cycle life test of another cell shown in *Figure 3-23*, however, has a much lower capacity of 118 mAh/g and a capacity retention of 80%. *Figure 3-24* and *Figure 3-22* exhibit the voltage profiles of the cells cycled between the voltage window of -0.05 V and 1 V. The Nano Graphite + Silicon Nanoparticles cell performs excellently when compared to the datum cell and Nano Graphite cell in the first-rate test, however, the results overall were inconsistent, with the cell undergoing the cycle life tests performing >50% of the specific capacity of the datum cell. These results strongly suggest that further research is needed to refine the manufacturing process and optimize the material properties as poorly fabricated slurry and anodes were a result of issues at the casting stage as described in Graphite + Silicon Nanoparticles and Nano graphite + Silicon Nanoparticles Slurry and Electrode Preparation. As seen in the nano graphite fabrication process, the inconsistent results could possibly be a result of the challenges faced at the process stage. The SEM images displayed in *Figure 3-25*, show the nano graphite + silicon nanoparticles electrode micrograph after before a) and after b) c), 60 cycles. Pores in the surface structure of the electrode can be seen as well as a loss in structure all together which could explain the capacity loss. Despite these challenges, the nano graphite-silicon composite material shows potential as a good material for battery applications, and further research could help to refine the manufacturing process and address the challenges associated with working with this material.

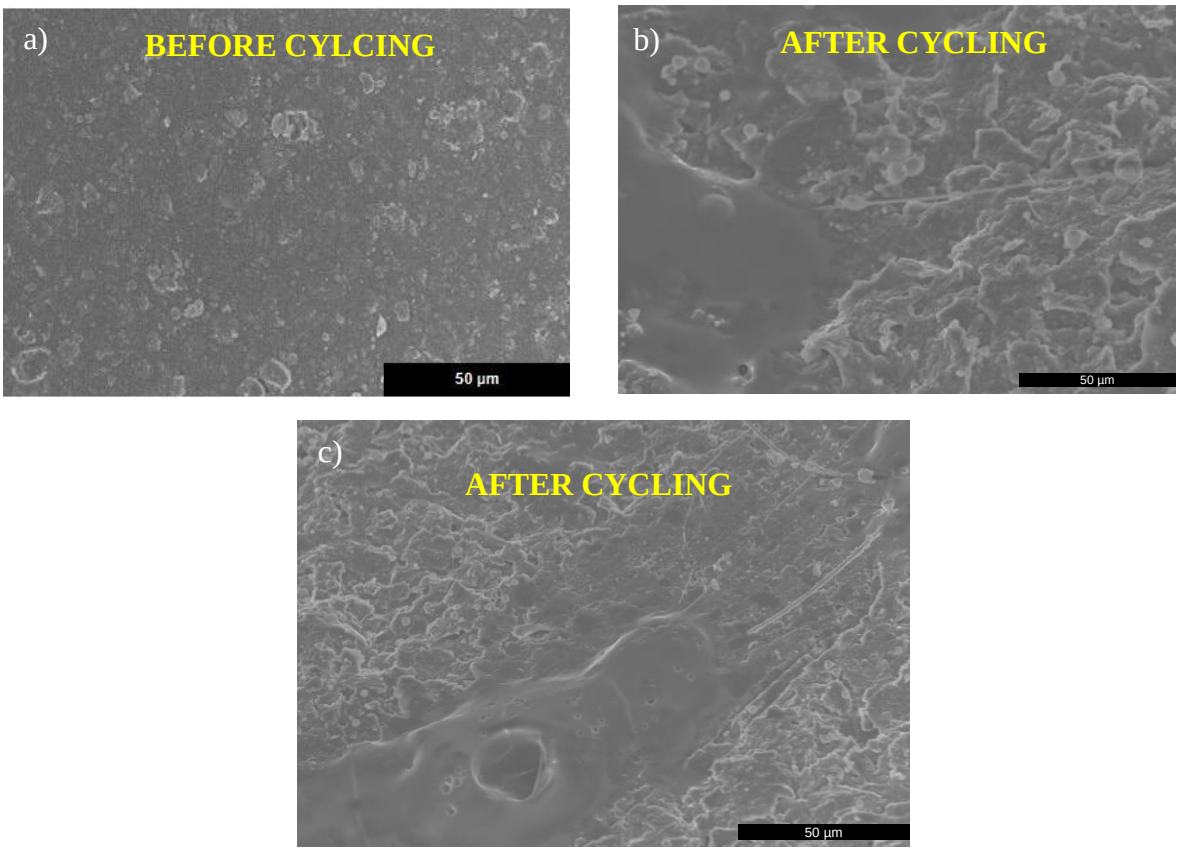

Figure 3-25- SEM images of a) Nano graphite + silicon electrodes before 60 cycles b) after 60 cycles and c) after 60 cycles showing porous and degraded surface. Images captured by Doctoral student Dan Gillard at Swansea University.

3.22 Anode Type Electrochemical Results Comparison

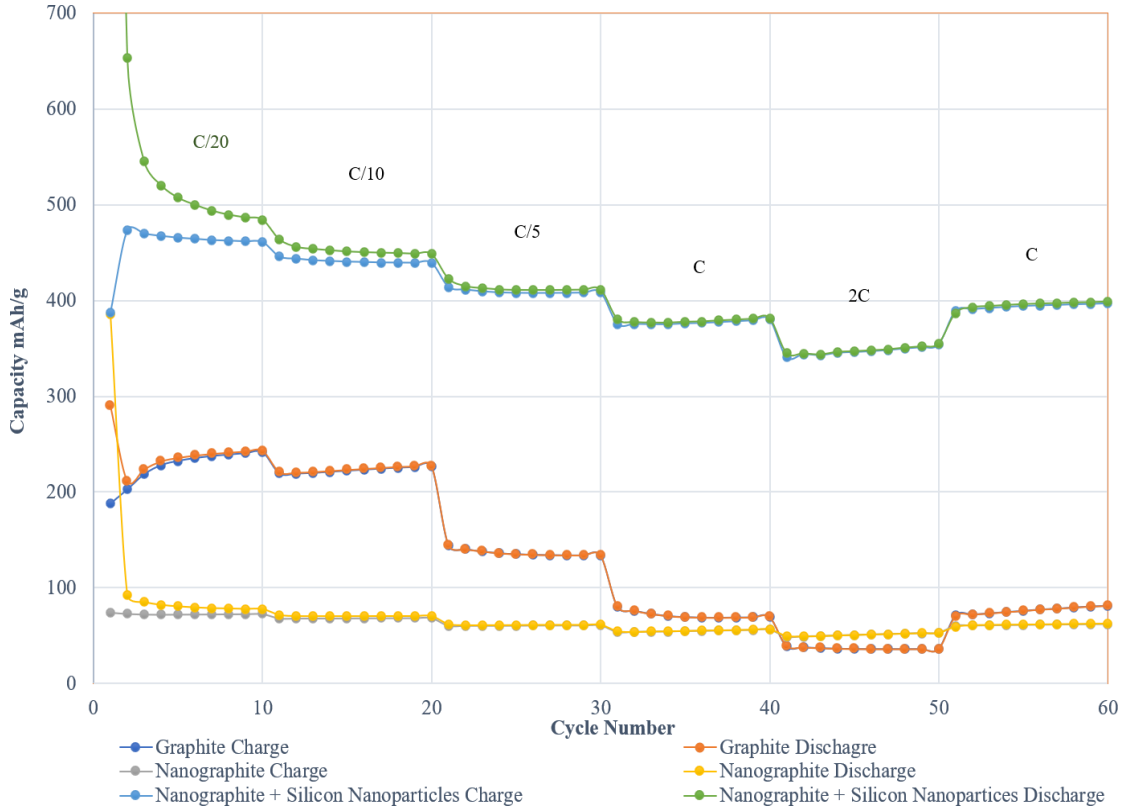

Figure 3-26 – Anode Type Comparison Graph using the Rate Test Results comparing the best performing cell from each anode variation.

Figure 3-26 presents a comparative analysis of rate tests conducted on three different anode types: Graphite, Nano Graphite, and Nano Graphite + Silicon nanoparticles. It is worth noting that the rate test cell incorporating the Graphite + Silicon nanoparticles failed, resulting in the absence of usable data.

The electrochemical results demonstrate that Nano graphite + silicon nanoparticles exhibit the highest capacity among the tested anode types. Additionally, the rate retention, which represents the ratio of initial capacity to final capacity, is relatively high for the Nano graphite + Silicon nanoparticles, as indicated by the flat shape of the corresponding graph. The flatter the graph, the higher the rate retention.

3.23 Electrochemical Testing Results Closure

In this study, four different types of cells were tested and compared, using the composite fabrication methods other than the MACS approach, of which are described in Chapter 3: graphite, nano graphite, Graphite + Silicon Nanoparticles, and Nano Graphite + Silicon Nanoparticles composites. The results were varied and highlighted some important findings. The Graphite cells produced reproducible and consistent results, which were expected based on the literature. This suggests that the methodology used for testing was satisfactory when fabricating conventional materials. The nano graphite is problematic when it comes to making a slurry as there is significant variability in results, as well as cell failure. The Nano Graphite cells had consistently low capacity, which is consistent with literature on the poor performance of this material. However, the challenges of working with nano graphite, including issues in the casting stage and cracking, suggest that this material may be more difficult to work with than graphite.

The Silicon composite cells produced mixed results, with some cells performing well and others performing poorly. The Nano Graphite + Silicon composite cell produced promising results in one cell but were inconsistent overall, likely due to the process challenges in the fabrication and casting stage. However, the results of the best performing cell suggest that the silicon material has potential for use in batteries, provided that the manufacturing and fabrication process can be optimized. Finally, the graphite-silicon composite cells completely failed. Overall, this study underscores the importance of carefully controlling the manufacturing process and optimizing material properties when working with different types of battery materials as well as the difficulty in doing so, and the sensitive nature of battery research. While some materials may perform well in certain conditions, others may prove more challenging to work with. The findings suggest that further research is needed to refine the manufacturing process and optimize material properties for each of these battery materials. Additionally, the

study highlights the importance of using reliable testing methodologies to ensure that results are reproducible and consistent across different cell types.

Furthermore, it should be noted that out of the 33-coin cells that were fabricated, 8 cells failed completely and only results from 15 cells could be recovered. In the context of this study, cell failure is identified as the point at which a cell ceases to yield any additional electrochemical results from the testing software. Further investigation is recommended to understand completely the failure mechanism. This highlights the difficulties in conducting reliable electrochemical testing within a limited time frame and emphasizes the need for improved repeatability in future work. Based on the statistics provided, the failure rate of the fabricated coin cells would be approximately 24% (8 out of 33 cells failed completely due to fabrication issues), and 12 out the 33 cells failed due to software issues which and furthermore the failure rate would be approximately 36% due to software testing issues.

Chapter 4.0 Feasibility Study: Matrix Assembly Cluster Source

4.1 Introduction

This chapter will present preliminary work on the synthesis of Graphite + Silicon Clusters nanocomposites using the Matrix Assembly cluster source (MACS), a novel technique that allows for the controlled assembly of nanoparticles into larger structures with precise control over their size, shape, and composition. This chapter will also outline the future work that will build on this feasibility study with the aim of developing high-performance graphite + silicon composites with enhanced mechanical, electrical, and thermal properties.

This chapter will first describe the experimental setup used to create the nanocomposite using the Matrix Assembly cluster source, as well as the materials and methods used in the experiment. This chapter will then present and discuss the preliminary results of the experiment, including the surface composition of the composite and any observed properties. Finally, the electrochemical results of this novel material, Graphite + Silicon Nanoparticles outline the planned future work, including the research question or objective, the experimental or analytical methods to be used, and the expected outcomes and potential impact of the future work.

4.1 Background

Graphite and Silicon nanocomposites have garnered considerable interest in recent years, thanks to their exceptional properties. However, as highlighted in Chapter 3, the fabrication process for Silicon Carbon composites presents challenges due to its inherent nature. This necessitates a feasibility study for the development of a novel Nanocomposite fabrication method and the Matrix Assembly Cluster Source.

Nanocomposites have emerged as a promising class of materials with enhanced mechanical, electrical, and thermal properties due to their high surface area-to-volume ratio and unique nanoscale structure. Various methods have been employed to fabricate nanocomposite materials, including solution mixing, melt blending, and in situ polymerization. However, these methods often suffer from issues such as poor dispersion of the nanoparticles, low interfacial adhesion, and the use of toxic solvents. Recently, a novel method called matrix assembly cluster source has been developed, which offers a solvent-free and physical approach to fabricate nanocomposites. This method involves a cluster beam deposition method with the deposition of nanoclusters onto a substrate, followed by the assembly of these clusters into a matrix material using low-energy ion irradiation. This method has been shown to produce nanocomposites with improved mechanical and thermal properties (80). The solvent-free nature of this method also makes it an attractive option for the fabrication of environmentally friendly nanocomposites. Thus, the matrix assembly cluster source method presents a promising approach for the fabrication of high-quality nanocomposite materials, which could have a wide range of applications in fields such as electronics, energy, and biomedicine. The specific device has been built in Swansea University and studies by Palmer et al, Cai et al and Spadaro et al explore the applications and working principles of the Matrix Assembly cluster source (83) (84) (85).

4.1 Fabricate Graphite + Silicon Nanocomposites usingthe Matrix Assembly Cluster Source

The preliminary work section of this thesis focuses on developing an experimental setup for fabricating graphite-silicon nanocomposites using the Matrix Assembly cluster source. The resulting nanocomposites are characterized using various techniques to assess their structural and electrochemical properties and are evaluated as active materials in anode slurry and tested as coin cells. The insights gained from this preliminary work aims to investigate the possibility

of the fabrication of a graphite-silicon nanocomposites using the Matrix Assembly Cluster Source and this methods suitability for making nanocomposites for high performance anodes in lithium-ion batteries.

4.1.1 Experimental techniques

4.1.1.1 Matrix Assembly Cluster Source – Nanocomposites Fabrication

The Matrix Assembly Cluster Source (MACS) is a novel technique for synthesizing nanostructured materials. In this method, a target material is heated by a laser or electron beam, which results in the ejection of atoms or clusters from the target. These clusters are then condensed onto a substrate to form a thin film or nanocomposite. The MACS process has several advantages, including the ability to control the size and composition of the clusters, and the ability to deposit materials without the use of solvents (86) (87).

The experimental setup for the MACS system in this project, is now the third version MACS 3 of this cluster beam source technique. The MACS 3 consists of a vacuum chamber, a target material, a substrate, and a laser or electron beam source. The target material is typically made of the material to be deposited as clusters onto the substrate, while the substrate can be any suitable material such as glass, silicon, or metal. The vacuum chamber is used to remove any residual gas molecules that may interfere with the deposition process.

During the deposition process, the target material is heated by a laser or electron beam, which causes atoms or clusters to be ejected from the target. These ejected clusters travel through the vacuum chamber and eventually reach the substrate, where they condense to form a thin film or nanocomposite. The size and composition of the clusters can be controlled by adjusting the laser or electron beam parameters, such as the energy and spot size.

Several studies have utilized methods similar to that of the MACS technique for synthesizing nanostructured materials, such as metal nanoparticles (88) metal oxide nanocrystals (Koike et al., 2012), and carbon-based nanomaterials (75). The MACS method has been shown to

produce high-quality films with a high degree of control over the size and composition of the clusters. Studies including a study by Martelli et al. (86) explored the use of producing nanoclusters using the MACS technique for catalysis. *Figure 4-1* shows a schematic of the Matrix Assembly Cluster Source and *Figure 4-2*, a real-life image of the MACS in Swansea University in April 2022 and *Figure 4-3* an Engineering Rendering.

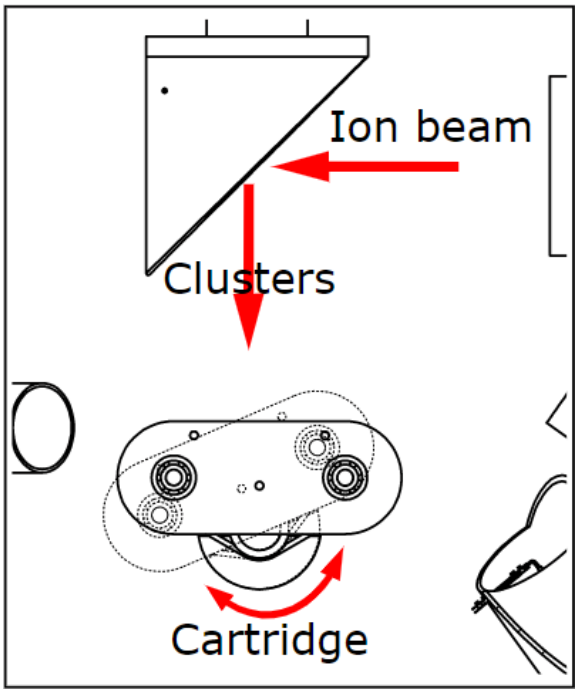

Figure 4-1 - MACS Schematic of inside the vacuum chamber showing the cold head and matrix assembly working principle.

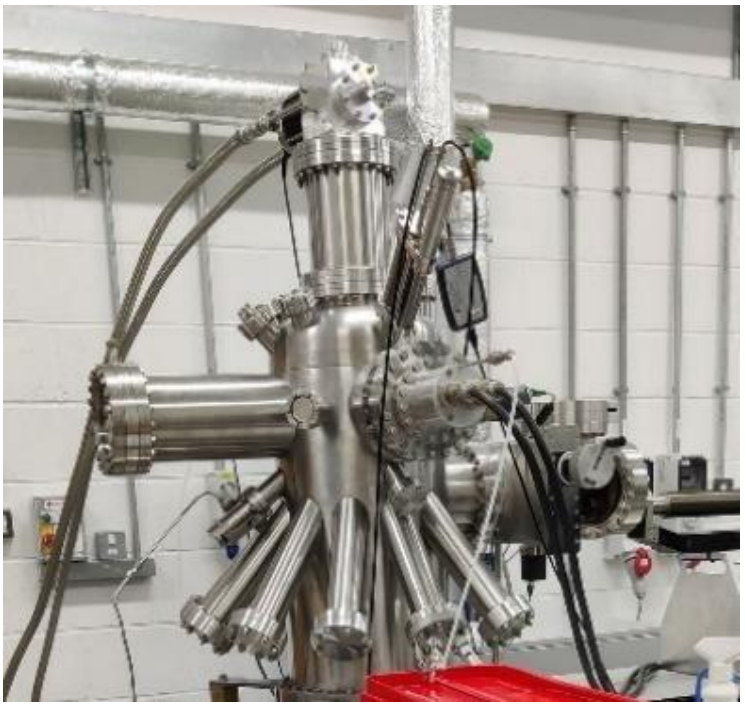

Figure 4-2 - MACS at WCPC - Swansea University April 2022

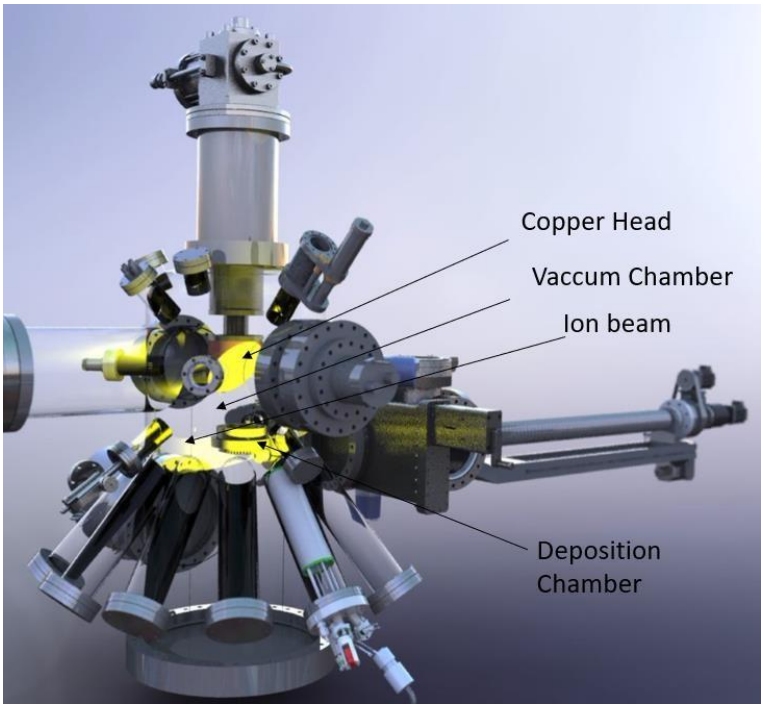

Figure 4-3- Engineering Rendering of the MACS created by Doctoral Student Morris Matthews.

4.1.1.1 Fabrication of MACS Graphite + Silicon Nanocomposites

In this study, the MACS system was used to synthesize graphite-silicon nanocomposites for use as Novel nanostructured anodes for lithium-ion batteries. The SFG15 graphite was used as the substrate, while silicon was deposited as clusters using the MACS method. The resulting nanocomposites were characterized using various technique described in Chapter 2 to assess their structural and electrochemical properties. The details of the experimental setup and the characterization techniques used are described in the following sections.

During the preliminary work done prior to this project, it was found that to achieve the desired nanocomposite material, it was essential to install an e-beam evaporator to evaporate the silicon. This is because silicon has a high melting point (1414ºC), making it difficult to deposit using the Matrix Assembly cluster source alone. The SFG15 substrate (500 mg) was placed in the deposition cup as shown in *Figure 4-1*. The e-beam evaporator was loaded with 1g of silicon metal. A composite of argon atoms and metal atoms, in this case silicon, matrix is then formed in the vacuum chamber, on the helium cooled copper cold head which is approximately 10 K. The matrix consists of small metal atoms (or clusters thereof) embedded in a film of frozen Argon atoms. An ion-beam is then fired at the argon silicon composite matrix and a cascade of collision results in metal silicon clusters of approximately 1 nm depositing on the SFG15 substrate material. The deposition rate was not optimized at this stage, as this was preliminary work, and the focus was on characterizing the resulting material, as the specific amount of silicon clusters deposited onto the substrate cannot be confirmed and only approximated after deposition. To attempt to determine the amount of silicon nanoparticles deposited onto the resulting MACS powder nanocomposite (SFG15 Graphite + Silicon clusters), the resulting material was characterized using techniques described in Chapter 2, such as scanning electron microscopy (SEM), energy dispersive X-ray spectroscopy (EDS), and X-ray photoelectron spectroscopy (XPS).

A 6% deposition rate with this percentage calculated through the hypothesis of creating 1nm thick silicon shell around a carbon atom, calculating that the required ratio of this nanocomposite should be 6% silicon 94% carbon. A schematic is included in Appendix A5. The resulting nanocomposite that is removed from the deposition chamber is in powder form and is referred to as the MACS powder (Graphite + Silicon nanoclusters). This powder is then used as active powder in the slurry preparation process for electrode fabrication.

4.1.1.2 Slurry Preparation and Electrode Fabrication

The slurry and electrodes for the MACS Graphite + Silicon nanocomposite was manufactured using the same methodologies outlined in Chapter 2. *Figure 4-4* shows the punched electrodes used in the MACS half coin-cells.

Figure 4-4 - MACS Graphite + Silicon Electrodes

4.1.1.3 Electrochemical Testing techniques.

The MACS Graphite + Silicon Electrode material was tested in a half coin cell configuration, identical to other cell types in this project using the MACCOR testing software in the Johnson Matthey technology centre. The cells were tested using a rate test and cycle life test.

4.2 Results and Discussion (Preliminary)

4.2.1 Powder and Electrode Characterization

Table 4-1 - XPS stoichiometric results for MACS Powder (Graphite + Silicon nanoclusters) and Electrode of MACS Graphite + Silicon Nanocomposite.

Sample Identifier	Al 2p component %	C 1s %	Cl 2p %	Cu 2p1/2 %	Cu 2p3/2 %	Fe 2p %	Na 1s %	O 1s %	Si 2p %
MACS Electrode	0	0.0	85.3	0.0	0.00	0.03	0.1	1.8	12.9
MACS Electrode	0	0.0	85.9	0.0	0.01	0.02	0.1	1.7	12.3
MACS Powder	0	0.0	98.2	0.0	0.00	0.00	0.0	0.0	1.8
MACS Powder	0	0.0	98.2	0.0	0.00	0.00	0.0	0.0	1.8

Table 4-1 displays the stoichiometric analysis results obtained from XPS surface analysis of the material in two forms: The MACS powder which refers to the graphite SFG15 after the material has been decorated with silicon nanoclusters (approx. 1nm) and is now a graphite silicon nanocomposite used as active powder and the MACS electrode which is the casted electrode after slurry and electrode fabrication with the MACS powder. The XPS analysis did not detect the presence of silicon on the electrode's surface. It has been shown that XPS is capable of successfully detecting platinum nanoparticles on graphite and so it is likely that silicon is not presents and the MACS technique could have added extra defects to the graphite. Further investigation using complementary analytical techniques may be necessary to confirm the presence or absence of silicon in the electrode. TEM and EDS are recommended for both elemental composition characterization technique and observation of the individual clusters. *Figure 4-6 a)* illustrates graphite electrode before the MACS addition of silicon nanoclusters and *Figure 4-6b)* shows a graphite electrode after addition of silicon nanoclusters.

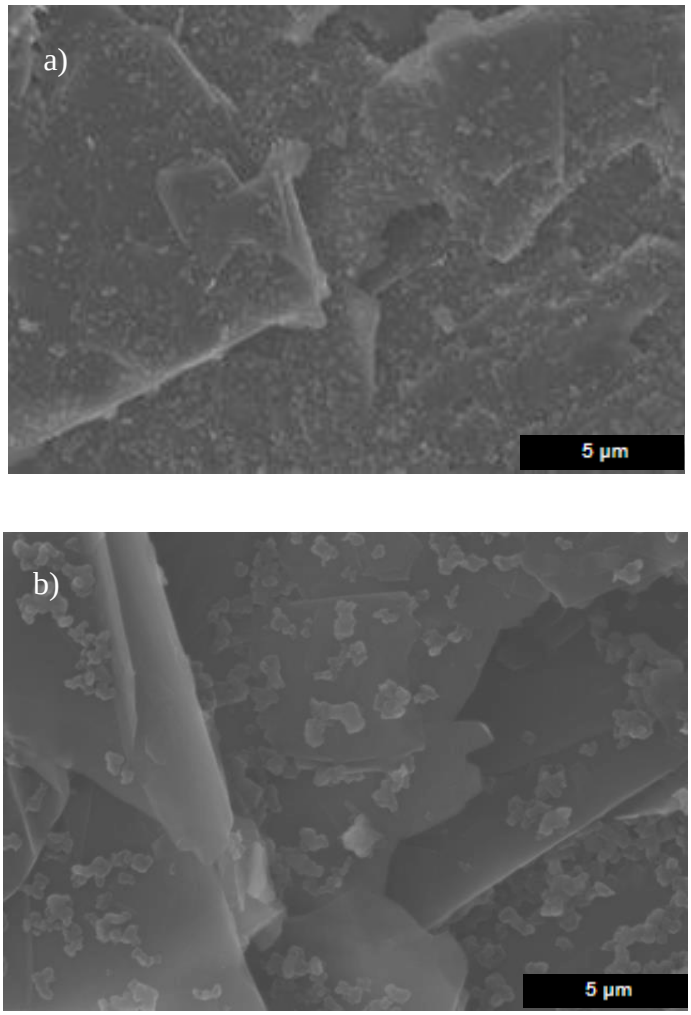

Figure 4-5 – a) SEM image of Graphite electrode b) SEM image of MACS Graphite + Silicon Electrode. Images captured and prepared by Doctoral student Dan Gillard.

The SEM image did not show any clear evidence of silicon nanoparticles on the electrode surface. This could be due to several reasons, such as the imaging conditions, the small size or low concentration of the particles, their uniform dispersion, or the presence of surface contaminants. The SEM image can be closely compared to the SEM micrograph of the Graphite electrode without any addition of silicon. Additional characterization techniques, such as TEM or XRD, may be necessary to confirm the presence and distribution of silicon nanoparticles. Unfortunately, due to time limitations within the project, further characterization techniques such as TEM or XRD were not pursued in this preliminary work.

4.2.2 Electrochemical Results (Preliminary)

The following section presents the graphical electrochemical results of the MACS cells, tested using both the rate test and cycle life test. *Figure 4-6, Figure 4-7* and *Figure 4-8* show the graphical electrochemical results of the MACS cells that were tested using the Rate Test, and *Figure 4-9* an *Figure 4-10* illustrate the Cycle Life test results.

4.2.2.1 Rate Test

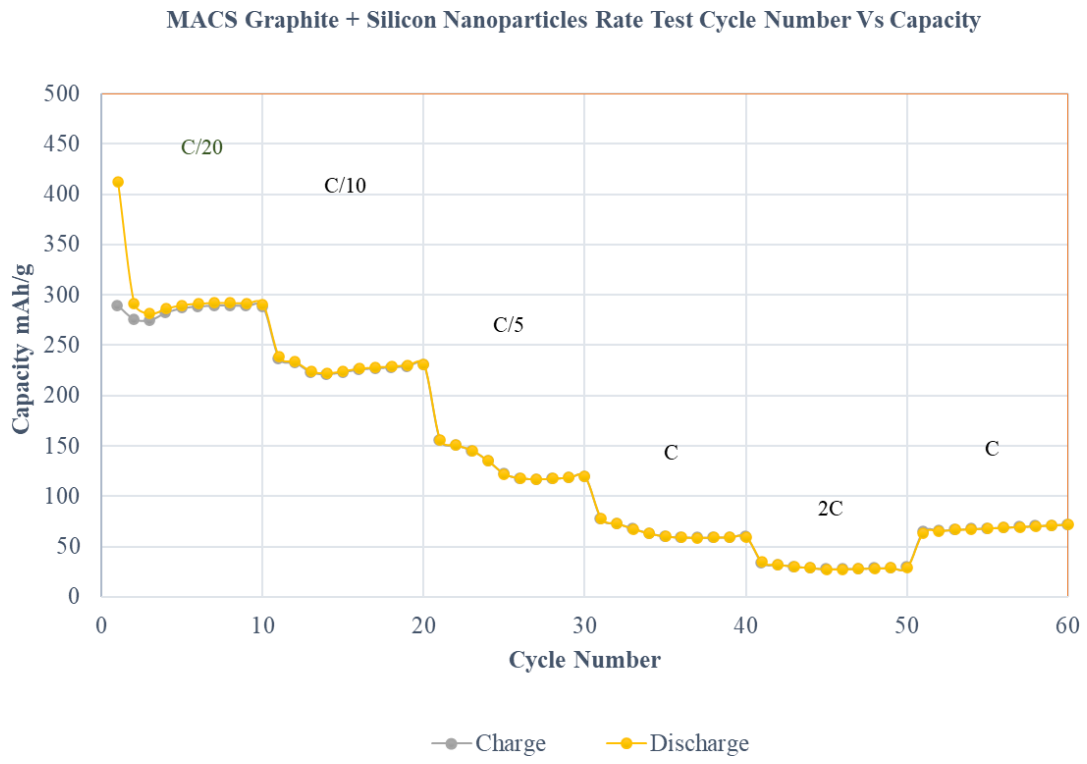

Figure 4-6 - Rate Test, MACS Cells 1.

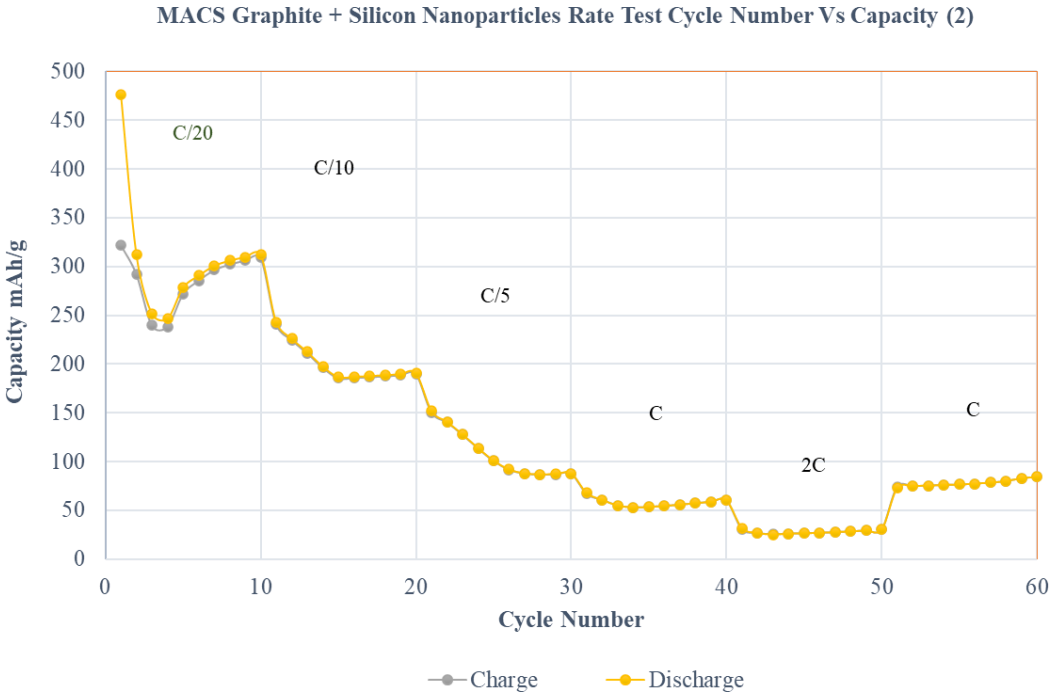

Figure 4-7 - Rate Test, MACS Cells 2

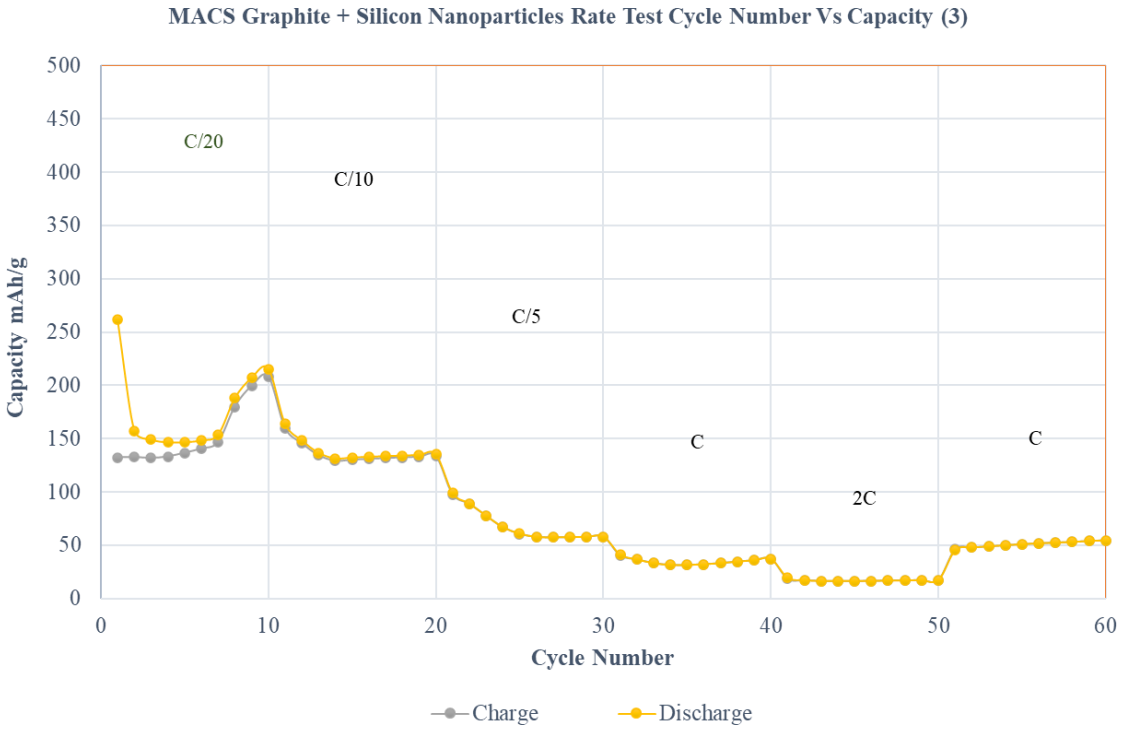

Figure 4-8 - Rate Test, MACS Cell 3.

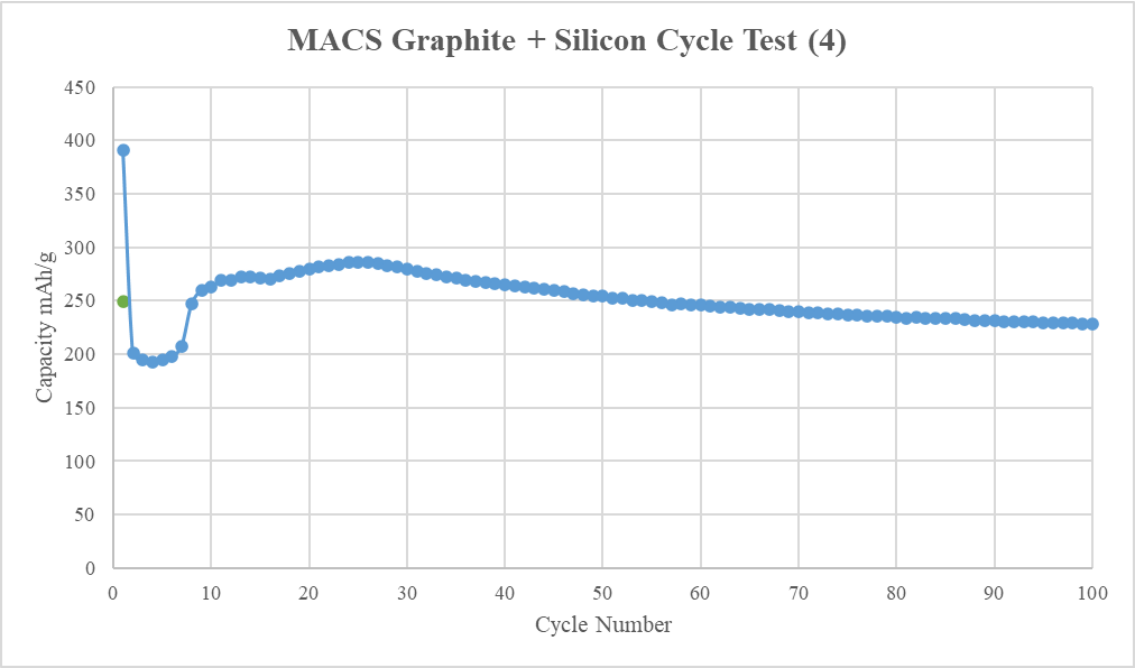

Figure 4-9 – Cycle Life Test, MACS Cell 4.

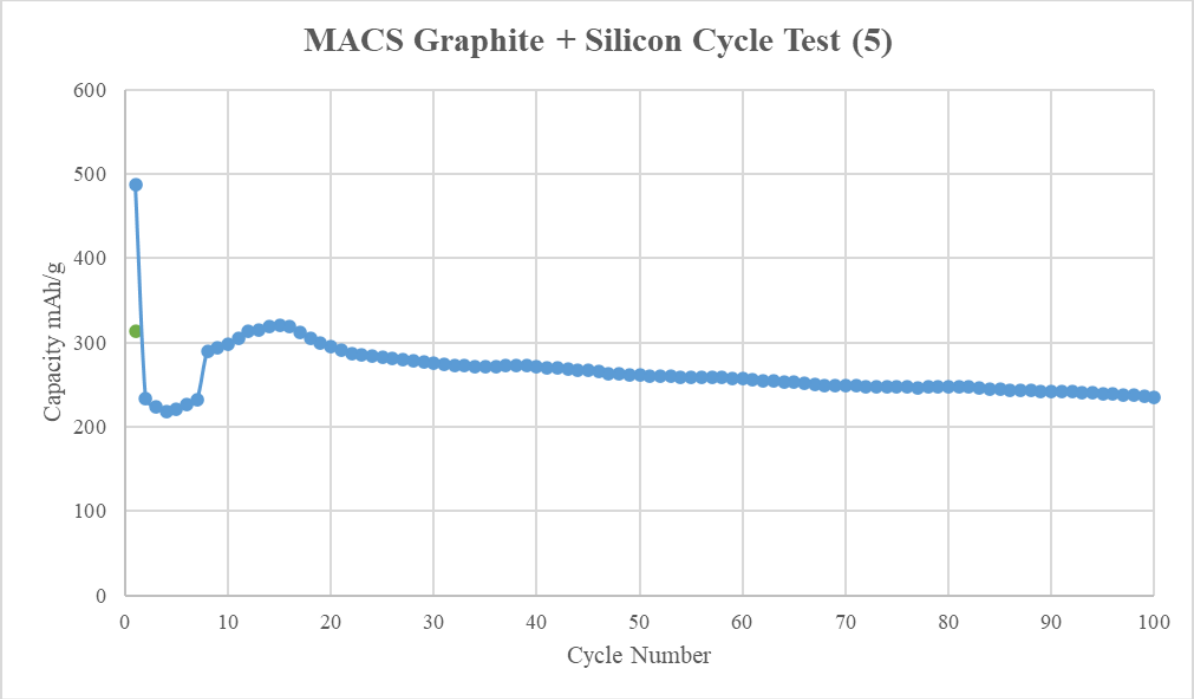

Figure 4-10 – Cycle Life Test, MACS Cell 5.

The MACS Graphite + Silicon Clusters Cell 1 rate test exhibits an initial discharge capacity of 406 mAh/g at C/20, as illustrated in *Figure 4-6* From cycle 30 to cycle 60 after a cycling at 1C, 2C and 1C for 10 cycles respectively, the cell has a capacity retention of 100% and an overall retention of 22% from cycle 2 to cycle 60. The MACS Graphite + Silicon Clusters Cell 2 *(Figure 4-7)* exhibits an initial discharge capacity of 475 mAh/g and after formation of the SEI layer drops to 295 mAh/g after cycle 1 at C/20. At cycle 30, from 1C over 10 cycles, 2C over 10 cycles and 1C over 10 cycles, the capacity retention is approximately 96% with an overall capacity retention after cycle 1 of 16%. Cell 3 *(Figure 4-8)* rate test shows a significantly lower initial discharge capacity of 150 mAh/g after cycle 1 but also with a retention rate of 100% through cycle 30 to 60 at 1C, 2C and 1C. The cycle life tests, presented in *Figure 4-9* and *Figure 4-10* represent MACS Graphite + Silicon clusters Cell 4 and 5. As seen across all cells, both Cell 4 and 5 have high initial discharge capacities of 495 mAh/g and 395 mAh/g respectively, which is 115 mAh/g and 15 mAh/g higher than the datum cell and around 4 times higher than the Graphite + Silicon nanoparticles, which exhibited mostly cell failure and a discharge capacity of 75 mAh/g.

As can be seen, the cells exhibit higher initial discharge capacities and excellent capacity retention rates throughout multiple cycles. The MACS powder also proves to be easier to process compared to the other tested Silicon nanocomposites, in the slurry preparation and electrode fabrication process. This could be since there may not be Silicon present and further investigation of chemical composition characterization techniques and methodology refinement is paramount. These findings highlight the possibility of the MACS as a method of developing Silicon Carbon nanocomposites for use as anodes in lithium-ion batteries.

4.2 Overall Project Closure, Discussion and Future Works

In conclusion, the results of this study suggest that the tested MACS Graphite + Silicon clusters anode has some potential to improve the performance of electrodes in energy storage devices, but further testing is needed. This study also demonstrates that it is possible to use the MACS approach to produce carbon silicon nanocomposites for application as an anode for lithium-ion batteries and it's ESS potential. The Nano graphite + Silicon nanoparticles anode also showed an increased capacity compared to regular Graphite, good retention rate, and consistent, repeatable results are promising.

However, the variation in results across the Nano Graphite, Nano Graphite + Silicon, and Gaphite + Silicon suggests that there may be issues in process optimisation at the slurry, electrode, andcoin cell fabrication stages.

The cycle life test showed that the nano graphite + silicon nanoparticles had a lower capacity than the datum cell. However, the capacity remained stable and consistent over multiple cycles, indicating that the material has good cycle life characteristics. This is an important finding, as cycle life is a critical factor in the performance of electrodes in energy storage devices. The stable and consistent performance of the material over multiple cycles suggests that it could be a promising candidate for use in such devices.

Several studies have investigated the use of silicon-based materials as an electrode material for energy storage devices, and the results of this study are consistent with those findings for the best performing cell. To conclude, repeats are essential. For example, a study by Zhang et al. (87) found that the incorporation of silicon into graphite-based electrodes led to improved electrochemical performance, including increased capacity and stability. The results of this study are consistent with these findings, as the tested material exhibited increased capacity and stable cycle life characteristics. However, it is important to note that the tested material is a

novel composite material that has not been extensively studied in the literature, and further research will be necessary to fully understand its potential as an electrode material.

This study represents only preliminary work, and further refinement of the methodology is necessary. In future work, more in-depth characterization techniques, such as TEM or XRD, could be used to better understand the structure and composition of the material. Additionally, the performance of the all-anode materials could be evaluated under different operating conditions to determine its suitability for practical applications. Further refinement of the methodology and more in-depth characterization techniques will be necessary to fully understand and optimize the performance of the material.

The battery manufacturing and testing process is lengthy and can take anywhere from a week to three months for a single cell to complete testing. Given the one-year timeframe for this master's project, there were some difficulties encountered in repeating results when cells failed during testing. Moreover, the preparation of slurries, which takes approximately four days to complete, is another factor that adds to the complexity of the testing process. These slurries are susceptible to moisture, which can have an impact on the results of the cell. As a result, it was important to take measures to ensure that the manufacturing process was as consistent as possible, to minimize any variability that could arise due to issues such as moisture contamination.

This study provides a foundation for further exploration of the potential of the tested material as an electrode material for energy storage devices as well as the MACS approach for silicon carbon nanocomposite fabrication, in particular Nano Graphite + Silicon clusters made by the MACS to ‘complete the story’ and compare electrochemcial results and performance of this combination of nanocompiste. This would be highly reccomended as the next step for progression of this project.

Bibliography

1. ***Electrical Energy Storage for the grid: a battery of choice.*** **Dunn, B., H.Kamath and Tarascon, J.M. s.l. : Science, 2011, Vol. Nov 18.**

2. ***Silicon-based anodes for lithium-ion batteries: From fundamentals to practical applications.*** **Wang.C, Li.L and Wange.Z. 31, s.l. : 1602230, Vol. 13.**

3. ***Fundamentals of Batteries.*** **s.l. : Elsevier, 2019, Vol. 2, pp. 1–22.**

4. ***Introduction to Battery Full-Lifespan Management.*** **L, Kailong., Y, Wang. and X., Lai. 2nd, 2019, Vol. Springer, pp. 1-22.**

5. . ***Handbook of Batteries.*** **s.l. : McGraw-Hill Education, 2011, Vol. Vol. 4.**

6. ***Electrochemical Methods: Fundamentals and Applications.*** **Bard, A.J and Faulker, L.R. s.l. : Wiley, 2001.**

7. ***On the Electricity Excited by the Mere Contact of Conducting Substances of Different Kinds.*** **Volta, A. London : The Royal Society of London, 1832, Vol. 90, pp. 403–431.**

8. ***The Correspondence of Michael Faraday.*** **Farady, M. London : R. and J.E. Taylor., 1834, Vol. 1.**

9. ***What are Batteries, Fuel Cells, and Supercapacitors?*** **Brodd. R, Winder. M. s.l. : Chemical Reviews, 2004, American Chemical Society, Vol. 104(10), pp. 4245-4269.**

10. ***Lithium batteries and cathode materials.*** **Whittingham, M.S. 10, 2004, Chemical Reviews, Vol. 104, pp. 4271-4301.**

11. ***The Li-ion rechargeable battery: A perspective.*** **Goodenough, J.B and Park, K.S. Journal of the American Chemical Society, Vol. 135(4), pp. 1167-1176.**

12. ***History of lithium batteries.*** **s.l. : Journal of Solid State Electrochemistry, 2011, Vol. 15, pp. 1623-1630.**

13. ***Lithium ion, lithium metal and altrnative rechargeable battery technologies: the odyssey for high.*** **Placke, T. Berlin : Journal of Solid State Electrochemistry, 2017, Vol. 21, pp. 1939-1964.**

14. ***Challenges in the development of advanced Li-ion batteries.*** **Etacheri, V and al, et. 9, s.l. : Energy & Environmental Science,, 2011, Energy & Environmental Science.**

15. 'Lithium', 2016. Archived from the orginial on 30 November 2016. Retrieved 23 January 2023.

16. ***3. Brief History of Early Lithium-Battery Development.*** **Reddy, M and al, et. Basel : Journal of Materials, 2020, PubMed.**

17. ***he road towards highly efficient rechargeable lithium–sulfur batteries: enabling approaches and restraining factors.*** **Meng, Y.S and Arroyo-de Dompablo, M.E. 47, Journal of Materials Chemistry, Vol. 19, pp. 8943-8962.**

18. ***The lithium-ion battery: State of the art and future perspectives.*** **Zubi, G, et al. s.l. : Elsevier, 18 June 2018, Renewable and Sustainable Energy Reviews, Vols. Vol. 89,, pp. 292-308.**

19. ***Electrical energy stroage and intercalation chemistry.*** **Whittingham, M.S. s.l. : Science, 1976, Science, Vol. 192, pp. 1126-1127.**

20. ***The electrochemical properties of ionic alkali metal aand NR4-graphite intercalation compounds.*** **J.O., Besenhard. s.l. : Elsevier, Carbon, Vol. 14, pp. 111-115.**

21. ***Synthesis and properties of lithium-graphite intercalation compounds.*** **Basu, S: et al. 3, s.l. : Elsevier, 1979, Materials Science & Engineering, Vol. 38, pp. 275-283.**

22. ***A reversible graphite-lithium negative electrode for electrochemical generators.*** **Yazami. R, Touzain. Ph. s.l. : Elsevier, 1983, Journal of Power Sources, Vol. 9, pp. 365-371.**

23. ***Lithium-ion battery characteristics and applications.*** **Assad, M: et al. s.l. : Science Direct, 2021, Design and Performance Optimization of Renewable Energy Systems, pp. 205-219.**

24. ***Recent progress of advance anode materials of lithium-ion batteries.*** **Cheng, H, et al. s.l. : Elsevier, 2021, Journal of Enegry Chemistry, Vol. 57, pp. 451-468.**

25. ***Solvated Ion Intercalation in Graphite: Sodium and Beyond.*** **Park, J, Zheng, Long, X and Kang, K. Seoul : Frontiers, 2020, Jounral of Frontiers in Chemistry.**

26. ***Building Better Batteries.*** **Armand, M and Tarascon, J.M. s.l. : Nature, 2008, Vol. 451, pp. 652-657.**

27. ***Lithium Batteries: Status, Prospects and Future.*** **Scrosati, B and Garche, J. 9, s.l. : Journal of Power Sources, 2009, Vol. 195, pp. 2419–2430. 0378-7753.**

28. ***Solvated Ion Intercalation in Graphite: Sodium and Beyond.*** **Park, J, Xu, L and Kang, K. 2020, Journal of Frontiers in Chemistry.**

29. Targray. Graphite Anode. ***Targray.*** **[Online] 8 Febuary 2021. [Cited: 14 January 2022.]**

30. ***Lithium-ion battery characteristics and applications*** **. Wang, S and Chen, Z. 2021, Science Direct.**

31. ***Intercalation chemistry of graphite: alkali metal ions and beyond.*** **Li.Y, Yaxiang.P, Adelhelm.P, Titrici.M.M, Hu. Y.S. s.l. : Publishing, 2019, Chem. Soc. Rev,, Vol. 48, pp. 4655-4687.**

32. ***Carbon materials for ion-intercaltion involved rechargeable battery technologies.*** **G, Wang., Minghao.Y and Feng.X. Germany : Publishing, 2020., Royal Soc. of Chemistry.**

33. ***A review of lithium-ion battery safety concerns: The issues, stragtegies and testing standards.*** **Chen, Y, Zhao, Y and Wang, L. 414(6861, s.l. : Nature, 2021, Journal of Energy Chemistry, Vol. 59, pp. 359-367.**

34. ***Solvated Ion Intercalation in Graphite: Sodium and Beyond.*** **Jooha, P, Zheng-Long, Xu and Kang, K. Seoul : Frontiers, Department of Materials Science and Engineering, 2020, Vol. 8.**

35. ***High-performance lithium battery anodes using silicon nanowires.*** **Lawes, S and al, Et. 3(1), s.l. : Nature nanotechnology, 2018, Nano Energy, pp. 313-321.**

36. ***High-performance lithium battery anodes using silicon nanowires.*** **Chan, Candace K and al, Et. s.l. : Nature nanotechnology, 2008, Nature Nanotechnology, Vol. 3 (1), pp. 31-35.**

37. ***Scalable and Low-Cost Synthesis of Porous Silicon Nanoparticles as High Peformance Lithium-ion Battery Anodes.*** **Yan, Z. 2022, Materials Today Nano.**

38. ***Designing Nanostructured Si anodes for high energy lihtium ion batteries.*** **Cui, Y. Wu, H. 2012, Nanotoday, Vol. 7, pp. 414-429.**

39. ***Silicon and Carbon Nanocomposite Spheres with enhanced conductivity and stability as high-performance anodes for lithium-ion batteries.*** **Wang, W and al, Et. 44838 , s.l. : Journal of Power Sources, 2017, Scientific Reports, Vol. 7, pp. 10-16.**

40. ***High-performance graphite/silicon composite anodes for lithium-ion batteries.*** **al, Zhang et. 135279, (2020) : Electrochimica Acta, Vol. 331.**

41. ***Enhanced Stability Lithium-Ion Battery Based on Optimized Graphene/Si Nanocomposites by Templated Assembly.*** **Liu, L and al, et. s.l. : National Library of Medicine, 2019.**

42. N, Choi., et al. ***Recent Progress on Polymeric Binders for Silicon Anodes in Lithium Ion Batteries.*** **s.l. : Journal of Electrochemical Science and Technology, 2015. Vol. 6.**

43. R, Masse., et al. ***Energy Storage through intercalation reactions: electrodes for rechargeable batteries.*** **s.l. : National Science Review, 2017.**

44. ***Studying the kinetics of crystalline siliocn nanoparticle lithiation with in situ transmission electron microscopy.*** **McDowell, M, et al. s.l. : Adv Mater, 2012.**

45. ***Silicon nanoparticles coated with nanopourous carbon as a promising anode material for lithium ion batteries.*** **H. Xu, M. Ding, D. Li, Y. Jiang, B. Xue. Changchun : New Journal of Chemistry, 2020.**

46. ***Scanning Electron Microscopy and X-Ray Microanalysis: A Text for Biologists, Materials Scientists, and Geologists. .*** **Goldstein, J.I, et al. s.l. : Springer, 2017.**

47. TWI. ***TWI global.*** **[Online] [Cited: 20 September 2022.] https://www.twi-global.com/what-we-do/services-and-support/failure-analysis-and-repair/microscopy/scanning-electron-microscopy-sem-analysis-and-imaging.**

48. ***Transmission Electron Microscopy: A Textbook for Materials Science. .*** **Williams, D.B and Carter, C.B. s.l. : Springer., 2009.**

49. ***Quantitative electron spectroscopy of surfaces: A standard data base for electron inelastic mean free paths in solids.*** **Seah, M.P and Dench, W.A. 2, s.l. : Surface and Interface Analysis, 1996, Vol. 3, pp. 18-22.**

50. ***Binders for Li-ion battery electrodes: Challenges, progress, and perspectives.*** **Li.J, et al. s.l. : Energy Storage Materials,, Vol. 9, pp. 140-164.**

51. ***nsights into the effect of the binder content on the performance of anodes for lithium-ion batteries.*** **Li, M, et al. s.l. : Journal of Power Sources, 2020, Vol. 400, pp. 306-313.**

52. Fritsch International. https://www.fritsch-international.com/. ***https://www.fritsch-international.com/.*** **[Online] Fritsch International. [Cited:]**

53. TMAX Battery Equipments. Laboratory Electric Rolling Press Machine Calener Machine. ***battery-equipments.com.*** **[Online] TMAX. [Cited: 25 January 2023.]**

54. MTI Coorporation. Disc Cutters. ***mtixtl.com.*** **[Online] MTI Coorportation. [Cited: 25 January 2023.]**

55. ***Construction and Testing of Coin Cells of Lithium Ion Batteries.*** **Kayyar, A, Huang J., Samiee, M, Luo J. 4104, s.l. : PMCID, 2012, Vol. 66.**

56. Richardson, M. ***Increasing battery capacity: going Si high.*** **[prod.] Mewburn Ellis. 2020.**

57. Garcia, J.L. Electrical Power Systems. [book auth.] Battistini. S, Maphurs. B. Cappeletti.C. ***Cubesat Handbook.*** **s.l. : Academic Press, 2021.**

58. Fluorinated hybrid solid-electrolyte-interphase for dendrite-free lithium deposition. **Pathak, R et al. South Dakota : Nature Communications, 2020.**

59. ***Lithium-ion battery characteristics and applications.*** **Shunli Wang, Yongcun Fan, Daniel-Ioan Stroe, Carlos Fernandez, Chunmei Yu, Wen Cao, Zonghai C. s.l. : Elsevier, 2021, pp. 1-46.**

60. BioLogic. How to read battery cycling curves. ***BioLogic.*** **[Online] 11 November 2021. https://www.biologic.net/topics/how-to-read-cycling-curves/.**

61. ***Facile Synthesize of Pyrite (FeS 2 /C) nanoparticles as Electrode Material for Non-Aqueous Hybrid Electrochemical Capacitors.*** **Pham, D.T, et al. 2018.**

62. ***Highly Stable Cycling of Silicon-Nanographite Aerogel-Based Anode for Lithium-Ion Batteries.*** **Pati, R et al. 2021, ACS Omega, pp. 6600-6606.**

63. A comparison of Lithium-Ion Cell Performance across Three Different Cell Formats. **Bridgewater, G, Capener M, Brandon J, Lain J, Copey M, Kendrick E. 38, Coventry : Batteries, 2021, Vol. 7.**

64. ***High power TiO2 and high capacity Sn-doped TiO2 nanomaterial anodes for lithium-ion batteries.*** **Luebke, M, et al. s.l. : Journal of Power Sources, Vol. 294.**

65. ***1.10 - Surface Oxidation of Siliocn Ultra-Fine Particles.*** **Iijima, S. s.l. : Science Direct, 1995, Science Direct, pp. 82-87.**

66. ***Highly Stable Cycling of Silicon-Nanographite Aerogel-Based Anode.*** **Patil, R, et al. 6, s.l. : ACS Omega, 2021, pp. 6600-6606.**

67. ***Optimization of slurry mixing process for silicon anodes in lithium-ion batteries.*** **227008, s.l. : Journal of Power Sources, Vol. 438.**

68. ***A graphene coating layer for silicon anodes in lithium ion batteries.*** **Li, Y and al, Et. 2013, Journal of Materials Chemistry, pp. 5188-5194.**

69. ***Effects of graphite particle size on lithium-ion battery anode performance.*** **Li, Y and al, et. s.l. : Journal of Energy Chemistry,, 2017, pp. 712-718.**

70. ***X-ray microscopy: principles and prospects.*** **Chao, W, Kriz, J and D.Sayre. s.l. : Journal of Optical Society of America B, 1998.**

71. ***Contribution of X-ray photoelectron spectroscopy study on the electrochemical reaction of graphite in lithium ion battery.*** **Dedryvere, R, et al. s.l. : Journal of Power Sources, 2003, Chemistry of Materials, Vols. 119-121, pp. 585-589.**

72. ***Quantitative surface analysis by XPS.*** **Swingle, R. s.l. : John Wiley & Sons., 1975, Analytical Chemistry, Vol. 47, pp. 21-24.**

73. ***Surface analysis by Auger and X-ray photoelectron spectroscopy.*** **Tuner, N and Schreifels, J. s.l. : IM Publications., 2003, Analytical Chemistry, pp. 309-332.**

74. XPS Analysis of Carbon-Based Materials. In X-Ray Photoelectron Spectroscopy. **Morgan, D. s.l. : Springer., 2014.**

75. ***Growth of carbon nanotubes on magnetic iron oxide nanoparticles using plasma enhanced chemical vapor deposition.*** **Yuan, W, et al. 2014, Journal of Nanoparticle Research, p. 2227.**

76. ***Rate-dependent capacity fading mechanisms of graphite anodes studied by in-situ rate and in-situ capacity tests.*** **Eom, K and al, et. s.l. : Journal of Power Sources, Vol. 382, pp. 160-166.**

77. ***Studies on capacity fading mechanism of graphite anode for Li-ion battery.*** **Fu, L, et al. 1, s.l. : Journal of Power Sources , 2006, Vol. 162.**

78. ***Hierarchical structured silicon-graphite composite as anode material for high-energy lithium-ion batteries.*** **Mai, L and al, Et. 9, s.l. : ACS Applied Materials & Interfaces, Vol. 6, pp. 6522-6529.**

79. ***Structural changes in silicon anodes during lithium insertion/extraction.*** **. Obrovac, M.N and Christensen, L. 5, s.l. : Electrochemical and Solid-State Letters, Vol. 7. A93-A96.**

80. ***Nano/Microstructured Silicon-graphite Composite Anode for High-Energy Density Li-ion Battery.*** **Li, P, Huang, J.Y and Kook Sun, Y. s.l. : American Chemical Society, 2019.**

81. ***Review of advanced materials for lithium-ion battery electrodes.*** **Marom, R, et al. 3, MRS Bulletin, Vol. 36, pp. 170-176.**

82. ***Graphene-wrapped sulfur particles as a rechargeable lithium-sulfur battery cathode material with high capacity and cycling stability.*** **Wang, C and al, et. 7, s.l. : Nano Letters, Vol. 11, pp. 2644-2647.**

83. ***Synthesis without Solvents: The Cluster (Nanoparticle) Beam Route.*** **Palmer, R.E, Cai, R and Vernieres, J. Swansea : Accounts of chemical research, 2018, Vol. 51, pp. 2296-2304.**

84. ***A new method to prepare colloids of size-controlled clusters from a matrix assembly cluster source.*** **Cai, R, et al. Birmingham : APL Materials, 2017, Vol. 5.**

85. ***Angular dependence of nanoparticle generation in the matrix assembly.*** **Spadaro, M, et al. 12, Swansea : Nano Research, 2019, Vol. 12.**

86. ***Scale-Up of Cluster Beam Deposition to the Gram Scale with the Matrix Assembly Cluster Source for Heterogeneous Catalysis (Catalytic Ozonation of Nitrophenol in Aqueous Solution).*** **Cai, R, et al. 2020, American Chemical Society, pp. 12,22.**

87. Angular dependence of nanoparticle generation in the matrix assembly cluster source. **Spadaro, M and al, et. 2019, Nano Research, pp. 3069-3074.**

88. ***Synthesis of metal nanoparticles by magnetron sputtering gas aggregation source and their size control.*** **Koike, H, et al. 2012, Materials Transactions, pp. 1096-1100.**

89. ***Highly Stable Cycling of Silicon-Nanographite Aerogel-Based Anode.*** **Patil.R, Phadatare.M, Blomquist.N, Ortegren. J, Hummelgard.M, Meshram.J, Dubal.D, Olin.H. s.l. : American Chemical Society, 21 March 2021, ACS Omega, pp. 6600-6606.**

90. ***Graphene and silicon composite anodes for lithium ion batteries. Journal of Power Sources.*** **Journal of Power Sources, Vol. 254, pp. 72-79.**

91. ***Facile synthesis of silicon/carbon composites from rice husks for high-performance lithium-ion batteries. .*** **158126, s.l. : Journal of Alloys and Compounds, 2021, Vol. 855.**

92. ***Building better batteries.*** **7179, s.l. : Nature., 2008, Vol. 451, pp. 652-657.**

93. ***Standard Potentials in Aqueous Solution.*** **New York : Springer:, 1985.**

94. ***Influence of material properties on the specific energy density of cylindrical lithium-ion batteries.*** **s.l. : Journal of Power Sources., 2014, Vol. 267, pp. 799-806.**

95. https://www.pinterest.co.uk/edgefx/. [Online] 22 January 2021. [Cited: 2023 April 24.]

96. ***ilicon nanoparticles-embedded graphite/carbon composite anode for high-capacity lithium batteries.*** **2010, Vol. 6(9), pp. 1000-1005.**

97. ***Review- Nano-Silicon/Carbon Composite Anode Materials Towards Practical Applications for Next Generation Li-ion Batteries.*** **Luo, F et al. 14, s.l. : Journal of the Electrochemical Society, 2015, Vol. 162. A2509.**

98. ***Synthesis and Catalysis.*** **Schafhaeul.C and Prakt.J. 1840, Faculty of Natural Science, Vol. 21, pp. 129-157.**

99. ***Recent Progress of Advance Anode Materials of lithium-ion batteries.*** **Cheng, G, et al. 2021, Journal of Energy Chemistry, pp. 451-468.**

100. ***Review of Nanotechnology for Anode Materials in Batteries.*** **Goutain, S. s.l. : Emerging Nanotechnologies in Rechargeable Energy Storage Systems, 2017, Emerging Nanotechnologies in Rechargeable Energy Storage Systems.**

101. ***Advances in structure and property optimizations of battery electrode materials.*** **Meng, J and al, Et. (2017), Joule, pp. 522-547.**

102. ***Understanding the lithium-ion battery graphite-silicon composite anode through in-situ and operando X-ray spectroscopy techniques.*** **Bak, S.M. s.l. : Nano Energy, 2017, Nature Journal, Vol. 41, pp. 454-466.**

103. ***Graphene-silicon nanocomposites for lithium-ion battery anodes.*** **Sehrawat, P. s.l. : Carbon Based Nanomaterials for Advanced Thermal and Electrochemical Energy Storage and Conversion, 2018, Science Direct.**

104. ***Recent advances in silicon/graphite composite anodes for high-performance lithium-ion batteries.*** **Wang and al, Et. s.l. : Nanomaterials, 2019, Vol. 9(7).**

105. ***Estimating lithium-ion battery behavior from half-cell data.*** **s.l. : Energy Reports, 2021.**

106. Graphite as anode materials: Fundamental mechanism, recent progress and advances. **Beijing : Institute of Nuclear and New Energy Technology,, 2020. 100084.**

107. ***Use of lithium-ion batteries in electric vehicles.*** **s.l. : Journal of Power Sources, 2000. Vol. 90.**

108. ***Secondary Batteries Lithium Rechargeable Systems: Electrolytes: Solid Sulfide.*** **s.l. : Encyclopedia of Electrochemical Power Sources, 2009.**

109. Research progress on silicon/carbon composite anode materials for lithium-ion battery,. **s.l. : Journal of Energy Chemistry, 2018.**

110. ***Research on Advanced Materials for Li-ion Batteries.*** **2009. Vol. 21.**

111. Research progress on silicon/carbon composite anode materials for lithium-ion battery. **s.l. : Journal of Energy Chemistry, 2018. Vol. 27.**

112. ***Electrochemical Impedance Spectroscopy*** **. s.l. : Encyclopedia of Analytcial Science Edition, 2005.**

113. ***Electrochemical Impedance Spectroscopy.*** **s.l. : Fuel Cell Systems Explained, 2004.**

114. BioLogic. What is Electrochemical Impedance Spectroscopy (EIS) (Electrochemisty). ***Biologic.net.*** **[Online] BioLogic, 13 June 2022. [Cited: 19 December 2022.] https://www.biologic.net/topics/what-is-eis/.**

115. ***Electrode fabrication process and its influence in lithium-ion battery performance: State of the art and future trends.*** **Goncalves, R et. al. s.l. : Electrochemistry Communications, 2022, Vol. 135.**

116. The Role of Current Collector in Enabling the High Performance of Li/S Battery. **Benitez, A et. al. 37, s.l. : ChemistrySelect, 2018, Vol. 3, pp. 10371-10377.**

117. ***Understanding the Corrosion of Mg and Mg Alloys.*** **Atrens A, Dargusch M.S. s.l. : Encyclopedia of Interfacial Chemistry, 2018.**

118. ***Effects of HF on the Lihtiation Behaviour of the Silicon Anode in LiPF6 Organic Electrolyte Solution.*** **Lin, H., Noguchi, H., Uosaki, K. 5, s.l. : ACS Omega, 31 January 2020, Vol. 5, pp. 2081-2087.**

119. ***Electrochemical behavior of lithium intercalation into graphite. Journal of Power Sources,.*** **Novak, P, Muller, K and Santhanam, K.S.V. 2, 1997, Vol. 68, pp. 538-541.**

120. ***Multi-time-scale investigation of graphite anode behavior in Li-ion batteries using rate and electrochemical impedance tests.*** **Zhang, Y and al, Et. 470, s.l. : Journal of Power Sources, Vol. 228413.**

121. ***Silicon nanowires terminated with methyl functionalities exhibit stronger Si-C bonds than equivalent 2D surfaces.*** **s.l. : Physical chemistry chemical physics, 2009, Vol. 11, pp. 3845-8.**

122. ***Spectroscopic study using FTIR, Raman, XPS and NEXAFS of carbon nitride thin films deposited by RF magnetron sputtering.*** **Fabre-Bouchet, B, et al. 1-2, s.l. : Thin Solid Films, 2005, Vol. 482, pp. 167-171.**

Appendix

A1. Coin Cell Table

Table A-0-1 describes all coin cells that were manufactured and tested in this project and weather the cells failed or worked. ‘Outage’ means where the results of the cell were lost due to a power outage.

Table A.0-1 - Cell Type Table

Cell No.	Cell Type	Testing and Manufacturing Site	Testing Software	Fail/Worked
1	Graphite	Swansea University	Astrol	Fail
2	Graphite	Swansea University	Astrol	Fail
3	Graphite	Swansea University	Astrol	Fail
4	Graphite	Swansea University	Astrol	Fail
5	Graphite	Swansea University	BioLogic	Worked
6	Graphite	Swansea University	BioLogic	Worked
7	Graphite	Johnson Matthey	MACCOR	Worked
8	Graphite	Johnson Matthey	MACCOR	Worked
9	Graphite	Johnson Matthey	MACCOR	Worked
10	Graphite	Johnson Matthey	MACCOR	Worked
11	Graphite	Johnson Matthey	MACCOR	Failed
12	Nano graphite	Johnson Matthey	MACCOR	Worked
13	Nano graphite	Johnson Matthey	MACCOR	Worked
14	Nano graphite	Johnson Matthey	MACCOR	Worked

15	Nano graphite	Johnson Matthey	MACCOR	Worked
16	Nano graphite	Johnson Matthey	MACCOR	Worked
17	Nano graphite	Swansea University	BioLogic	Outage
18	Nano graphite	Swansea University	BioLogic	Outage
19	Graphite + Silicon	Swansea University	BioLogic	Outage
20	Graphite + Silicon	Swansea University	BioLogic	Outage
21	Graphite + Silicon	Swansea University	BioLogic	Outage
22	Graphite + Silicon	Swansea University	BioLogic	Failed
23	Graphite + Silicon	Swansea University	BioLogic	Failed
24	Graphite + Silicon	Swansea University	BioLogic	Worked
25	Graphite + Silicon	Swansea University	BioLogic	Worked
26	Nano graphite + Silicon	Swansea University	BasyTech	Worked
27	Nano graphite + Silicon	Swansea University	BasyTech	Worked
28	Nano graphite + Silicon	Swansea University	BasyTech	Worked

29	Nano graphite + Silicon	Swansea University	MACCOR	Worked
30	Nano graphite + Silicon	Swansea University	MACCOR	Worked
31	Nano graphite + Silicon	Swansea University	MACCOR	Worked
32	Nano graphite + Silicon	Swansea University	MACCOR	Failed
33	Nano graphite + Silicon	Swansea University	MACCOR	Failed

A2. Graphite Electrochemical Results

The following section shows other completed cell results that have been processed.

Figure A0-1 - Graphite Rate Test Result Cell 2

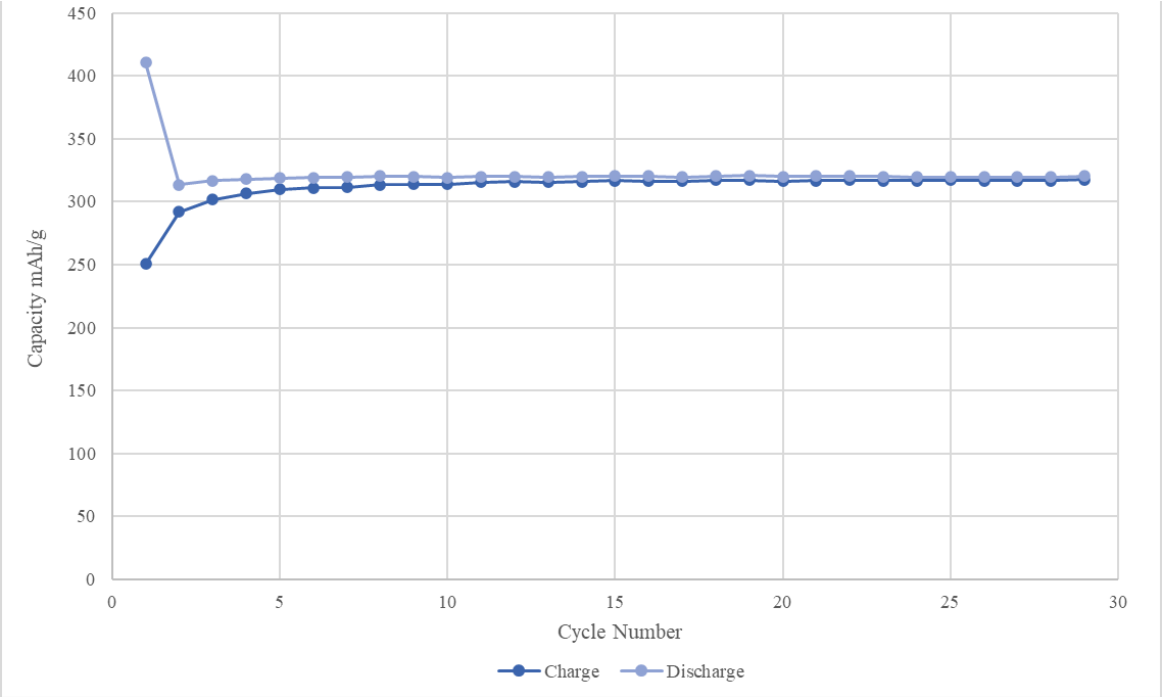

Figure A0-2 - Graphite Cycle Life Test Result Cell 3 (C/10)

A3. Nano graphite Electrochemical Tests

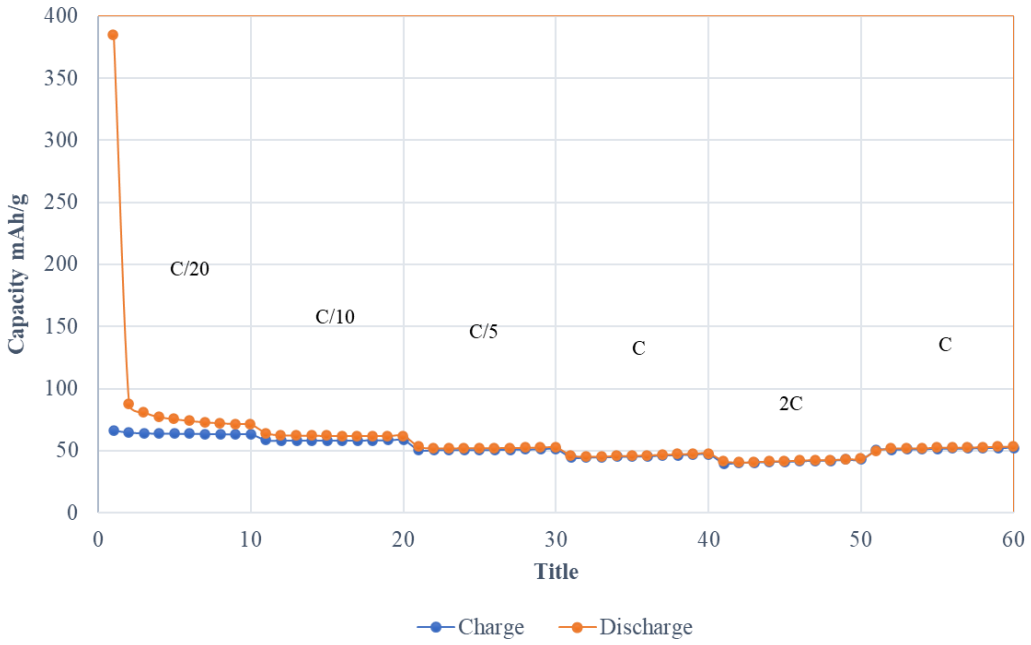

Figure A0-3 – Nano graphite Rate Test Cell 2

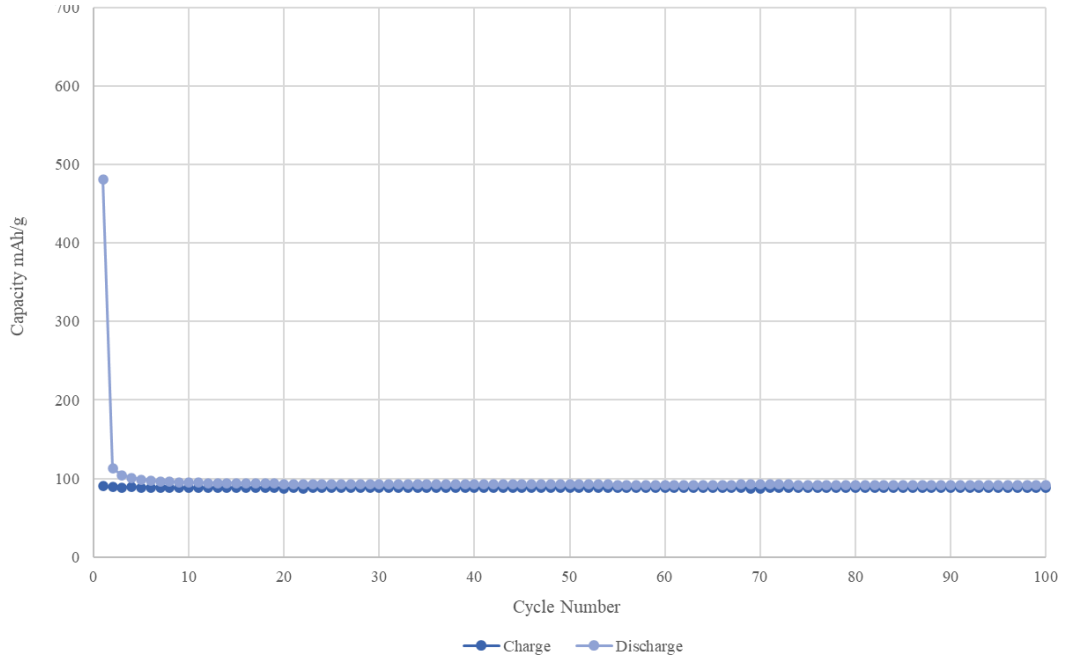

Figure A0-4 – Nano graphite Cycle Life Test Cell 3

A4. Full XPS Results

Table A0-2 - Full stoichiometric XPS Results

Sample Identifier	Al 2p component %	C 1s %	Cl 2p %	Cu 2p1/2 %	Cu 2p3/2 %	Fe 2p %	Na 1s %	O 1s %	Si 2p %
G	0	84	0	0	0	0.5	1.7	13.6	0.1
G	0	84.3	0	0	0	0.5	1.8	13.2	0.2
G	0	82.8	0	0	0	0.5	1.9	14.7	0.2
NG	1.3	69.3	0	0.01	0.02	0.2	1.7	25.4	2
NG	1.3	69.8	0	0.02	0.01	0.3	1.8	25.6	2.1
NG	1.3	68.8	0	0.02	0.03	0.2	1.9	26.1	2.2
Gr+NSi	0	81.2	0	0	0	0	1.7	14.8	2.2
Gr+NSi	0	81.3	0	0	0	0	1.7	14.9	2.1
NGr +NSi	0.7	61.7	0.4	0.04	0.07	1.3	0.2	30.3	5.3
NGr + NSi	2	64	0.1	0.23	0.63	0.7	1.2	27.9	3.2
NGr + NSi	2.1	64.1	0.1	0.24	0.62	0.6	1.2	27.9	3.2
MACS Electrode	0	73228.7	17.8381	3.49498	21.9048	47.1168	1510.83	11051.6	0
MACS Electrode	0	71127.9	4.01196	6.45692	19.6729	68.5204	1421.76	10149.1	0
MACS Powder	0	36211.7	0	0	0	0	0	658.029	0
MACS Powder	0	15776.2	0	0	0	0	0	290.708	0

A5. Silicon loading theory.

Figure A 0-5 illustrates the Silicon loading theory based on the idea that a 1 nm silicon shell would surround a carbon atom. Although this will not be the morphology of the composite atoms, it acted as basis for desired silicon loading.

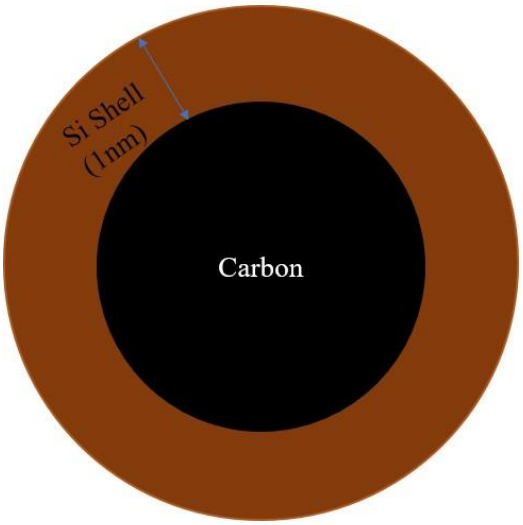

Figure A6-5 - 1nm Silicon Shell coating a Carbon atom, showing the theory of why a 94:6 ratio was chosen for Graphite + Silicon cluster nanocomposite not to scale.